Open Quantum Systems with Applications to Precision Measurements

by

David Tieri

B.A., University of Colorado - Boulder, 2009

M.S., University of Colorado - Boulder, 2013

A thesis submitted to the

Faculty of the Graduate School of the

University of Colorado in partial fulfillment

of the requirements for the degree of

Doctor of Philosophy

Department of Physics

2015

This thesis entitled:
Open Quantum Systems with Applications to Precision Measurements
written by David Tieri
has been approved for the Department of Physics

_____

Murray Holland

_____

John Bohn

Date _____

The final copy of this thesis has been examined by the signatories, and we find that both the
content and the form meet acceptable presentation standards of scholarly work in the above
mentioned discipline.

Tieri, David (Ph.D., Physics)

Open Quantum Systems with Applications to Precision Measurements

Thesis directed by Prof. Murray Holland

A spectrally pure coherent light source is an important component in precision measurement applications, such as an atomic clock. The more spectrally pure the coherent light source, or the narrower the linewidth of its power spectrum, the better for atomic clock experiments. A coherent light light source, such as a laser, is intrinsically an open quantum system, meaning that it gains and loses energy from an external environment.

The aim of this thesis is to study various open quantum systems in an attempt to discover a scheme in which an extremely spectrally pure coherent light source might be realized. Therefore, this thesis begins by introducing the two main approaches to treating open quantum systems, the quantum master equation approach, and the quantum Langevin equation approach. In addition to deriving these from first principles, many of the solution methods to these approaches are given and then demonstrated using computer simulations. These include the quantum jump algorithm, the quantum state diffusion algorithm, the cumulant expansion method, and the method of c-number Langevin equations.

Using these methods, the theory of the crossover between lasing and steady state superradiance is presented. It is shown that lasing and steady state superradiance might be demonstrated in the same physical system, but in different parameter regimes. The parameter space between these two extreme limits is explored, and the benefits and drawbacks of operating a system at a given set of parameters, i.e. to achieve the most spectrally pure light source, are discussed.

We also consider the phase stability of a laser that is locked to a cavity QED system comprised of atoms with an ultra-narrow optical transition. Although the atomic motion introduces Doppler broadening, the standing wave nature of the cavity causes saturated absorption, which can be used to achieve an extremely high degree of phase stabilization. The inhomogeneity introduced by finite

atomic velocities can also cause optical bistability to disappear, resulting in no regions of dynamic instability that would otherwise restrict operational parameters in the experiment to be tuned outside of the optimum region where the minimum linewidth occurs.

Dedication

This thesis is dedicated to my Grandma, Mom and Dad, Michael, Granny and Bob, Theo, UJ and Aunt Laura, Auntie Lori, Aunt Cathy and both of my Grandfathers.

Acknowledgements

I would like to thank Jinx Cooper for teaching me to never accept that something is true just because someone else says it is. I know it took a lot of convincing. Thank you Murray Holland for providing me with such amazing opportunities throughout my physics career. I would like to also thank Minghui Xu for being a good friend; I can honestly say I would not have gotten a PhD without you. To Dominic Meiser and Brandon Peden, thanks for being mentors to me, and for spending so much of your time teaching me stuffs. Thanks Jose D'Ianco for being an awesome person, Ron Pepino, Rajiv Bhat, Meret Krämer for being so welcoming when I first started in the group, Andrew Sykes for always being there to chat over a beer, Brandon Ruzic for being a good friend through it all, especially all semester last semester. Ryan Wilson, Victor Colussi, Jon Pfeiffer, you guys are awesome too. Thanks Jon for switching rooms with me when we lived together and I didn't like my room.

I would also like to thank Mary Nelson for teaching me Calculus in her office at 7am every morning for half a year, Ben Safdi for getting me started in physics, and staying up until 3am helping me do my homework, and then starting on his. Thank you to Noel Clark for telling me to go home and have a beer after a hard exam, to Mark Ablowitz for taking the time to tell me "Its ok, you're doing a good job, buddy", when I was totally stressed out in his office ten minutes before a homework trying to get the answers out of him. Thank you Will Forsythe for inspiring me each week, Kim Browne, Jeff Walters, Marika, Jimie and Scott, Ryan at Robb's Music, Andrew and Amanda, and everyone from Pekoe. Thanks to Bihui and Athreya, and to Jan Thomsen and his group for a great collaboration. And thanks to everyone else I forgot to thank.

Contents

Figures

Figure

Chapter 1

Introduction

1.1   Background

Our understanding of the interaction between light and matter is important, both fundamentally, and because it allows for the development of applications that are integral to the operation of our society. For instance, it was this understanding that allowed for the invention of the laser in 1960, which was then called "a solution looking for a problem" [82]. Since then, lasers have become ubiquitous in our society, with a vast scope of applicability, ranging from medical applications, such as cancer diagnosis and treatment [25, 26, 36], eye and general surgeries [21], and medical imaging [33], to industrial applications, such as cutting and welding [5]. Lasers are also used in nuclear fusion research to deliver a tremendous amount of energy to an extremely small fuel cell, in an attempt to achieve conditions where nuclear fusion [53, 54] will happen. If achieved, this internal confinement nuclear fusion would provide an inexaustible source of clean energy.

In fundamental biology research, optical tweezers, which rely on a highly focused laser and can hold microscopic particles in place [3], have opened the doors to new experiments, including the study of motor proteins [78], which are the mechanism behind transport phenomenon in neurons. The information obtained from optical tweezer experiments could allow for the development of a new generation of drugs and treatments to fight disease related to motor proteins [61].

Our understanding of the interaction between light and matter also has allowed for the development of the atomic clock. The idea was proposed in 1945 by Rabi [4, 72], and by 1955, an atomic clock based on a microwave transition in Cesium was built [29, 28, 30], which surpassed in

accuracy and precision, the best quartz based clocks of the day [20, 47]. This led in 1967 to the redefinition of the second, in terms of the frequency between two atomic levels in Cesium [72].

Since then, atomic clocks have increased in accuracy and precision by about an order of magnitude every decade [46], and a vast number of new technologies, including GPS, have followed. GPS is a space-based system that uses multiple synchronized atomic clocks to provide time and location information anywhere on Earth, and it has revolutionized navigation in all aspects of our society.

Recently, a new generation of atomic clocks based on optical transitions has been created [83, 41, 44, 8]. These new optical atomic clocks were made possible by the new techniques of trapping and cooling of atoms with lasers, and by the invention of the optical frequency comb. An optical frequency comb is a pulsed laser that acts like reduction gears in the frequency domain, allowing optical frequencies to be geared down to measurable microwave frequencies. Optical atomic clocks have now surpassed the cesium standard in precision and accuracy by orders of magnitude, and still are becoming even more precise and accurate [8]. In addition to "being another solution looking for a problem", more precise and accurate clocks could be used to detect potential slow changes to the fundamental constants of nature [7], or to confirm the existence of gravitational waves predicted in Einstein's general theory of relativity [6].

Currently, the precision and accuracy of these optical clocks are limited by the linewidth of the laser used to interrogate the atoms through the Dick effect [18, 71]. Here, the cyclical operation of these clocks causes an aliasing effect that translates the interrogation laser's phase noise into the feedback control loop that keeps the laser on the atomic resonance. The noise in the interrogation laser is a bottleneck which limits the achievement of better precision and accuracy, and a narrower linewidth interrogation laser is needed to increase the precision and accuracy of these clocks.

Much effort has already been invested in making a narrow linewidth interrogation laser. The current state-of-the-art is to send laser light into an ultra-stable reference cavity to reduce the laser's linewidth [42, 23, 91, 51, 50]. This method has made for orders of magnitude reduction in interrogation laser linewidth, but it is limited in further reducing this linewidth by the cavity

length fluctuations due to the thermal vibrations of the cavity mirrors. Even when using these cavity stabilized lasers, optical clocks still suffer from the Dick effect, so that further reducing the linewidth of the interrogation laser would directly allow more accurate and precise clocks. Reduction of a laser's linewidth by this method, past the current state of the art, is very difficult.

Because of this difficulty, alternative methods of producing a narrow linewidth laser have been considered. It was proposed, that in addition to a laser, coherent light can be produced in an atom-cavity system that is operated in an exotic parameter regime. In this regime, the cavity decay rate is much larger than the collective atomic decay rate, which is smaller than the decay rate of independent atoms [66, 65, 64]. In this so called "bad cavity" or superradiance regime, the linewidth can actually be smaller than the atomic transition itself, due to collective effects. In fact, this light could be used directly as the frequency measure for a clock, circumventing the need for an interrogation laser all together [13]. This type of coherent light source has been explored only in the extreme superradiance limit, and the crossover between superradiance and the more familiar lasing limit has only recently been explored [81].

Another proposed method of producing a narrow linewidth laser is to place atoms with an extremely narrow transition inside an optical cavity, and to stabilize a laser to an atomic transition, instead of to an empty cavity resonance [63]. Such a system, which again lies in the bad cavity, or superradiance parameter regime, is insensitive to thermal cavity length fluctuations, and therefore circumnavigates the main bottleneck of further reducing the linewidth of empty reference cavity systems. An experimental effort to realize such a system has been made [86], but in contrast to the original proposal [63], the atoms had a non-negligible velocity, making Doppler effects important. Still, it was shown theoretically how these systems could be optimized to allow for linewidths comparable, or even narrower, than the state of the art reference cavity systems [80].

In this thesis, we will explore in detail the topic of the crossover theory from lasing to superradiance, and demonstrate the potential for a crossover system to be used in precision measurement applications [81]. We will also explore the theory of the stabilization of a laser to narrow linewidth atoms inside a cavity, including the effects due to atomic motion [86, 80, 15].

Before these topics are explored, the background material necessary for their understanding will be discussed. Specifically, these aforementioned systems are inherently open, meaning that they are able to lose and gain energy. Therefore, the equations that describe open quantum systems will be derived. Exact solution methods to these equations will be discussed. However, these methods are only able to describe small systems, with ~ 10 atoms. A solution method does exist which exploits an underlying symmetry in the derived equations, and therefore drastically reduces complexity, allowing for larger systems to be analyzed [90]. Still, this method is limited to systems having ~ 100 atoms, and therefore cannot be used to directly describe many realistic experiments, which can have $\sim 10^5$ or more atoms. To describe these larger experimental systems, approximate solution methods must be used. Therefore, we discuss several approximate solution methods. In addition to their ability to describe the specific systems previously mentioned, these approximate solution methods are able to capture the essential physical phenomenon in a wide class of devices, including the synchronization between two different ensembles of atoms [89].

1.2   Overview

In Chapter 2, the quantization of the electromagnetic field will be discussed. This will prove necessary in order to correctly describe the Hamiltonian dynamics of our open quantum systems when few photons are present. Also, it will be necessary in order to describe spontaneous irreversible processes, such spontaneous emission. The power spectrum, and its relation to two-time correlation functions will also be discussed. This will allow the spectral properties of a system, such as the linewidth of the power spectrum, to be calculated.

In Chapter 3, the equation for open quantum systems in the Schrödinger picture of quantum mechanics, known as the master equation, will be derived. Exact solution methods to the master equation, such as the quantum jump and quantum state diffusion methods, will be discussed. In addition, computer simulations of these methods are demonstrated. The cumulant expansion method, which yields an approximate set of coupled equations for expectation values of system observables, is then discussed.

Chapter 4 will begin by deriving the quantum Langevin equations, which describe open quantum systems in the Heisenberg picture of quantum mechanics. Although these equations can prove useful for some analytical work, for computer simulations, they are very difficult to work with. Therefore the Fokker-Planck equation for a quazi-probability distribution describing the system, and its equivalent set of c-number (complex number) Langevin equations will be discussed. These c-number Langevin equations can be simulated on a computer with relative ease. Once this proof-of-principle procedure for deriving the c-number Langevin equations is shown, a more practical way to derive c-number Langevin equations is given. This new procedure becomes more and more advantageous as system complexity increases. Computer simulations of the c-number Langevin equations for several systems will be demonstrated.

Chapter 5 will use several of the methods of the previous chapters to present the theory of the crossover between lasing and steady state superradiance. Although lasing and steady state super-radiance seem to be disjoint phenomena, it will be shown that they should actually be thought of as the extreme limits of a single and more general phenomenon. In a laser, the phase information that allows for coherence is stored in the light field. In steady state superradiance, the phase information that allows for coherence is stored in the atomic ensemble. In the in-between parameter region, or crossover region, phase information that allows for coherence can be stored in the light field and the atomic ensemble simultaneously. The properties of systems that lie in the superradiance, lasing and crossover parameter regions will be compared.

The rate at which energy is re-supplied to a typical laser allows the system to operate just above the lasing threshold. It will be seen that a crossover system operating at this same rate of re-supplying energy will be much farther above threshold, which can allow the linewidth of the power spectrum to be orders of magnitude smaller than the laser. Such a system also exhibits a much larger intracavity intensity than a superradiant system, so that the crossover system is more experimentally accessible. The linewidth and intracavity intensity will then be shown to be insensitive to atomic dephasing in all parameter regions, so long as the rate of atomic dephasing is smaller than the rate of energy being resupplied to the system.

It will also be demonstrated that a system in the superradiance region is insensitive to fluctuations in cavity frequency, while a system in the lasing region is insensitive to fluctuations in the atomic frequency. A crossover system is less sensitive to fluctuations in cavity frequency than a laser system, and less sensitive to fluctuations in atomic frequency than a superradiant system. This is important, since fluctuations in cavity length are the cause of the current limit on the further reduction of the linewidth in today's best ultrastable lasers.

In Chapter 6, we will consider the phase stability of a local oscillator (or laser) locked to a cavity QED (Quantum Electrodynamics) system comprised of atoms with an ultra-narrow optical transition. The atoms will be modeled as being cooled to millikelvin temperatures and then released into the optical cavity. Although the atomic motion introduces Doppler broadening, the standing wave nature of the cavity causes saturated absorption features to appear, which are much narrower than the Doppler width. These features can be used to achieve an extremely high degree of phase stabilization, competitive with the current state-of-the-art. A comparison between the developed theory, and the results of an experiment on the system that we consider will be given. Finally, it will be seen that the inhomogeneity introduced by finite atomic velocities can cause optical bistability to disappear, resulting in no regions of dynamic instability and thus enabling a new regime accessible to experiments where optimum stabilization may be achieved.

Finally, chapter 7 will give a conclusion of the presented material.

Chapter 2

Preliminaries

The equations that describe open quantum systems are comprised of both coherent Hamiltonian dynamics, and incoherent dynamics. In the systems that we will consider, the Hamiltonian parts will describe atoms interacting reversibly with an electromagnetic field, meaning that energy is transferred between the two, but is not lost to an external environment. If there are only a few photons present in the field, a quantized electromagnetic field will be necessary for an accurate description. A quantized electromagnetic field will also be required to describe the incoherent parts of the systems, in which energy is lost to an external environment. These parts are derived by coupling the system to a continuum of quantized electromagnetic field modes in vacuum.

In addition, the spectral properties of the light produced by a system will be of interest to us. This aspect concerns the Wiener-Khinchin theorem. This theorem relates the power spectrum to a two-time correlation function of field variables. In many cases the two-time correlation function can be obtained with relative ease.

2.1   Quantization of the Electromagnetic Field

We begin by formulating the quantized theory of the electromagnetic radiation and demonstrating the discrete photon excitations that this implies. Maxwell's equations in vacuum and

without sources are,

$$\nabla \cdot \mathbf{E}(\mathbf{r}, t) = 0 \tag{2.1}$$

$$\nabla \cdot \mathbf{B}(\mathbf{r}, t) = 0 \tag{2.2}$$

$$\nabla \times \mathbf{E}(\mathbf{r}, t) = -\frac{\partial \mathbf{B}(\mathbf{r}, t)}{\partial t} \tag{2.3}$$

$$\nabla \times \mathbf{B}(\mathbf{r}, t) = \mu_0 \epsilon_0 \frac{\partial \mathbf{E}(\mathbf{r}, t)}{\partial t}. \tag{2.4}$$

Eq. 2.2 allows $\mathbf{B}(\mathbf{r}, t)$ to be written as the curl of a vector potential $\mathbf{A}(\mathbf{r}, t)$,

$$\mathbf{B}(\mathbf{r}, t) = \nabla \times \mathbf{A}(\mathbf{r}, t). \tag{2.5}$$

In the Coulomb gauge, where $\nabla \cdot \mathbf{A}(\mathbf{r}, t) = 0$, $\mathbf{E}(\mathbf{r}, t)$ can be written as,

$$\mathbf{E}(\mathbf{r}, t) = -\frac{d\mathbf{A}(\mathbf{r}, t)}{dt}. \tag{2.6}$$

Substituting Eqns. 2.5 and 2.6 in Eq. 2.4 yields,

$$\nabla^2 \mathbf{A}(\mathbf{r}, t) = \mu_0 \epsilon_0 \frac{\partial^2 \mathbf{A}(\mathbf{r}, t)}{\partial t^2}. \tag{2.7}$$

The general solution to Eq. 2.7 inside a cubical volume of side length L, with boundary conditions corresponding to standing wave modes is,

$$\mathbf{A}(\mathbf{r}, t) = \sum_{\mathbf{k}} \left(A_{\mathbf{k}} \mathbf{u}_{\mathbf{k}}(\mathbf{r}) e^{-\imath \omega_k t} + A_{\mathbf{k}}^* \mathbf{u}_{\mathbf{k}}^*(\mathbf{r}) e^{\imath \omega_k t} \right), \tag{2.8}$$

where,

$$\mathbf{k} = \frac{2\pi}{L} \mathbf{n} \quad , \quad \mathbf{n} = (n_x, n_y, n_z) \quad , \quad n_i = 0, \pm 1, \pm 2, \pm \ldots, \tag{2.9}$$

and,

$$\omega_k = c \left| \mathbf{k} \right|. \tag{2.10}$$

The mode functions $\mathbf{u}_{\mathbf{k}}(\mathbf{r})$ are given by,

$$\mathbf{u}_{\mathbf{k}}(\mathbf{r}) = \left(\frac{2}{L} \right)^{3/2} \sin(\mathbf{k} \cdot \mathbf{r}) \mathbf{e}_{\mathbf{k}}, \tag{2.11}$$

where $\mathbf{e_k}$ is a unit polarization vector orthogonal to $\mathbf{k}$. These mode functions satisfy,

$$\nabla^2 \mathbf{u_k}(\mathbf{r}) = -\frac{\omega_k^2}{c^2} \mathbf{u_k}(\mathbf{r}), \tag{2.12}$$

where $c = 1/\sqrt{\mu_0 \epsilon_0}$ is the speed of light in a vacuum. Also, they form a complete orthonormal basis, i.e.,

$$\int_V \mathbf{u_k^*}(\mathbf{r}) \mathbf{u_{k'}}(\mathbf{r}) d\mathbf{r} = \delta_{\mathbf{kk'}}, \tag{2.13}$$

where the integral is over the cubical volume V, and $\delta_{\mathbf{kk'}}$ is the Kronecker delta. Note that for simplicity we have neglected the discrete polarization index, but that can be accounted for by letting the index $\mathbf{k} \to \mathbf{k}\lambda$ and also summing over λ, the discrete polarization index.

The energy H stored in the electromagnetic field is

$$H = \frac{1}{2} \int dV \left[\epsilon_0 \left(\mathbf{E}(\mathbf{r}, t) \cdot \mathbf{E}(\mathbf{r}, t) \right) + \frac{1}{\mu_0} \left(\mathbf{B}(\mathbf{r}, t) \cdot \mathbf{B}(\mathbf{r}, t) \right) \right]. \tag{2.14}$$

From Eqns. 2.5 and 2.6, $\mathbf{E}(\mathbf{r}, t)$ and $\mathbf{B}(\mathbf{r}, t)$ are therefore given by,

$$\mathbf{E}(\mathbf{r}, t) = i \sum_{\mathbf{k}} \omega_k \left(A_{\mathbf{k}} \mathbf{u_k}(\mathbf{r}) e^{-i\omega_k t} - A_{\mathbf{k}}^* \mathbf{u_k^*}(\mathbf{r}) e^{i\omega_k t} \right), \tag{2.15}$$

$$\mathbf{B}(\mathbf{r}, t) = \sum_{\mathbf{k}} \left(A_{\mathbf{k}} (\boldsymbol{\nabla} \times \mathbf{u_k}(\mathbf{r})) e^{-i\omega_k t} + A_{\mathbf{k}}^* (\boldsymbol{\nabla} \times \mathbf{u_k^*}(\mathbf{r})) e^{i\omega_k t} \right). \tag{2.16}$$

Eqns. 2.15 and 2.16 may be substituted into Eq. 2.14, and after evaluating the integrals using Eq. 2.13, Eq. 2.14 becomes,

$$H = \sum_{\mathbf{k}} H_{\mathbf{k}}, \tag{2.17}$$

where

$$H_{\mathbf{k}} = \epsilon_0 V \omega_k^2 \left(A_{\mathbf{k}} A_{\mathbf{k}}^* + A_{\mathbf{k}}^* A_{\mathbf{k}} \right). \tag{2.18}$$

After defining the variables $q_{\mathbf{k}}$ and $p_{\mathbf{k}}$ as,

$$A_{\mathbf{k}} = \frac{1}{2\omega_k \sqrt{\epsilon_0 V}} (\omega_k q_{\mathbf{k}} + i p_{\mathbf{k}})$$

$$A_{\mathbf{k}}^* = \frac{1}{2\omega_k \sqrt{\epsilon_0 V}} (\omega_k q_{\mathbf{k}} - i p_{\mathbf{k}}), \tag{2.19}$$

Eq. 2.18 becomes,

$$H_{\mathbf{k}} = \frac{1}{2} (p_{\mathbf{k}} + \omega_k^2 q_{\mathbf{k}}). \tag{2.20}$$

This Hamiltonian has the form as a harmonic oscillator with position $q_{\mathbf{k}}$ and its conjugate momentum $p_{\mathbf{k}}$, with unit mass. Thus each mode of the electromagnetic field can be formally mapped into a harmonic oscillator degree of freedom.

The quantization procedure is now preformed in the typical way of quantum mechanics by demanding that the variables $q_{\mathbf{k}}$ and $p_{\mathbf{k}}$ become quantum mechanical operators,

$$q_{\mathbf{k}} \to \hat{q}_{\mathbf{k}} \ , \ p_{\mathbf{k}} \to \hat{p}_{\mathbf{k}}, \tag{2.21}$$

that obey the commutation relations,

$$[\hat{q}_{\mathbf{k}}, \hat{p}_{\mathbf{k}}] = \imath \hbar \delta_{\mathbf{k}, \mathbf{k}'}. \tag{2.22}$$

Then, Eq. 2.20 becomes the Hamiltonian for the quantum harmonic oscillator,

$$\hat{H}_{\mathbf{k}} = \frac{1}{2}(\hat{p}_{\mathbf{k}} + \omega_k^2 \hat{q}_{\mathbf{k}}). \tag{2.23}$$

This quantization procedure turns each variable $H_{\mathbf{k}}$ into an operator $\hat{H}_{\mathbf{k}}$ that acts on an infinite dimension Hilbert space. Therefore, the total Hamiltonian $\hat{H}$ is a sum over each one of these Hilbert spaces with each individual space corresponding to a mode of the electromagnetic field. Formally, to sum over Hilbert spaces means to construct the following:

$$\begin{aligned} \hat{H} \ = \ & \hat{H}_{\mathbf{k}_1} \otimes \hat{\mathbb{1}} \otimes \hat{\mathbb{1}} \otimes \hat{\mathbb{1}} \otimes \cdots \\ & + \hat{\mathbb{1}} \otimes \hat{H}_{\mathbf{k}_1} \otimes \hat{\mathbb{1}} \otimes \hat{\mathbb{1}} \otimes \cdots \\ & + \cdots, \end{aligned} \tag{2.24}$$

where $\hat{\mathbb{1}}$ is the identity operator on each Hilbert space. With this implied meaning, Eq. 2.24 is written simply as,

$$\hat{H} = \sum_{\mathbf{k}} \hat{H}_{\mathbf{k}}. \tag{2.25}$$

It is convenient to work with annihilation operators $\hat{a}_{\mathbf{k}}$ and creation operators $\hat{a}_{\mathbf{k}}^{\dagger}$ which are dimensionless and defined by,

$$\begin{aligned} \hat{a}_{\mathbf{k}} \ &= \ \frac{1}{\sqrt{2\hbar\omega_k}}(\omega_k \hat{q}_{\mathbf{k}} + \imath \hat{p}_{\mathbf{k}}), \\ \hat{a}_{\mathbf{k}}^{\dagger} \ &= \ \frac{1}{\sqrt{2\hbar\omega_k}}(\omega_k \hat{q}_{\mathbf{k}} - \imath \hat{p}_{\mathbf{k}}), \end{aligned} \tag{2.26}$$

where the commutation relations for $\hat{a}_{\mathbf{k}}$ and $\hat{a}_{\mathbf{k}}^{\dagger}$ follow from Eq. 2.22, and are given by,

$$\left[\hat{a}_{\mathbf{k}}, \hat{a}_{\mathbf{k}}^{\dagger}\right] = \delta_{\mathbf{k},\mathbf{k}'}. \tag{2.27}$$

The Hamiltonian for each mode indexed by different values of $\mathbf{k}$ can now be written as,

$$\hat{H}_{\mathbf{k}} = \frac{1}{2}\hbar\omega_k \left(\hat{a}_{\mathbf{k}}\hat{a}_{\mathbf{k}}^{\dagger} + \hat{a}_{\mathbf{k}}^{\dagger}\hat{a}_{\mathbf{k}}\right), \tag{2.28}$$

or by using Eq. 2.27,

$$\hat{H}_{\mathbf{k}} = \hbar\omega_k \left(\hat{a}_{\mathbf{k}}^{\dagger}\hat{a}_{\mathbf{k}} + \frac{1}{2}\right). \tag{2.29}$$

The eigenbasis of Eq. 2.29 are the quantum harmonic oscillator number states, which obey,

$$\hat{a}_{\mathbf{k}}|n\rangle_{\mathbf{k}} = \sqrt{n}|n-1\rangle_{\mathbf{k}}$$
$$\hat{a}_{\mathbf{k}}^{\dagger}|n\rangle_{\mathbf{k}} = \sqrt{n+1}|n+1\rangle_{\mathbf{k}}. \tag{2.30}$$

with $\hat{a}_{\mathbf{k}}|n\rangle_{\mathbf{k}} = 0$ and integer $n \geq 0$. It is now obvious that the above quantization procedure is equivalent to letting,

$$A_{\mathbf{k}} \rightarrow \sqrt{\frac{\hbar}{2\omega_k\epsilon_0 V}}\hat{a}_{\mathbf{k}} \ , \ A_{\mathbf{k}}^* \rightarrow \sqrt{\frac{\hbar}{2\omega_k\epsilon_0 V}}\hat{a}_{\mathbf{k}}^{\dagger}. \tag{2.31}$$

Therefore, the electric and magnetic field operators, $\hat{\mathbf{E}}(\mathbf{r},t)$ and $\hat{\mathbf{B}}(\mathbf{r},t)$ are given by,

$$\hat{\mathbf{E}}(\mathbf{r},t) = \imath\sum_{\mathbf{k}}\sqrt{\frac{\hbar\omega_k}{2\epsilon_0}}\left(\hat{a}_{\mathbf{k}}\mathbf{u}_{\mathbf{k}}(\mathbf{r})e^{-\imath\omega_k t} - \hat{a}_{\mathbf{k}}^{\dagger}\mathbf{u}_{\mathbf{k}}^*(\mathbf{r})e^{\imath\omega_k t}\right), \tag{2.32}$$

$$\hat{\mathbf{B}}(\mathbf{r},t) = \sum_{\mathbf{k}}\sqrt{\frac{\hbar}{2\omega_k\epsilon_0}}\left(\hat{a}_{\mathbf{k}}(\boldsymbol{\nabla}\times\mathbf{u}_{\mathbf{k}}(\mathbf{r}))e^{-\imath\omega_k t} + \hat{a}_{\mathbf{k}}^{\dagger}(\boldsymbol{\nabla}\times\mathbf{u}_{\mathbf{k}}^*(\mathbf{r}))e^{\imath\omega_k t}\right). \tag{2.33}$$

Eqns. 2.32 and 2.33 are operators in the Heisenberg picture, since they contain the explicit time dependence. Specifically, they include the time dependence of the free evolution of the field under Eq. 2.25. This can be seen by considering the frame transformation,

$$e^{\frac{\imath}{\hbar}\hat{H}t}\hat{a}_{\mathbf{k}}e^{-\frac{\imath}{\hbar}\hat{H}t} = \hat{a}_{\mathbf{k}}e^{-\imath\omega_k t}$$
$$e^{\frac{\imath}{\hbar}\hat{H}t}\hat{a}_{\mathbf{k}}^{\dagger}e^{-\frac{\imath}{\hbar}\hat{H}t} = \hat{a}_{\mathbf{k}}^{\dagger}e^{\imath\omega_k t}. \tag{2.34}$$

Therefore, in the Schrödinger picture the fields may be written as,

$$\hat{\mathbf{E}}(\mathbf{r}, t) = i \sum_{\mathbf{k}} \sqrt{\frac{\hbar \omega_k}{2 \epsilon_0}} \left(\hat{a}_{\mathbf{k}} \mathbf{u}_{\mathbf{k}}(\mathbf{r}) - \hat{a}_{\mathbf{k}}^\dagger \mathbf{u}_{\mathbf{k}}^*(\mathbf{r}) \right), \tag{2.35}$$

$$\hat{\mathbf{B}}(\mathbf{r}, t) = \sum_{\mathbf{k}} \sqrt{\frac{\hbar}{2 \omega_k \epsilon_0}} \left(\hat{a}_{\mathbf{k}} (\boldsymbol{\nabla} \times \mathbf{u}_{\mathbf{k}}(\mathbf{r})) + \hat{a}_{\mathbf{k}}^\dagger (\boldsymbol{\nabla} \times \mathbf{u}_{\mathbf{k}}^*(\mathbf{r})) \right). \tag{2.36}$$

For a single mode cavity field of frequency $\omega_c = ck$, oriented in the z direction satisfying standing wave boundary conditions, Eq. 2.11 becomes,

$$u(z) = \sqrt{\frac{2}{V}} \sin(kz), \tag{2.37}$$

where V is the volume of the cavity. Since we will be mainly focused on the properties of $\hat{\mathbf{E}}(z, t)$ rather than $\hat{\mathbf{B}}(z, t)$, it will be convenient to us to put $\hat{\mathbf{E}}(z, t)$ in its simplest form. We therefore let $\hat{a} \to -i\hat{a}$ in the expressions for $\hat{\mathbf{E}}(z, t)$ and $\hat{\mathbf{B}}(z, t)$. Then, for the case of linear polarization in the $\mathbf{x}$ direction, Eqns. 2.32 and 2.33 become,

$$\hat{\mathbf{E}}(z, t) = \sqrt{\frac{\hbar \omega_c}{V \epsilon_0}} \left(\hat{a} e^{-i\omega_c t} + \hat{a}^\dagger e^{i\omega_c t} \right) \sin(kz) \frac{\mathbf{x}}{|\mathbf{x}|} \tag{2.38}$$

$$\hat{\mathbf{B}}(z, t) = -i \sqrt{\frac{\hbar \omega_c \mu_0}{V}} \left(\hat{a} e^{-i\omega_c t} - \hat{a}^\dagger e^{i\omega_c t} \right) \cos(kz) \frac{\mathbf{y}}{|\mathbf{y}|}, \tag{2.39}$$

where $\frac{\mathbf{x}}{|\mathbf{x}|}$ and $\frac{\mathbf{y}}{|\mathbf{y}|}$ are unit vectors in the direction $\mathbf{x}$ and $\mathbf{y}$ directions, and the fact that $c = 1/\sqrt{\mu_0 \epsilon_0}$ has been used. The Hamiltonian $\hat{H}$ for a single mode cavity field is,

$$\hat{H}_c = \hbar \omega_c \left(\hat{a}^\dagger \hat{a} + \frac{1}{2} \right). \tag{2.40}$$

Since the zero energy definition is arbitrary, the factor of $\hbar \omega_c / 2$ can be dropped from Eq. 2.40 without loss of generality, resulting in,

$$\hat{H}_c = \hbar \omega_c \hat{a}^\dagger \hat{a}. \tag{2.41}$$

In the Schrödinger picture, where the time dependence of $\hat{H}_c$ will appear on to the state vector of the system under consideration, instead of on $\hat{a}$, Eqns. 2.38 and 2.39 are,

$$\hat{\mathbf{E}}(z, t) = \sqrt{\frac{\hbar \omega_c}{V \epsilon_0}} \left(\hat{a} + \hat{a}^\dagger \right) \sin(kz) \frac{\mathbf{x}}{|\mathbf{x}|} \tag{2.42}$$

$$\hat{\mathbf{B}}(z, t) = -i \sqrt{\frac{\hbar \omega_c \mu_0}{V}} \left(\hat{a} - \hat{a}^\dagger \right) \cos(kz) \frac{\mathbf{y}}{|\mathbf{y}|}. \tag{2.43}$$

2.2   Jaynes Cummings Model

The Jaynes Cummings model describes a single two level atom interacting with a single quantized cavity field mode. Besides being a prototypical cavity QED system, it is used to describe the Hamiltonian part of the open quantum system that will later be considered. We will find that, in the Jaynes Cummings model, the atom oscillates between its excited and ground states, similar to the case where the cavity field is treated classically. However, it differs from the classical case, since these oscillations can occur even when there are no photons present. Although these oscillations are reversible, this model provides good motivation for describing the irreversible spontaneous processes such as spontaneous emission, which are caused by the coupling of a system to the many modes of the electromagnetic field in vacuum.

2.2.1   Jaynes Cummings Hamiltonian

The Hamiltonian describing the free evolution of a two level atom is given by,

$$\hat{H}_a = \frac{\hbar\omega_a}{2}\left(|e\rangle\langle e| - |g\rangle\langle g|\right), \tag{2.44}$$

where $|e\rangle$ and $|g\rangle$ are the excited and ground states of the atom, which form an orthonormal basis, and where $\hbar\omega_a$ is the energy difference between the two levels.

The energy of an atom with dipole moment operator $\hat{\mathbf{d}}$ interacting with a single mode electromagnetic field in a cavity $\hat{\mathbf{E}}(\mathbf{R}, t)$ is described by,

$$\hat{H}_I = -\hat{\mathbf{d}} \cdot \hat{\mathbf{E}}(\mathbf{R}, t), \tag{2.45}$$

where $\mathbf{R}$ is the position of the center of mass of the atom. It is valid to evaluate the electric field $\hat{\mathbf{E}}(\mathbf{R}, t)$ at $\mathbf{R}$ since we are interested in electromagnetic fields with wavelengths much larger than atomic dimensions. Therefore, in this approximation, known as the dipole approximation, the electric field is treated as constant over the dimensions of an atom. After inserting the identity

operator $\hat{\mathbb{1}} = (|e\rangle \langle e| + |g\rangle \langle g|)$ on both sides of $\hat{\mathbf{d}}$ in Eq. 2.45, it becomes,

$$
\begin{aligned}
\hat{H}_I &= -(|e\rangle \langle e| + |g\rangle \langle g|)\, \hat{\mathbf{d}}\, (|e\rangle \langle e| + |g\rangle \langle g|) \cdot \hat{\mathbf{E}}(\mathbf{R}, t) \\
&= -\left(\langle e| \hat{\mathbf{d}} |g\rangle |e\rangle \langle g| + \langle g| \hat{\mathbf{d}} |e\rangle |g\rangle \langle e| \right) \cdot \hat{\mathbf{E}}(\mathbf{R}, t),
\end{aligned}
\tag{2.46}
$$

where $\langle e| \hat{\mathbf{d}} |e\rangle = \langle g| \hat{\mathbf{d}} |g\rangle = 0$. This is because under transformation by the parity operator $\hat{\Pi}$, the dipole operator becomes $\hat{\Pi}^\dagger \hat{\mathbf{d}} \hat{\Pi} = -\hat{\mathbf{d}}$, and since $\hat{\Pi} |e\rangle = -|e\rangle$ and $\hat{\Pi} |g\rangle = -|g\rangle$, it follows that $\langle e| \hat{\mathbf{d}} |e\rangle = -\langle e| \hat{\mathbf{d}} |e\rangle = \langle g| \hat{\mathbf{d}} |g\rangle = -\langle g| \hat{\mathbf{d}} |g\rangle = 0$. After substituting Eq. 2.38, Eq. 2.46 becomes,

$$
\hat{H}_I = \hbar g \left(|e\rangle \langle g| + |g\rangle \langle e|\right) \left(\hat{a} e^{-\imath \omega_c t} + \hat{a}^\dagger e^{\imath \omega_c t} \right).
\tag{2.47}
$$

Here, the coupling rate g between the atom and field is given by,

$$
g \equiv -\sqrt{\frac{\omega_c}{\hbar V \epsilon_0}} \sin(k z_0) \langle e| \hat{\mathbf{d}} \cdot \frac{\mathbf{x}}{|\mathbf{x}|} |g\rangle,
\tag{2.48}
$$

where z_0 is the position of the center of mass of the atom.

2.2.2   The Rotating Wave Approximation

We move into an interaction picture that puts the time dependence of the free evolution of the atom on the atomic operators, defined by,

$$
\begin{aligned}
\widetilde{|e\rangle \langle g|} &\equiv e^{\frac{\imath}{\hbar} \hat{H}_a t} |e\rangle \langle g| e^{-\frac{\imath}{\hbar} \hat{H}_a t} = |e\rangle \langle g| e^{-\imath \omega_a t} \\
\widetilde{|g\rangle \langle e|} &\equiv e^{\frac{\imath}{\hbar} \hat{H}_a t} |g\rangle \langle e| e^{-\frac{\imath}{\hbar} \hat{H}_a t} = |g\rangle \langle e| e^{\imath \omega_a t},
\end{aligned}
\tag{2.49}
$$

where the tilde over the operators indicates that they are in an interaction picture. After substitution of Eqns. 2.49, Eq. 2.47 becomes,

$$
\begin{aligned}
\hat{H}_I &= \hbar g \left(\widetilde{|e\rangle \langle g|} e^{\imath \omega_a t} + \widetilde{|g\rangle \langle e|} e^{-\imath \omega_a t} \right) \left(\hat{a} e^{-\imath \omega_c t} + \hat{a}^\dagger e^{\imath \omega_c t} \right) \\
&= \hbar g \Big(\hat{a} \widetilde{|e\rangle \langle g|} e^{\imath (\omega_a - \omega_c) t} + \hat{a}^\dagger \widetilde{|e\rangle \langle g|} e^{\imath (\omega_a + \omega_c) t} \\
&\quad + \hat{a} \widetilde{|g\rangle \langle e|} e^{-\imath (\omega_a + \omega_c) t} + \hat{a}^\dagger \widetilde{|g\rangle \langle e|} e^{-\imath (\omega_a - \omega_c) t} \Big).
\end{aligned}
\tag{2.50}
$$

Close to resonance, i.e. when $\omega_c \approx \omega_a$, terms with $\omega_a + \omega_c$ in the exponential oscillate much more rapidly than terms with $\omega_a - \omega_c$ in the exponential. These fast oscillating terms average to zero on

a time scale that is much faster than the time in which the slowly oscillating terms would average to zero, and therefore the fast oscillating terms can be dropped. In this approximation, called the rotating wave approximation, Eq 2.50 becomes,

$$\hat{H}_I \quad = \quad \hbar g \left(\hat{a} \widetilde{|e\rangle \langle g|} e^{i(\omega_a - \omega_c)t} + \hat{a}^\dagger \widetilde{|g\rangle \langle e|} e^{-i(\omega_a - \omega_c)t} \right). \tag{2.51}$$

Moving back to the Schrödinger picture, where the time dependence due to Eq. 2.40 is not on the operator $\hat{a}$ and the time dependence due to Eq. 2.44 is not on the operator $|g\rangle \langle e|$, we have,

$$\hat{H}_I \quad = \quad \hbar g \left(\hat{a} \, |e\rangle \langle g| + \hat{a}^\dagger \, |g\rangle \langle e| \right). \tag{2.52}$$

Adding together the Eqns. 2.41, 2.44 and 2.51, we arrive at the Jaynes-Cummings Hamiltonian,

$$\hat{H}_{JC} \quad = \quad \hbar \omega_c \hat{a}^\dagger \hat{a} + \frac{\hbar \omega_a}{2} \left(|e\rangle \langle e| - |g\rangle \langle g| \right) + \hbar g \left(\hat{a} \, |e\rangle \langle g| + \hat{a}^\dagger \, |g\rangle \langle e| \right). \tag{2.53}$$

2.2.3   Rabi Flopping

The Schrödinger equation with Eq. 2.53 as the Hamiltonian,

$$i\hbar \frac{d}{dt} |\psi(t)\rangle = \hat{H}_{JC} |\psi(t)\rangle , \tag{2.54}$$

can be solved by first noting that Eq. 2.53 only couples the state $|e\rangle |n\rangle$, where the atom is in the excited state and the field has n excitations, to the state $|g\rangle |n + 1\rangle$, where the atom is in the ground state and the field has $n+1$ excitations. Therefore, $\hat{H}_{JC}$ can be split up into independent two-state manifolds, which can be described by the basis $\{ |e\rangle |n\rangle , |g\rangle |n + 1\rangle \}$. The manifold of Eq. 2.53 with n excitations may be represented as the 2×2 matrix in the reduced subspace,

$$\hat{H}_{JC} \dot{=} \hbar \begin{pmatrix} \left(\frac{1}{2}\omega_a + n\omega_c \right) & g\sqrt{n + 1} \\ g\sqrt{n + 1} & \left(-\frac{1}{2}\omega_a + (n+1)\omega_c \right). \end{pmatrix} \tag{2.55}$$

The time dependent state vector $|\psi(t)\rangle$ of the system is given by solving the Schrödinger equation with this Hamiltonian,

$$|\psi(t)\rangle = c_1(t) \, |e\rangle |n\rangle + c_2(t) \, |g\rangle |n + 1\rangle , \tag{2.56}$$

where $c_1(t) = (\langle e | \langle n |) | \psi(t) \rangle$ and $c_2(t) = (\langle g | \langle n+1 |) | \psi(t) \rangle$. Projecting Eq. 2.56 on to $| e \rangle | n \rangle$ and $| g \rangle | n+1 \rangle$, and using Eq. 2.54, yields,

$$
\begin{aligned}
\imath \frac{d}{dt} c_1(t) &= \left(\frac{1}{2} \omega_a + n \omega_c \right) c_1(t) + g \sqrt{n+1} c_2(t) \\
\imath \frac{d}{dt} c_2(t) &= \left(-\frac{1}{2} \omega_a + (n+1) \omega_c \right) c_2(t) + g \sqrt{n+1} c_1(t).
\end{aligned}
\tag{2.57}
$$

We now assume exact resonance, $\omega_a = \omega_c$, and define an interaction picture as,

$$
\tilde{c}_1(t) = e^{\imath \omega_c (n+1/2) t} c_1(t) \qquad \tilde{c}_2(t) = e^{\imath \omega_c (n+1/2) t} c_2(t).
\tag{2.58}
$$

In this interaction picture, Eqns. 2.57 become,

$$
\begin{aligned}
\frac{d}{dt} \tilde{c}_1(t) &= -\imath g \sqrt{n+1} \tilde{c}_2(t) \\
\frac{d}{dt} \tilde{c}_2(t) &= -\imath g \sqrt{n+1} \tilde{c}_1(t)
\end{aligned}
\tag{2.59}
$$

The solutions to Eqns. 2.59 with initial conditions $c_1(0) = 1$ and $c_2(0) = 0$ are,

$$
\begin{aligned}
\tilde{c}_1(t) &= \cos(g \sqrt{n+1} t) \\
\tilde{c}_2(t) &= -\imath \sin(g \sqrt{n+1} t),
\end{aligned}
\tag{2.60}
$$

so that the probability of the system being in the excited and ground states, respectively, are,

$$
\begin{aligned}
|\tilde{c}_1(t)|^2 &= \cos^2(g \sqrt{n+1} t) \\
|\tilde{c}_2(t)|^2 &= \sin^2(g \sqrt{n+1} t).
\end{aligned}
\tag{2.61}
$$

Eqns. 2.61 tell us that the dynamics of the system is to oscillate, or flop, between the excited and ground state with Rabi frequency $g \sqrt{n+1}$. It is interesting to note that even when there are initially no excitations in the field i.e. $n = 0$ to stimulate an excited atom to emit its photon, the system will exhibit Rabi flopping. Although the expectation value of the electromagnetic field in the vacuum state $| 0 \rangle$ is zero,

$$
\begin{aligned}
\langle 0 | \hat{\mathbf{E}}(z, t) | 0 \rangle &= \sqrt{\frac{\hbar \omega_c}{V \epsilon_0}} \langle 0 | \left(\hat{a} + \hat{a}^\dagger \right) | 0 \rangle \sin(kz) \frac{\mathbf{x}}{|\mathbf{x}|} \\
&= 0,
\end{aligned}
\tag{2.62}
$$

the expectation value for the intensity of the field in the vacuum state is non-zero,

$$
\begin{aligned}
\langle 0| \left| \hat{\mathbf{E}}(z,t) \right|^2 |0\rangle &= \frac{\hbar \omega_c}{V \epsilon_0} \langle 0| \left(\hat{a} + \hat{a}^\dagger \right)^2 |0\rangle \sin^2(kz) \\
&= \frac{\hbar \omega_c}{V \epsilon_0} \sin^2(kz).
\end{aligned}
\tag{2.63}
$$

It can be seen from Eqns. 2.62 and 2.63 that even though the electromagnetic field in vacuum is on average zero, it fluctuates. Therefore, the Rabi flopping that occurs when there are initially no excitations in the field is caused by fluctuations in the vacuum electromagnetic field. This is a consequence of the quantum mechanical treatment of the electromagnetic field; an excited atom in a classical field that contains no energy would never decay.

Rabi flopping between excited and ground state is a reversible process, unlike spontaneous emission in which the photon leaves and never comes back. To correctly model the irreversible dissipative processes that are observed in nature, such as spontaneous emission, the system must be coupled to a continuum of modes. Models that include irreversible dissipative processes will be derived in Chapters 3 and 4.

2.3   Wiener-Khinchin Theorem

We will be frequently interested in information regarding the frequency content of the light that is produced by an open quantum system. The open quantum system that we consider may for instance consist of atoms interacting with an electromagnetic field inside a cavity. The spectral information about the cavity field, which is described by the annihilation operator $\hat{a}(t)$, can be obtained from the power spectral density $S(\omega)$, which is defined by,

$$
S(\omega) \equiv \lim_{T \to \infty} \frac{1}{T} \left\langle \hat{a}_T^\dagger(\omega) \hat{a}_T(\omega) \right\rangle,
\tag{2.64}
$$

where,

$$
\hat{a}_T(\omega) \equiv \int_{-T/2}^{T/2} dt \, e^{-i\omega t} \hat{a}(t).
\tag{2.65}
$$

Eq. 2.64 tells us how the total energy that is contained in the cavity field is distributed as a function of frequency ω. The power spectral density, described by Eq. 2.64, will often consist of a

distribution of frequencies around a central frequency. The width of this distribution, called the linewidth, denoted by $\Delta\nu$, is measure of the spectral purity of the light emitted by the considered system.

Since many of the solution methods to the equations of open quantum systems do not give direct access to $\hat{a}(t)$, it will often be difficult to calculate the power spectral density from Eq. 2.64 directly. However, an alternative method to obtain Eq. 2.64 is possible. This is demonstrated by substituting Eq. 2.65 into Eq. 2.64, which yields,

$$S(\omega) = \lim_{T\to\infty} \frac{1}{T} \int_{-T/2}^{T/2} dt \int_{-T/2}^{T/2} dt' e^{-i\omega(t'-t)} \left\langle \hat{a}^\dagger(t)\hat{a}(t') \right\rangle. \tag{2.66}$$

After changing variables to $\tau \equiv t' - t$, Eq. 2.66 becomes,

$$\begin{aligned}
S(\omega) &= \lim_{T\to\infty} \frac{1}{T} \left\{ \int_{-T}^{0} d\tau \int_{-T/2-\tau}^{T/2} dt e^{-i\omega\tau} \left\langle \hat{a}^\dagger(t)\hat{a}(t+\tau) \right\rangle \right. \\
&\quad \left. + \int_{0}^{T} dt \int_{-T/2}^{T/2-\tau} dt e^{-i\omega\tau} \left\langle \hat{a}^\dagger(t)\hat{a}(t+\tau) \right\rangle \right\}.
\end{aligned} \tag{2.67}$$

We assume that the system under consideration is in steady state, so that $\left\langle \hat{a}^\dagger(t)\hat{a}(t') \right\rangle$ is independent of t, and only depends on τ. Then, Eq. 2.67 becomes,

$$\begin{aligned}
S(\omega) &= \lim_{T\to\infty} \frac{1}{T} \int_{-T}^{T} d\tau e^{-i\omega\tau} \left\langle \hat{a}^\dagger(t)\hat{a}(t+\tau) \right\rangle (T - |\tau|). \\
&= \int_{-\infty}^{\infty} d\tau e^{-i\omega\tau} \left\langle \hat{a}^\dagger(t)\hat{a}(t+\tau) \right\rangle,
\end{aligned} \tag{2.68}$$

or since $S(\omega)$ is real,

$$\begin{aligned}
S(\omega) &= \int_{-\infty}^{\infty} d\tau e^{-i\omega\tau} \left\langle \hat{a}^\dagger(t+\tau)\hat{a}(t) \right\rangle \\
&= 2Re\left[\int_{0}^{\infty} d\tau e^{-i\omega\tau} \left\langle \hat{a}^\dagger(t+\tau)\hat{a}(t) \right\rangle \right].
\end{aligned} \tag{2.69}$$

Eq. 2.69 is known as the Wiener-Khinchin Theorem. It says that the power spectrum is the Fourier transform of the two-time correlation function $\left\langle \hat{a}^\dagger(t+\tau)\hat{a}(t) \right\rangle$. Therefore, the power spectrum $S(\omega)$ and its linewidth $\Delta\nu$, can be obtained from $\left\langle \hat{a}^\dagger(t+\tau)\hat{a}(t) \right\rangle$, which in many cases can be directly accessed.

Chapter 3

Master Equation

To correctly incorporate dissipation into a quantum mechanical system, the system is assumed to be small, and weakly coupled to a much larger reservoir. Since we only care about keeping track of system variables, the combined system and reservoir are evolved to second order in perturbation theory, and then the reservoir variables are averaged over. The resulting equation, called the master equation, keeps track of system variables only, and allows the system to lose or gain energy from its weak coupling to the large reservoir.

This approach is in the Schrödinger picture, where the time dependence is put on the state vector of the combined system and reservoir. Because the reservoir will be averaged over, the system will evolve into a statistical mixture of states, and it will no longer be able to be described by a single state vector. Instead, it will be necessary to describe the system by a reduced density operator, which can account for the system evolving into a statistical mixture of states.

3.1   Density Operator

Operators corresponding to system observables do not act on the reservoir part of the total Hilbert space. Therefore, if some sort of a partial expectation value over the reservoir part of the the state vector describing the combined system and reservoir could be performed, the complexity of the problem would be drastically reduced from the start. Unfortunately, a partial expectation value of a state vector can not be taken, but an analogous operation can be performed on a density

operator, which is defined as

$$\hat{\chi}(t) \equiv |\Psi(t)\rangle \langle \Psi(t)|, \tag{3.1}$$

where $|\Psi(t)\rangle$ is the state vector for the combined system and reservoir.

Let $\hat{\theta}_{SR}$ be an arbitrary operator of the system and reservoir Hilbert spaces. The trace of $\hat{\chi}(t)$ and $\hat{\theta}_{SR}$ is given by,

$$
\begin{aligned}
Tr\left[\hat{\chi}(t)\hat{\theta}_{SR}\right] &= \sum_s \sum_r \langle s| \langle r| \hat{\chi}(t)\hat{\theta}_{SR} |s\rangle |r\rangle \\
&= \sum_s \sum_r \langle s| \langle r|\Psi(t)\rangle \langle \Psi(t)| \hat{\theta}_{SR} |s\rangle |r\rangle \\
&= \sum_s \sum_r \langle \Psi(t)| \hat{\theta}_{SR} |s\rangle |r\rangle \langle s| \langle r|\Psi(t)\rangle \\
&= \langle \Psi(t)| \hat{\theta}_{SR} \left(\sum_s \sum_r |s\rangle |r\rangle \langle s| \langle r| \right) |\Psi(t)\rangle \\
&= \langle \Psi(t)| \hat{\theta}_{SR} |\Psi(t)\rangle,
\end{aligned}
$$

$$\tag{3.2}$$

where the states $|s\rangle$ are a basis for the system Hilbert space, and the states $|r\rangle$ are a basis for the reservoir Hilbert space. This tells us that performing the trace of $\hat{\chi}(t)$ and $\hat{\theta}_{SR}$ is equivalent to taking the expectation value of $\hat{\theta}_{SR}$.

If we are only interested observables associated with the system, we can preform partial trace over the reservoir Hilbert space, and arrive at a reduced density operator for the system only. Let $\hat{\theta}_S$, be an arbitrary system operator. The trace of $\hat{\chi}(t)$ and $\hat{\theta}_S$ is,

$$
\begin{aligned}
Tr\left[\hat{\chi}(t)\hat{\theta}_S\right] &= \sum_s \sum_r \langle s| \langle r| \hat{\chi}(t)\hat{\theta}_S |s\rangle |r\rangle \\
&= \sum_s \sum_r \langle s| \langle r| \hat{\chi}(t) |r\rangle \hat{\theta}_S |s\rangle \\
&= \sum_s \langle s| \left(\sum_r \langle r| \hat{\chi}(t) |r\rangle \right) \hat{\theta}_S |s\rangle \\
&= \sum_s \langle s| \hat{\rho}(t)\hat{\theta}_S |s\rangle, \tag{3.3}
\end{aligned}
$$

where,

$$\hat{\rho}(t) \;=\; \sum_r \langle r | \, \hat{\chi}(t) \, | r \rangle$$
$$=\; Tr_R \left[\hat{\chi}(t) \right],$$

(3.4)

where $\hat{\rho}(t)$ is the reduced density operator of the system. From Eq. 3.3 it can be seen that if the expectation value of a system operator is desired, it is valid to first take the partial trace of $\hat{\chi}(t)$ over the reservoir Hilbert space to get $\hat{\rho}(t)$ and then later take the remaining partial trace of $\hat{\rho}(t)$ and $\hat{\theta}$ to get the total trace. In the next section, the equation of motion for a combined system and reservoir will be considered, and a partial trace over the reservoir Hilbert space will be preformed. This will leave us with an equation of motion for the reduced density operator of the system. It is a drastic simplification to not have to keep track of the reservoir Hilbert space.

A consequence of performing a partial trace over the reservoir Hilbert space is that we will no longer have complete information about combined system and reservoir. This causes the the reduced density operator to be a mixed state, or a statistical ensemble of states. It will therefore not be possible to rewrite the reduced density it in terms of state vectors. Therefore, the reformulation of the problem in terms of density matrices is not only for convenience, it is essential.

The equation of motion for $\hat{\chi}(t)$ that is equivalent to the Schrödinger equation, $i\hbar \frac{d}{dt} | \Psi(t) \rangle = \hat{H}(t) | \Psi(t) \rangle$, is called the Von Neumann equation. It is derived by taking a time derivative of $\hat{\chi}(t)$ and substituting in the Schroödinger equation,

$$\frac{d}{dt} \hat{\chi}(t) \;=\; \frac{d}{dt} \left(| \Psi(t) \rangle \langle \Psi(t) | \right)$$
$$=\; \left(\frac{d | \Psi(t) \rangle}{dt} \langle \Psi(t) | + | \Psi(t) \rangle \frac{d \langle \Psi(t) |}{dt} \right)$$
$$=\; \frac{1}{i\hbar} \left(\hat{H}(t) | \Psi(t) \rangle \langle \Psi(t) | - | \Psi(t) \rangle \langle \Psi(t) | \hat{H}(t) \right)$$
$$=\; \frac{1}{i\hbar} \left[\hat{H}(t), \hat{\chi}(t) \right].$$

(3.5)

3.2 The Master Equation for a Damped Harmonic Oscillator

To derive the master equation [67], we will need to make two approximations. First, the interaction between system and reservoir is assumed to be weak, so that it is sufficient to evolve the system to leading order in perturbation theory. This is the Born approximation. Also, the frequency bandwidth of the reservoir is assumed to be very large, so that in the time domain, reservoir correlations decay away very fast. In the limiting case of infinite bandwidth, the reservoir is delta correlated in time. This is the Markov approximation.

In order to best illuminate the approximations and the physics involved, the master equation is derived for a simple system instead of in full generality. Once our foot is in the door, it is easy to generalize to more complicated systems, since the derivation for those systems follow in an almost identical manner.

3.2.1 Derivation

Consider a quantum harmonic oscillator of frequency ω_c, which is coupled to many other quantum harmonic oscillators of frequencies ω_j. This could be, for instance, used to model the the coupling of a cavity mode to all other modes of the electromagnetic field in a system cavity QED system. The Hamiltonian of the combined system and reservoir $\hat{H}$, is given by,

$$\hat{H} = \hat{H}_S + \hat{H}_R + \hat{H}_{SR}, \tag{3.6}$$

where $\hat{H}_S$ is the Hamiltonian for the system,

$$\hat{H}_S = \hbar\omega_c \hat{a}^\dagger \hat{a}, \tag{3.7}$$

$\hat{H}_R$ is the Hamiltonian for the reservoir,

$$\hat{H}_R = \hbar \sum_j \omega_j \hat{r}_j^\dagger \hat{r}_j \tag{3.8}$$

and $\hat{H}_{SR}$ is the Hamiltonian for the coupling between the system and reservoir,

$$\hat{H}_{SR} = \hbar \sum_j \left(\lambda_j \hat{a}^\dagger \hat{r}_j + \lambda_j^* \hat{a} \hat{r}_j^\dagger \right), \tag{3.9}$$

where $\hat{a}$ is the annihilation operator in the system Hilbert space and $\hat{r}_j$ is the annihilation operator of the jth mode in the reservoir Hilbert space, and λ_j is the coupling between the system and the jth mode in the reservoir.

At time $t = t_0$, it is assumed that there are no correlations between the system and reservoir, and therefore $\hat{\chi}(t_0)$ is of the separable form,

$$\hat{\chi}(t_0) = \hat{\rho}(t_0) \otimes \hat{R}, \tag{3.10}$$

where $\hat{\rho}(t)$ is the reduced density operator of the system, and $\hat{R}$ is the reduced density operator of the reservoir, which are defined respectively as,

$$\hat{\rho}(t) \equiv tr_R\left\{\hat{\chi}(t)\right\}, \tag{3.11}$$

and

$$\hat{R} \equiv tr_S\left\{\hat{\chi}(t)\right\}. \tag{3.12}$$

The reservoir density operator, $\hat{R}$, has no time dependence because we are assuming that the reservoir is broadband, so that in the time domain, it returns to its steady state value on a time scale much faster than system dynamics. Therefore at later times we can also assume that $\hat{\chi}(t)$ will be seperable,

$$\hat{\chi}(t) = \hat{\rho}(t) \otimes \hat{R}. \tag{3.13}$$

The reservoir is assumed to be in thermal equilibrium at temperature T, which is described by,

$$\hat{R} = \frac{e^{-\frac{\hat{H}_R}{k_B T}}}{tr_R\left\{e^{-\frac{\hat{H}_R}{k_B T}}\right\}}. \tag{3.14}$$

The first step in our derivation is to move into an interaction picture, so that the time dependence of $\hat{H}_S$ and $\hat{H}_R$ can be rotated out. This is done by the following transformation:

$$\tilde{\chi}(t) = e^{\frac{i}{\hbar}(\hat{H}_S + \hat{H}_R)t}\hat{\chi}(t)e^{-\frac{i}{\hbar}(\hat{H}_S + \hat{H}_R)t}. \tag{3.15}$$

It is worth noting that Eq. 3.14 implies that $\hat{R}$ is unaffected by this transformation, since an operator commutes with an exponential of itself, so that,

$$\tilde{\hat{R}} = \hat{R} \tag{3.16}$$

To find the time evolution in the interaction picture, the derivative of both sides of Eq. 3.15 is first found,

$$
\begin{aligned}
\dot{\tilde{\chi}}(t) &= -\frac{1}{i\hbar}\left(\hat{H}_S + \hat{H}_R\right)e^{\frac{i}{\hbar}(\hat{H}_S+\hat{H}_R)t}\hat{\chi}(t)e^{-\frac{i}{\hbar}(\hat{H}_S+\hat{H}_R)t} \\
&\quad + e^{\frac{i}{\hbar}(\hat{H}_S+\hat{H}_R)}\left(\dot{\hat{\chi}}(t)e^{-\frac{i}{\hbar}(\hat{H}_S+\hat{H}_R)t} + \hat{\chi}(t)\left(\frac{1}{i\hbar}\left(\hat{H}_S + \hat{H}_R\right)\right)e^{-\frac{i}{\hbar}(\hat{H}_S+\hat{H}_R)t}\right). \quad (3.17)
\end{aligned}
$$

Upon substitution of Eq. 3.5 into Eq. 3.17, it becomes,

$$
\begin{aligned}
\dot{\tilde{\chi}}(t) &= -\frac{1}{i\hbar}\left(\hat{H}_S + \hat{H}_R\right)\tilde{\chi}(t) \\
&\quad + e^{\frac{i}{\hbar}(\hat{H}_S+\hat{H}_R)}\left(\frac{1}{i\hbar}\left[\hat{H}(t),\hat{\chi}(t)\right]\right)e^{-\frac{i}{\hbar}(\hat{H}_S+\hat{H}_R)t} + \frac{1}{i\hbar}\tilde{\chi}(t)\left(\hat{H}_S + \hat{H}_R\right). \quad (3.18)
\end{aligned}
$$

Finally, we now use Eq. 3.6 and simplify, and arrive at,

$$
\begin{aligned}
\dot{\tilde{\chi}}(t) &= -\frac{1}{i\hbar}\left(\hat{H}_S + \hat{H}_R\right)\tilde{\chi}(t) + \frac{1}{i\hbar}\tilde{\chi}(t)\left(\hat{H}_S + \hat{H}_R\right) \\
&\quad + e^{\frac{i}{\hbar}(\hat{H}_S+\hat{H}_R)}\frac{1}{i\hbar}\left(\left(\hat{H}_S + \hat{H}_R + \hat{H}_{SR}(t)\right)\hat{\chi}(t) - \hat{\chi}(t)\left(\hat{H}_S + \hat{H}_R + \hat{H}_{SR}(t)\right)\right)e^{-\frac{i}{\hbar}(\hat{H}_S+\hat{H}_R)t} \\
&= e^{\frac{i}{\hbar}(\hat{H}_S+\hat{H}_R)}\frac{1}{i\hbar}\left(\hat{H}_{SR}(t)\hat{\chi}(t) - \hat{\chi}(t)\hat{H}_{SR}(t)\right)e^{-\frac{i}{\hbar}(\hat{H}_S+\hat{H}_R)t} \\
&= \frac{1}{i\hbar}e^{\frac{i}{\hbar}(\hat{H}_S+\hat{H}_R)}\left(\hat{H}_{SR}(t)e^{-\frac{i}{\hbar}(\hat{H}_S+\hat{H}_R)}e^{\frac{i}{\hbar}(\hat{H}_S+\hat{H}_R)}\hat{\chi}(t)\right. \\
&\quad \left. - \hat{\chi}(t)e^{-\frac{i}{\hbar}(\hat{H}_S+\hat{H}_R)}e^{\frac{i}{\hbar}(\hat{H}_S+\hat{H}_R)}\hat{H}_{SR}(t)\right)e^{-\frac{i}{\hbar}(\hat{H}_S+\hat{H}_R)t} \\
&= \frac{1}{i\hbar}\left[\tilde{\hat{H}}_{SR}(t),\tilde{\chi}(t)\right], \quad (3.19)
\end{aligned}
$$

where,

$$
\tilde{\hat{H}}_{SR}(t) \equiv e^{\frac{i}{\hbar}(\hat{H}_S+\hat{H}_R)t}\hat{H}_{SR}(t)e^{-\frac{i}{\hbar}(\hat{H}_S+\hat{H}_R)t}. \quad (3.20)
$$

Next, both sides of Eq. 3.19 are integrated,

$$
\tilde{\chi}(t) - \tilde{\chi}(t_0) = \frac{1}{i\hbar}\int_{t_0}^{t}dt'\left[\tilde{\hat{H}}_{SR}(t'),\tilde{\chi}(t')\right], \quad (3.21)
$$

and then substitute this back into itself to obtain,

$$
\tilde{\chi}(t) - \tilde{\chi}(t_0) = \frac{1}{i\hbar}\int_{t_0}^{t}dt'\left[\tilde{\hat{H}}_{SR}(t'),\tilde{\chi}(t_0)\right] - \frac{1}{\hbar^2}\int_{t_0}^{t}dt'\int_{t_0}^{t'}dt''\left[\tilde{\hat{H}}_{SR}(t'),\left[\tilde{\hat{H}}_{SR}(t''),\tilde{\chi}(t'')\right]\right]. \quad (3.22)
$$

After taking the partial trace over the reservoir of both sides of Eq. 3.22, it is given by,

$$\tilde{\rho}(t) - \tilde{\rho}(t_0) = -\frac{1}{\hbar^2} \int_{t_0}^{t} dt' \int_{t_0}^{t'} dt'' tr_R \left\{ \left[\tilde{\hat{H}}_{SR}(t'), \left[\tilde{\hat{H}}_{SR}(t''), \tilde{\chi}(t'') \right] \right] \right\}, \tag{3.23}$$

where the first term on the right hand side of Eq. 3.22 vanishes since the trace over the reservoir of $\hat{r}_j$ and $\hat{r}_j^\dagger$ are zero. The vanishing of this term is why Eq. 3.23 was expanded up to second order in $\tilde{\hat{H}}_{SR}$. The Born approximation is now made, by neglecting terms higher than this leading order in $\tilde{\hat{H}}_{SR}$.

We assume that the integration time interval $\tau \equiv t - t_0$ is short compared to the time it takes the reservoir to change, but long compared to the time it takes the system to change. Under this assumption, it is valid to approximate,

$$\frac{\tilde{\rho}(t_0 + \tau) - \tilde{\rho}(t_0)}{\tau} \approx \frac{d}{dt} \tilde{\rho}(\tau). \tag{3.24}$$

Under this approximation, Eq 3.23 is turned into a coarse-grained equation of motion for $\tilde{\rho}(t)$,

$$\frac{d}{d\tau} \tilde{\rho}(\tau) = -\frac{1}{\hbar^2 \tau} \int_0^\tau d\tau' \int_0^{\tau'} d\tau'' tr_R \left\{ \left[\tilde{\hat{H}}_{SR}(\tau'), \left[\tilde{\hat{H}}_{SR}(\tau''), \tilde{\chi}(t) \right] \right] \right\}, \tag{3.25}$$

where the independent variable has been changed from t to τ, and the time origin has been shifted by t_0.

In order to proceed, the form of $\hat{H}_{SR}$ in the interaction picture must be found. To do this, the time dependence of the system operator $\hat{a}$ and reservoir operators $\hat{r}_j$ in the interaction picture are found,

$$\begin{aligned}
\tilde{\hat{a}}(t) &= e^{\frac{i}{\hbar}(\hat{H}_S + \hat{H}_R)t} \hat{a} e^{-\frac{i}{\hbar}(\hat{H}_S + \hat{H}_R)t} \\
&= e^{\frac{i}{\hbar}\hat{H}_S t} \hat{a} e^{-\frac{i}{\hbar}\hat{H}_S t} \\
&= \hat{a} e^{-i\omega_c t},
\end{aligned} \tag{3.26}$$

$$\begin{aligned}
\tilde{\hat{r}}_j(t) &= e^{\frac{i}{\hbar}(\hat{H}_S + \hat{H}_R)t} \hat{r}_j e^{-\frac{i}{\hbar}(\hat{H}_S + \hat{H}_R)t} \\
&= e^{\frac{i}{\hbar}\hat{H}_R t} \hat{r}_j e^{-\frac{i}{\hbar}\hat{H}_R t} \\
&= \hat{r}_j e^{-i\omega_j t}.
\end{aligned} \tag{3.27}$$

Eqns. 3.26 – 3.27, and their Hermitian conjugates are substituted into Eq. 3.9, so that $\hat{H}_{SR}$ in the interaction picture is given by,

$$
\begin{aligned}
\tilde{\hat{H}}_{SR}(\tau) &= \hbar \sum_j \left(\lambda_j e^{i(\omega_c - \omega_j)\tau} \hat{a}^\dagger \hat{r}_j + \lambda_j^* e^{-i(\omega_c - \omega_j)\tau} \hat{a} \hat{r}_j^\dagger \right), \\
&= \imath\hbar \left(\hat{a}^\dagger \hat{F}(\tau) - \hat{a}\hat{F}^\dagger(\tau) \right),
\end{aligned}
\tag{3.28}
$$

where the reservoir operator $\hat{F}(\tau)$ is defined as,

$$
\hat{F}(\tau) \equiv -\imath \sum_j \lambda_j \hat{r}_j e^{i(\omega_j - \omega_c)\tau}.
\tag{3.29}
$$

After expanding the double commutator, and substituting in Eq. 3.28, Eq. 3.25 becomes,

$$
\begin{aligned}
\frac{d}{dt}\tilde{\hat{\rho}}(t) &= \frac{1}{\tau} \int_0^\tau d\tau' \int_0^{\tau'} d\tau'' tr_R \Bigg\{ \left(\hat{a}^\dagger \hat{F}(\tau') - \hat{a}\hat{F}^\dagger(\tau') \right) \left(\hat{a}^\dagger \hat{F}(\tau'') - \hat{a}\hat{F}^\dagger(\tau'') \right) \tilde{\hat{\chi}}(t) \\
&\quad - \left(\hat{a}^\dagger \hat{F}(\tau') - \hat{a}\hat{F}^\dagger(\tau') \right) \tilde{\hat{\chi}}(t) \left(\hat{a}^\dagger \hat{F}(\tau'') - \hat{a}\hat{F}^\dagger(\tau'') \right) \Bigg\} + H.C. \\
&= \frac{1}{\tau} \int_0^\tau d\tau' \int_0^{\tau'} d\tau'' \Bigg(\hat{a}^\dagger \hat{a}^\dagger \tilde{\hat{\rho}}(t) tr_R \left\{ \hat{F}(\tau')\hat{F}(\tau'')\hat{R} \right\} - \hat{a}^\dagger \hat{a} \tilde{\hat{\rho}}(t) tr_R \left\{ \hat{F}(\tau')\hat{F}^\dagger(\tau'')\hat{R} \right\} \\
&\quad - \hat{a}\hat{a}^\dagger \tilde{\hat{\rho}}(t) tr_R \left\{ \hat{F}^\dagger(\tau')\hat{F}(\tau'')\hat{R} \right\} + \hat{a}\hat{a} \tilde{\hat{\rho}}(t) tr_R \left\{ \hat{F}^\dagger(\tau')\hat{F}^\dagger(\tau'')\hat{R} \right\} \\
&\quad - \hat{a}^\dagger \tilde{\hat{\rho}}(t) \hat{a}^\dagger tr_R \left\{ \hat{F}(\tau')\hat{R}\hat{F}(\tau'') \right\} + \hat{a}^\dagger \tilde{\hat{\rho}}(t) \hat{a} tr_R \left\{ \hat{F}(\tau')\hat{R}\hat{F}^\dagger(\tau'') \right\} \\
&\quad + \hat{a}\tilde{\hat{\rho}}(t) \hat{a}^\dagger tr_R \left\{ \hat{F}^\dagger(\tau')\hat{R}\hat{F}(\tau'') \right\} - \hat{a}\tilde{\hat{\rho}}(t) \hat{a} tr_R \left\{ \hat{F}^\dagger(\tau')\hat{R}\hat{F}^\dagger(\tau'') \right\} \Bigg) + H.C.
\end{aligned}
\tag{3.30}
$$

Since $\hat{R}$ is diagonal in the reservoir eigenbasis, terms with two $\hat{F}(\tau)$ or two $\hat{F}^\dagger(\tau)$ in the reservoir trace will be zero. However, terms with one $\hat{F}(\tau)$ and one $\hat{F}^\dagger(\tau)$ in the reservoir trace will be non-zero. Consider, for example, the term proportional to,

$$
\begin{aligned}
\int_0^\tau d\tau' \int_0^{\tau'} d\tau'' tr_R \left\{ \hat{F}^\dagger(\tau')\hat{F}(\tau'')\hat{R} \right\} &= \int_0^\tau d\tau' \int_0^{\tau'} d\tau'' \sum_{i,j} \lambda_i^\star \lambda_j tr_R \left\{ \hat{r}_i^\dagger \hat{r}_j \hat{R} \right\} e^{-i(\omega_i - \omega_c)\tau'} e^{i(\omega_j - \omega_c)\tau''} \\
&= \int_0^\tau d\tau' \int_0^{\tau'} d\tau'' \sum_j |\lambda_j|^2 \, tr_R \left\{ \hat{r}_j^\dagger \hat{r}_j \hat{R} \right\} e^{i(\omega_c - \omega_j)(\tau' - \tau'')},
\end{aligned}
\tag{3.31}
$$

where the last line follows again from the fact that $\hat{R}$ is diagonal in the reservoir eigenbasis.

The sum is changed to an integral over ω by including a density of states $\mathcal{D}(\omega)$,

$$
\begin{aligned}
\int_0^\tau d\tau' \int_0^{\tau'} d\tau'' tr_R \left\{ \hat{F}^\dagger(\tau')\hat{F}(\tau'')\hat{R} \right\} &= \sum_j \Delta_j \, |\lambda_j|^2 \int_0^\tau d\tau' \int_0^{\tau'} d\tau'' tr_R \left\{ \hat{r}_j^\dagger \hat{r}_j \hat{R} \right\} e^{i(\omega_c - \omega_j)(\tau' - \tau'')} \\
&= \int_0^B d\omega \mathcal{D}(\omega) \, |\lambda(\omega)|^2 \int_0^\tau d\tau' \int_0^{\tau'} d\tau'' tr_R \left\{ \hat{r}^\dagger \hat{r} \hat{R} \right\} e^{i(\omega_c - \omega)(\tau' - \tau'')}
\end{aligned}
$$

$$(3.32)$$

where $\Delta_j = 1$ and B is the bandwidth of the reservoir. Since we assuming that the bandwidth of the reservoir is very large, the reservoir relaxation rate $\frac{1}{\tau_R}$ will be much larger than the systems relaxation rate $\frac{1}{\tau_S}$. Then, for $\tau << \tau_S$, $tr_R \left\{ \hat{r}^\dagger \hat{r} \hat{R} \right\}$ will be approximately constant, so that it can be factored outside of the integral,

$$
\begin{aligned}
\int_0^\tau d\tau' \int_0^{\tau'} d\tau'' tr_R & \left\{ \hat{F}^\dagger(\tau')\hat{F}(\tau'')\hat{R} \right\} \\
&= \int_0^B d\omega \mathcal{D}(\omega) \, |\lambda(\omega)|^2 \, tr_R \left\{ \hat{r}^\dagger \hat{r} \hat{R} \right\} \int_0^\tau d\tau' \int_0^{\tau'} d\tau'' e^{i(\omega_c - \omega)(\tau' - \tau'')} .
\end{aligned}
$$

$$(3.33)$$

The resulting integral of the exponential will then destructively interfere when $T \equiv \tau' - \tau'' >> \tau_R$, resulting in it averaging to zero. Therefore, after changing variables to T, the upper limit of integration on the T integral can be extended to $T = \infty$ with minimal error, so that Eq. 3.33 becomes,

$$
\begin{aligned}
\int_0^\tau d\tau' \int_0^{\tau'} d\tau'' tr_R & \left\{ \hat{F}^\dagger(\tau')\hat{F}(\tau'')\hat{R} \right\} \\
&= \int_0^B d\omega \mathcal{D}(\omega) \, |\lambda(\omega)|^2 \, tr_R \left\{ \hat{r}^\dagger \hat{r} \hat{R} \right\} \int_0^\tau d\tau' \int_0^\infty dT e^{i(\omega_c - \omega)T} \\
&= \int_0^B d\omega \mathcal{D}(\omega) \, |\lambda(\omega)|^2 \, tr_R \left\{ \hat{r}^\dagger \hat{r} \hat{R} \right\} \int_0^\tau d\tau' \left[\pi \delta(\omega - \omega_c) - i\mathcal{P}\left(\frac{1}{\omega - \omega_c} \right) \right],
\end{aligned}
$$

$$(3.34)$$

where we have used,

$$
\lim_{t \to \infty} \int_{t_0}^t dt' e^{i(\omega_c - \omega)(t - t')} = \lim_{t \to \infty} \int_0^{t - t_0} dT e^{i(\omega_c - \omega)T} = \pi \delta(\omega - \omega_c) - i\mathcal{P}\left(\frac{1}{\omega - \omega_c} \right).
$$

$$(3.35)$$

Neglecting the principal part, $\mathcal{P}\left(1/(\omega - \omega_c) \right)$, which leads to a negligible frequency shift, Eq. 3.34 becomes,

$$
\int_0^\tau d\tau' \int_0^{\tau'} d\tau'' tr_R \left\{ \hat{F}^\dagger(\tau')\hat{F}(\tau'')\hat{R} \right\} = \frac{\kappa \tau \bar{n}}{2},
$$

$$(3.36)$$

where,

$$\kappa = 2\pi \mathcal{D}(\omega_c)\left|\lambda(\omega_c)\right|^2, \tag{3.37}$$

and $\bar{n}$ is the average number of thermal excitations in the reservoir,

$$\bar{n} = tr_R\left\{\hat{r}^\dagger \hat{r} \hat{R}\right\}. \tag{3.38}$$

After evaluation of the other reservoir trace terms, which follow in almost an identical manner to the one demonstrated, Eq. 3.30 becomes the master equation for the damped harmonic oscillator,

$$\begin{aligned}
\frac{d}{dt}\tilde{\rho}(t) &= \frac{1}{2}\left(-\hat{a}^\dagger\hat{a}\tilde{\rho}(t)\kappa\left(\bar{n}+1\right) - \hat{a}\hat{a}^\dagger\tilde{\rho}(t)\kappa\bar{n} + \hat{a}^\dagger\tilde{\rho}(t)\hat{a}\kappa\bar{n} + \hat{a}\tilde{\rho}(t)\hat{a}^\dagger\kappa\left(\bar{n}+1\right)\right) + H.C. \\
&= -\frac{\kappa}{2}\left(\bar{n}+1\right)\left(\hat{a}^\dagger\hat{a}\tilde{\rho}(t) + \tilde{\rho}(t)\hat{a}^\dagger\hat{a} - 2\hat{a}\tilde{\rho}(t)\hat{a}^\dagger\right) - \frac{\kappa}{2}\bar{n}\left(\hat{a}\hat{a}^\dagger\tilde{\rho}(t) + \tilde{\rho}(t)\hat{a}\hat{a}^\dagger - 2\hat{a}^\dagger\tilde{\rho}(t)\hat{a}\right).
\end{aligned} \tag{3.39}$$

3.2.2 Analytic Solutions for Photon Number

Eq. 3.39 can be used to calculate the average photon number $\langle\hat{a}^\dagger\hat{a}\rangle$ since in the Schrödinger picture,

$$\frac{d}{dt}\left\langle\hat{a}^\dagger\hat{a}\right\rangle = tr\left[\hat{a}^\dagger\hat{a}\frac{d}{dt}\tilde{\rho}(t)\right]. \tag{3.40}$$

Now, Eq. 3.39 is substituted into Eq. 3.40 to obtain

$$\begin{aligned}
\frac{d}{dt}\left\langle\hat{a}^\dagger\hat{a}\right\rangle &= -\frac{\kappa}{2}\left(\bar{n}+1\right)tr\left[\hat{a}^\dagger\hat{a}\hat{a}^\dagger\hat{a}\tilde{\rho}(t) + \hat{a}^\dagger\hat{a}\tilde{\rho}(t)\hat{a}^\dagger\hat{a} - 2\hat{a}^\dagger\hat{a}\hat{a}\tilde{\rho}(t)\hat{a}^\dagger\right] \\
&\quad -\frac{\kappa}{2}\bar{n}tr\left[\hat{a}^\dagger\hat{a}\hat{a}\hat{a}^\dagger\tilde{\rho}(t) + \hat{a}^\dagger\hat{a}\tilde{\rho}(t)\hat{a}\hat{a}^\dagger - 2\hat{a}^\dagger\hat{a}\hat{a}^\dagger\tilde{\rho}(t)\hat{a}\right] \\
&= -\frac{\kappa}{2}\left(\bar{n}+1\right)tr\left[\hat{a}^\dagger\hat{a}\hat{a}^\dagger\hat{a}\tilde{\rho}(t) + \hat{a}^\dagger\hat{a}\hat{a}^\dagger\hat{a}\tilde{\rho}(t) - 2\hat{a}^\dagger\hat{a}^\dagger\hat{a}\hat{a}\tilde{\rho}(t)\right] \\
&\quad -\frac{\kappa}{2}\bar{n}tr\left[\hat{a}^\dagger\hat{a}\hat{a}\hat{a}^\dagger\tilde{\rho}(t) + \hat{a}\hat{a}^\dagger\hat{a}^\dagger\hat{a}\tilde{\rho}(t) - 2\hat{a}\hat{a}^\dagger\hat{a}\hat{a}^\dagger\tilde{\rho}(t)\right],
\end{aligned} \tag{3.41}$$

where in the last line, we have used the cyclic property of the trace,

$$tr\left[\hat{A}\hat{B}\hat{C}\right] = tr\left[\hat{C}\hat{A}\hat{B}\right] = tr\left[\hat{B}\hat{C}\hat{A}\right], \tag{3.42}$$

with $\hat{A}$, $\hat{B}$, and $\hat{C}$ being arbitrary operators. Eq. 3.41 can be simplified by using the commutation relations for creation and annihilation operators,

$$\left[\hat{a}, \hat{a}^\dagger\right] = \hat{a}\hat{a}^\dagger - \hat{a}^\dagger\hat{a} = \hat{\mathbb{1}}, \tag{3.43}$$

where $\hat{\mathbb{1}}$ is the identity operator. We find,

$$
\begin{aligned}
\frac{d}{dt}\left\langle \hat{a}^\dagger \hat{a} \right\rangle &= -\frac{\kappa}{2}\left(\bar{n}+1\right) tr\left[2\hat{a}^\dagger\left(\hat{a}^\dagger\hat{a}+1\right)\hat{a}\tilde{\rho}(t) - 2\hat{a}^\dagger\hat{a}^\dagger\hat{a}\hat{a}\tilde{\rho}(t)\right] \\
&\quad -\frac{\kappa}{2}\bar{n}tr\left[\left(\hat{a}\hat{a}^\dagger-1\right)\hat{a}\hat{a}^\dagger\tilde{\rho}(t) + \hat{a}\hat{a}^\dagger\left(\hat{a}\hat{a}^\dagger-1\right)\tilde{\rho}(t) - 2\hat{a}\hat{a}^\dagger\hat{a}\hat{a}^\dagger\tilde{\rho}(t)\right] \\
&= -\kappa\left\langle \hat{a}^\dagger\hat{a}\right\rangle + +\kappa\bar{n}.
\end{aligned} \tag{3.44}
$$

The solution to Eq. 3.44 is,

$$
\left\langle \hat{a}^\dagger\hat{a}\right\rangle(t) = \left\langle \hat{a}^\dagger\hat{a}\right\rangle(0)e^{-\kappa t} + \bar{n}\left(1 - e^{-\kappa t}\right). \tag{3.45}
$$

Eq. 3.45 will prove useful in sections 3.4 and 3.5 when we will wish to compare the numerical solution methods demonstrated in that section to an analytic solution. These numerical solution can be used to treat more complex systems, where analytic solutions are not possible.

3.2.3   The Quantum Regression Theorem

Consider the two-time expectation value of two arbitrary system operators $\hat{A}$ and $\hat{B}$,

$$
\left\langle \hat{A}(t+\tau)\hat{B}(t)\right\rangle = tr\left[e^{\frac{i}{\hbar}\hat{H}\tau}\hat{A}(t)e^{-\frac{i}{\hbar}\hat{H}\tau}\hat{B}(t)\hat{\rho}\right], \tag{3.46}
$$

where $\hat{H}$ is the total Hamiltonian of system and reservoir. Using the cyclic property of the trace, we find

$$
\begin{aligned}
\left\langle \hat{A}(t+\tau)\hat{B}(t)\right\rangle &= tr\left[e^{-\frac{i}{\hbar}\hat{H}\tau}\hat{B}(t)\hat{\rho}e^{\frac{i}{\hbar}\hat{H}\tau}\hat{A}(t)\right] \\
&= tr\left[\hat{S}(\tau)\hat{A}(t)\right],
\end{aligned} \tag{3.47}
$$

where,

$$
\hat{S}(\tau) \equiv e^{-\frac{i}{\hbar}\hat{H}\tau}\hat{B}(t)\hat{\rho}e^{\frac{i}{\hbar}\hat{H}\tau}. \tag{3.48}
$$

Eq. 3.48 says that $\hat{S}(\tau)$ obeys the same equation of motion as $\hat{\rho}$. Since $\hat{\rho}$ obeys the master equation, so does $\hat{S}(\tau)$. Taking the derivative with respect to τ of both sides of Eq. 3.47 yields,

$$
\frac{d}{d\tau}\left\langle \hat{A}(t+\tau)\hat{B}(t)\right\rangle = tr\left[\left(\frac{d}{d\tau}\hat{S}(\tau)\right)\hat{A}(t)\right]. \tag{3.49}
$$

Thus, since $\left(\frac{d}{d\tau}\hat{S}(\tau)\right)$ is known, the equation of motion for the two-time correlation function $\left\langle \hat{A}(t+\tau)\hat{B}(t)\right\rangle$ can be calculated. This is the the quantum regression theorem.

To demonstrate the quantum regression theorem, $\left\langle \hat{a}^\dagger(t+\tau)\hat{a}(t)\right\rangle$ is calculated for the damped harmonic oscillator. We let $\hat{A} \to \hat{a}^\dagger$ and $\hat{B} \to \hat{a}$ in Eq. 3.49,

$$\frac{d}{d\tau}\left\langle \hat{a}^\dagger(t+\tau)\hat{a}(t)\right\rangle = \left\langle \left(\frac{d}{d\tau}\hat{S}(\tau)\right)\hat{a}^\dagger(t)\right\rangle \tag{3.50}$$

Using Eq. 3.39 for $\hat{S}(\tau)$ yields,

$$\begin{aligned}
\frac{d}{d\tau}\left\langle \hat{a}^\dagger(t+\tau)\hat{a}(t)\right\rangle &= -\frac{\kappa}{2}\left(\bar{n}+1\right)tr\left[\hat{a}^\dagger\hat{a}\hat{S}(\tau)\hat{a}^\dagger + \hat{S}(\tau)\hat{a}^\dagger\hat{a}\hat{a}^\dagger - 2\hat{a}\hat{S}(\tau)\hat{a}^\dagger\hat{a}^\dagger\right] \\
&\quad -\frac{\kappa}{2}\bar{n}tr\left[\hat{a}\hat{a}^\dagger\hat{S}(\tau)\hat{a}^\dagger + \hat{S}(\tau)\hat{a}\hat{a}^\dagger\hat{a}^\dagger - 2\hat{a}^\dagger\hat{S}(\tau)\hat{a}\hat{a}^\dagger\right] \\
&= -\frac{\kappa}{2}\left(\bar{n}+1\right)tr\left[\hat{a}^\dagger\hat{a}^\dagger\hat{a}\hat{S}(\tau) + \hat{a}^\dagger\hat{a}\hat{a}^\dagger\hat{S}(\tau) - 2\hat{a}^\dagger\hat{a}^\dagger\hat{a}\hat{S}(\tau)\right] \\
&\quad -\frac{\kappa}{2}\bar{n}tr\left[\hat{a}^\dagger\hat{a}\hat{a}^\dagger\hat{S}(\tau) + \hat{a}\hat{a}^\dagger\hat{a}^\dagger\hat{S}(\tau) - 2\hat{a}\hat{a}^\dagger\hat{a}^\dagger\hat{S}(\tau)\right],
\end{aligned} \tag{3.51}$$

where in the last line, the cyclic property of the trace has been used. The commutation relations for creation and annihilation operators are used to simplify, yielding,

$$\begin{aligned}
\frac{d}{d\tau}\left\langle \hat{a}^\dagger(t+\tau)\hat{a}(t)\right\rangle &= -\frac{\kappa}{2}\left(\bar{n}+1\right)tr\left[\hat{a}^\dagger\hat{a}^\dagger\hat{a}\hat{S}(\tau) + \hat{a}^\dagger\left(\hat{a}^\dagger\hat{a}+\hat{\mathbb{1}}\right)\hat{S}(\tau) - 2\hat{a}^\dagger\hat{a}^\dagger\hat{a}\hat{S}(\tau)\right] \\
&\quad -\frac{\kappa}{2}\bar{n}tr\left[\left(\hat{a}\hat{a}^\dagger - \hat{\mathbb{1}}\right)\hat{a}^\dagger\hat{S}(\tau) + \hat{a}\hat{a}^\dagger\hat{a}^\dagger\hat{S}(\tau) - 2\hat{a}\hat{a}^\dagger\hat{a}^\dagger\hat{S}(\tau)\right] \\
&= -\frac{\kappa}{2}\left(\bar{n}+1\right)tr\left[\hat{a}^\dagger\hat{S}(\tau)\right] + \frac{\kappa}{2}\bar{n}tr\left[\hat{a}^\dagger\hat{S}(\tau)\right] \\
&= -\frac{\kappa}{2}tr\left[\hat{a}^\dagger\hat{S}(\tau)\right].
\end{aligned} \tag{3.52}$$

Eq. 3.48 is substituted with $\hat{B} \to \hat{a}$, and the cyclic property of the trace is again used. Then,

$$\begin{aligned}
\frac{d}{d\tau}\left\langle \hat{a}^\dagger(t+\tau)\hat{a}(t)\right\rangle &= -\frac{\kappa}{2}tr\left[\hat{a}^\dagger e^{-\frac{i}{\hbar}\hat{H}\tau}\hat{B}(t)\hat{\rho}e^{\frac{i}{\hbar}\hat{H}\tau}\right] \\
&= -\frac{\kappa}{2}tr\left[e^{\frac{i}{\hbar}\hat{H}\tau}\hat{a}^\dagger e^{-\frac{i}{\hbar}\hat{H}\tau}\hat{a}\hat{\rho}\right] \\
&= -\frac{\kappa}{2}tr\left[\hat{a}^\dagger(t+\tau)\hat{a}(t)\hat{\rho}(t)\right] \\
&= -\frac{\kappa}{2}\left\langle \hat{a}^\dagger(t+\tau)\hat{a}(t)\right\rangle.
\end{aligned} \tag{3.53}$$

The solution to Eq. 3.53 is,

$$\left\langle \hat{a}^\dagger(t+\tau)\hat{a}(t)\right\rangle = \left\langle \hat{a}^\dagger(t)\hat{a}(t)\right\rangle e^{-\kappa\tau/2}, \tag{3.54}$$

and from Eq. 3.45,

$$\left\langle \hat{a}^\dagger(t+\tau)\hat{a}(t)\right\rangle = \left(\left\langle \hat{a}^\dagger \hat{a}\right\rangle(0)e^{-\kappa t} + \bar{n}\left(1 - e^{-\kappa t}\right)\right) e^{-\kappa\tau/2}. \tag{3.55}$$

3.3   The Master Equation for a Damped Two Level Atom

The master equation for a two level atom coupled to a reservoir of harmonic oscillators follows almost instantaneously. This system could, for instance, describe the spontaneous emission of radiation from a two level atom due to its coupling to the many modes of the electromagnetic field. Describing how two level atoms are damped by a reservoir will be essential to systems that will be treated later.

The Hamiltonian of the combined system and reservoir, $\hat{H}$, is again given by Eq. 3.6, but now, the system Hamiltonian $\hat{H}_S$ is given by,

$$\hat{H}_S = \frac{\hbar\omega_a}{2}\hat{\sigma}^z, \tag{3.56}$$

where ω_a is the frequency difference between the two atomic levels. The Hamiltonian for the coupling between the system and reservoir, $\hat{H}_{SR}$, is now given by,

$$\hat{H}_{SR} = \hbar \sum_j \left(\lambda_j \hat{\sigma}^+ \hat{r}_j + \lambda_j^* \hat{\sigma}^- \hat{r}_j^\dagger\right), \tag{3.57}$$

where $\hat{r}_j$ is the annihilation operator of the jth mode in the reservoir Hilbert space, λ_j is coupling rate between the system and the jth mode of the reservoir, and $\hat{\sigma}^-$, $\hat{\sigma}^+$, and $\hat{\sigma}^z$ are the Pauli operators, which obey,

$$
\begin{aligned}
\left[\hat{\sigma}^+, \hat{\sigma}^-\right] &= \hat{\sigma}^z \\
\left[\hat{\sigma}^z, \hat{\sigma}^+\right] &= 2\hat{\sigma}^+ \\
\left[\hat{\sigma}^-, \hat{\sigma}^-\right] &= 2\hat{\sigma}^-.
\end{aligned}
\tag{3.58}
$$

To find Eq. 3.57 in the interaction picture, $\hat{\sigma}^-$ in the interaction picture must be found,

$$
\begin{aligned}
\tilde{\hat{\sigma}}^-(t) &= e^{\frac{i}{\hbar}(\hat{H}_S+\hat{H}_R)t}\hat{\sigma}^- e^{-\frac{i}{\hbar}(\hat{H}_S+\hat{H}_R)t} \\
&= e^{\frac{i}{\hbar}\hat{H}_S t}\hat{\sigma}^- e^{-\frac{i}{\hbar}\hat{H}_S t} \\
&= \hat{\sigma}^- e^{-i\omega_a t},
\end{aligned}
\tag{3.59}
$$

Eqns. 3.26 and 3.27, and their Hermitian conjugates are substituted into Eq. 3.57, so that $\hat{H}_{SR}$ in the interaction picture is given by,

$$
\begin{aligned}
\tilde{\hat{H}}_{SR}(\tau) &= \hbar \sum_j \left(\lambda_j e^{i(\omega_c-\omega_j)\tau}\hat{\sigma}^+\hat{r}_j + \lambda_j^* e^{-i(\omega_c-\omega_j)\tau}\hat{\sigma}^-\hat{r}_j^\dagger \right), \\
&= i\hbar \left(\hat{\sigma}^+\hat{F}(\tau) - \hat{\sigma}^-\hat{F}^\dagger(\tau) \right),
\end{aligned}
\tag{3.60}
$$

where $\hat{F}(\tau)$ is defined identically to the way it was defined in Eq. 3.29. After making the replacements $\hat{a} \to \hat{\sigma}^-$ and $\hat{a}^\dagger \to \hat{\sigma}^+$, Eq. 3.60 has the exact same form as Eq. 3.28, so the derivation is identical, except now the decay rate for the atoms, γ, is given by,

$$
\gamma = 2\pi \mathcal{D}(\omega_a)\left|\lambda(\omega_a)\right|^2,
\tag{3.61}
$$

The master equation for the damped two level atom is therefore,

$$
\begin{aligned}
\frac{d}{dt}\tilde{\hat{\rho}}(t) &= -\frac{\gamma}{2}(\bar{n}+1)\left(\hat{\sigma}^+\hat{\sigma}^-\tilde{\hat{\rho}}(t) + \tilde{\hat{\rho}}(t)\hat{\sigma}^+\hat{\sigma}^- - 2\hat{\sigma}^-\tilde{\hat{\rho}}(t)\hat{\sigma}^+ \right) \\
&\quad -\frac{\gamma}{2}\bar{n}\left(\hat{\sigma}^-\hat{\sigma}^+\tilde{\hat{\rho}}(t) + \tilde{\hat{\rho}}(t)\hat{\sigma}^-\hat{\sigma}^+ - 2\hat{\sigma}^+\tilde{\hat{\rho}}(t)\hat{\sigma}^- \right).
\end{aligned}
\tag{3.62}
$$

3.4   Quantum Jumps

The master equation can be solved numerically, without any approximations, by using the quantum jumps algorithm. In this algorithm, many random pieces, or trajectories, of the Dyson expansion of the master equation are found, and they are then averaged over. Because these trajectories are chosen with the correct weights to reproduce the Dyson expansion of the master equation, the correct evolution is given. The Dyson expansion of the master equation, how to find the correct weights of specific trajectories, and how to preform the algorithm are described.

3.4.1 The Dyson Expansion of the Master Equation

A general master equation can be written in the form,

$$\frac{d}{dt}\hat{\rho}(t) = -\frac{\imath}{\hbar}\left[\hat{H}_0, \hat{\rho}(t)\right] - \frac{1}{2}\sum_{k=1}^{N}\left\{\hat{S}_k^+\hat{S}_k^-\hat{\rho}(t) + \hat{\rho}(t)\hat{S}_k^+\hat{S}_k^- - 2\hat{S}_k^-\hat{\rho}(t)\hat{S}_k^+\right\}, \tag{3.63}$$

where $\hat{H}_0$ describes the coherent evolution of the system, and

$$\hat{S}_k = \sqrt{\gamma_k}\hat{s}_k, \tag{3.64}$$

is a jump operator, where $\hat{s}_k$ is a system operator, and γ_k is a system decay rate.

We define an effective Hamiltonian as

$$\hat{H}_{eff} \equiv \hat{H}_0 - \frac{\imath\hbar}{2}\sum_k \hat{S}_k^\dagger\hat{S}_k, \tag{3.65}$$

so that Eq. 3.63 becomes

$$\frac{d}{dt}\hat{\rho}(t) = -\frac{\imath}{\hbar}\left(\hat{H}_{eff}\hat{\rho}(t) - \hat{\rho}(t)\hat{H}_{eff}^\dagger\right) + \sum_k \hat{S}_k^\dagger\hat{\rho}(t)\hat{S}_k. \tag{3.66}$$

Eq. 3.66 can now be written in the form

$$\frac{d}{dt}\hat{\rho}(t) = \hat{\mathscr{L}}\hat{\rho}(t), \tag{3.67}$$

with

$$\hat{\mathscr{L}}\hat{\rho}(t) = \hat{\mathscr{L}}_0\hat{\rho}(t) + \hat{\mathscr{L}}_J\hat{\rho}(t), \tag{3.68}$$

where

$$\begin{aligned}
\hat{\mathscr{L}}_0\hat{\rho}(t) &= -\frac{\imath}{\hbar}\left(\hat{H}_{eff}\hat{\rho}(t) - \hat{\rho}(t)\hat{H}_{eff}^\dagger\right), \\
\hat{\mathscr{L}}_J\hat{\rho}(t) &= \sum_k \hat{S}_k\hat{\rho}(t)\hat{S}_k^\dagger.
\end{aligned} \tag{3.69}$$

In an interaction picture defined by the transformation,

$$\tilde{\rho}(t) = e^{-\hat{\mathscr{L}}_0 t}\hat{\rho}(t), \tag{3.70}$$

Eq. 3.67 reduces to

$$\frac{d}{dt}\tilde{\rho}(t) = e^{-\hat{\mathscr{L}}_0 t}\hat{\mathscr{L}}_J e^{\hat{\mathscr{L}}_0 t}\tilde{\rho}(t). \tag{3.71}$$

Both sides of Eq. 3.71 are integrated from $t' = 0$ to $t' = t$ to obtain,

$$\tilde{\rho}(t) = \tilde{\rho}(0) + \int_0^t dt' e^{-\hat{\mathscr{L}}_0 t'} \hat{\mathscr{L}}_J e^{\hat{\mathscr{L}}_0 t'} \tilde{\rho}(t'). \tag{3.72}$$

The above equation is substituted into its self to yield

$$\tilde{\rho}(t) = \tilde{\rho}(0) + \int_0^t dt' e^{-\hat{\mathscr{L}}_0 t'} \hat{\mathscr{L}}_J e^{\hat{\mathscr{L}}_0 t'} \tilde{\rho}(0) + \int_0^t dt' \int_0^{t'} dt'' e^{-\hat{\mathscr{L}}_0 t'} \hat{\mathscr{L}}_J e^{\hat{\mathscr{L}}_0 (t'-t'')} \hat{\mathscr{L}}_J e^{\hat{\mathscr{L}}_0 t''} \tilde{\rho}(t'') \tag{3.73}$$

This procedure can be repeated an infinite number of times to yield the Dyson expansion for $\tilde{\rho}(t)$,

$$
\begin{aligned}
\tilde{\rho}(t) &= \tilde{\rho}(0) + \int_0^t dt' e^{-\hat{\mathscr{L}}_0 t'} \hat{\mathscr{L}}_J e^{\hat{\mathscr{L}}_0 t'} \tilde{\rho}(0) + \int_0^t dt' \int_0^{t'} dt'' e^{-\hat{\mathscr{L}}_0 t'} \hat{\mathscr{L}}_J e^{\hat{\mathscr{L}}_0 (t'-t'')} \hat{\mathscr{L}}_J e^{\hat{\mathscr{L}}_0 t''} \tilde{\rho}(0) \\
&\quad + \int_0^t d_1 \int_0^{t'} dt'' \int_0^{t''} dt''' e^{-\hat{\mathscr{L}}_0 t'} \hat{\mathscr{L}}_J e^{\hat{\mathscr{L}}_0 (t'-t'')} \hat{\mathscr{L}}_J e^{\hat{\mathscr{L}}_0 (t''-t''')} \hat{\mathscr{L}}_J e^{\hat{\mathscr{L}}_0 t'''} \tilde{\rho}(0) + \cdots \\
&= \tilde{\rho}(0) + \sum_{n=1}^{\infty} \int_0^t dt_n \int_0^{t_n} dt_{n-1} \cdots \int_0^{t_3} dt_2 \int_0^{t_2} dt_1 \\
&\quad \times e^{-\hat{\mathscr{L}}_0 t_n} \hat{\mathscr{L}}_J e^{\hat{\mathscr{L}}_0 (t_n - t_{n-1})} \hat{\mathscr{L}}_J \cdots \hat{\mathscr{L}}_J e^{\hat{\mathscr{L}}_0 (t_2 - t_1)} \hat{\mathscr{L}}_J e^{\hat{\mathscr{L}}_0 t_1} \tilde{\rho}(0).
\end{aligned}
\tag{3.74}
$$

Applying the inverse transformation that was applied in Eq. 3.70 yields the Dyson expansion in the Schrödinger picture,

$$
\begin{aligned}
\hat{\rho}(t) &= e^{\hat{\mathscr{L}}_0 t} \hat{\rho}(0) + \sum_{n=1}^{\infty} \int_0^t dt_n \int_0^{t_n} dt_{n-1} \cdots \int_0^{t_3} dt_2 \int_0^{t_2} dt_1 \\
&\quad \times e^{\hat{\mathscr{L}}_0 (t-t_n)} \hat{\mathscr{L}}_J e^{\hat{\mathscr{L}}_0 (t_n - t_{n-1})} \hat{\mathscr{L}}_J \cdots \hat{\mathscr{L}}_J e^{\hat{\mathscr{L}}_0 (t_2 - t_1)} \hat{\mathscr{L}}_J e^{\hat{\mathscr{L}}_0 t_1} \hat{\rho}(0),
\end{aligned}
\tag{3.75}
$$

where $\tilde{\rho}(0) = \hat{\rho}(0)$, by definition. After plugging the more explicit form of the jump Liouvillian into Eq. 3.75, it becomes,

$$
\begin{aligned}
\hat{\rho}(t) &= e^{\hat{\mathscr{L}}_0 t} \hat{\rho}(0) + \sum_{n=1}^{\infty} \sum_{k_1, \cdots, k_n} \int_0^t dt_n \int_0^{t_n} dt_{n-1} \cdots \int_0^{t_3} dt_2 \int_0^{t_2} dt_1 \\
&\quad \times e^{\hat{\mathscr{L}}_0 (t-t_n)} \hat{\mathscr{L}}_J^{(k_n)} e^{\hat{\mathscr{L}}_0 (t_n - t_{n-1})} \hat{\mathscr{L}}_J^{(k_{n-1})} \cdots \hat{\mathscr{L}}_J^{(k_2)} e^{\hat{\mathscr{L}}_0 (t_2 - t_1)} \hat{\mathscr{L}}_J^{(k_1)} e^{\hat{\mathscr{L}}_0 t_1} \hat{\rho}(0),
\end{aligned}
$$

$$\tag{3.76}$$

where

$$\hat{\mathscr{L}}_J^{(k_i)} = \hat{S}_{k_i} \hat{\rho}(t) \hat{S}_{k_i}^{\dagger}. \tag{3.77}$$

3.4.2   Definition of Quantum Trajectories

Justifying the name later, we define a "trajectory" to be the quantity inside all of the sums

and integrals in Eq. 3.76,

$$\hat{\rho}_{t_1,k_1;t_2,k_2;\cdots;t_n,k_n}(t) = e^{\hat{\mathscr{L}}_0(t-t_n)}\hat{\mathscr{L}}_J^{(k_n)}e^{\hat{\mathscr{L}}_0(t_n-t_{n-1})}\hat{\mathscr{L}}_J^{(k_{n-1})}\cdots\hat{\mathscr{L}}_J^{(k_2)}e^{\hat{\mathscr{L}}_0(t_2-t_1)}\hat{\mathscr{L}}_J^{(k_1)}e^{\hat{\mathscr{L}}_0 t_1}\hat{\rho}(0). \quad (3.78)$$

A trajectory depends explicitly on the values of k_i and the values of t_i that appear in its definition.

In a trajectory, there are only two types of operations being performed. One is the free evolution

under $\hat{H}_{eff}$,

$$\hat{\rho}(t_i) = e^{\hat{\mathscr{L}}_0(t_i-t_{i-1})}\hat{\rho}(t_{i-1}), \quad (3.79)$$

which is the solution to the equation,

$$\begin{aligned} \frac{d}{dt_i}\hat{\rho}(t_i) &= \hat{\mathscr{L}}_0\hat{\rho}(t_i) \\ &= \frac{1}{\imath\hbar}\left(\hat{H}_{eff}\hat{\rho}(t_i) - \hat{\rho}(t_i)\hat{H}_{eff}^\dagger\right), \end{aligned} \quad (3.80)$$

and the other is the application of a jump operator,

$$\hat{\mathscr{L}}_J^{(k)}\hat{\rho}(t_i) = \hat{S}_k\hat{\rho}(t_i)\hat{S}_k^\dagger. \quad (3.81)$$

If the initial condition for the density operator is chosen to be in a pure state,

$$\hat{\rho}(0) = |\psi(0)\rangle\langle\psi(0)|, \quad (3.82)$$

evolution under $\hat{H}_{eff}$ preserves the purity of the state and therefore is equivalent to a Schrödinger

type evolution,

$$\frac{d}{dt_i}|\psi(t_i)\rangle = \frac{1}{\imath\hbar}\hat{H}_{eff}|\psi(t_i)\rangle. \quad (3.83)$$

Also, the application of a jump operator to a pure state preserves the purity of the state,

$$\hat{\mathscr{L}}_J^{(k)}|\psi(t_i)\rangle\langle\psi(t_i)| = \hat{S}_k|\psi(t_i)\rangle\langle\psi(t_i)|\hat{S}_k^\dagger \Longleftrightarrow \hat{S}_k|\psi(t_i)\rangle. \quad (3.84)$$

Therefore, the trajectory can be rewritten in terms of state vectors as

$$
\begin{aligned}
|\psi_{t_1,k_1;t_2,k_2;\cdots;t_n,k_n}(t)\rangle &= e^{-\frac{i}{\hbar}\hat{H}_{eff}(t-t_n)}\hat{S}_{k_n}e^{-\frac{i}{\hbar}\hat{H}_{eff}(t_n-t_{n-1})}\hat{S}_{k_{n-1}}\cdots \\
&\quad \times\hat{S}_{k_2}e^{-\frac{i}{\hbar}\hat{H}_{eff}(t_2-t_1)}\hat{S}_{k_1}e^{-\frac{i}{\hbar}\hat{H}_{eff}t_1}|\psi(0)\rangle \\
&= \hat{U}_{t,t_n}\hat{S}_{k_n}\hat{U}_{t_n,t_{n-1}}\hat{S}_{k_{n-1}}\cdots\hat{S}_{k_2}\hat{U}_{t_2,t_1}\hat{S}_{k_1}\hat{U}_{t_1,0}|\psi(0)\rangle , \qquad (3.85)
\end{aligned}
$$

where

$$
\hat{U}_{t_i,t_{i-1}} \equiv e^{-\frac{i}{\hbar}\hat{H}_{eff}(t_i-t_{i-1})}. \tag{3.86}
$$

Eq. 3.85 says that a quantum trajectory is constructed by evolving an initial state $|\psi(0)\rangle$ with $\hat{H}_{eff}$ from 0 to t_1, and then applying the jump operator $\hat{S}_{k_1}$, evolving this resulting state from t_1 to t_2, applying the jump operator $\hat{S}_{k_2}$, and repeating this procedure n times.

3.4.3   Unraveling the Master Equation

After taking the rest of the trace of Eq. 3.76, it can be written as,

$$
\begin{aligned}
1 &= \langle\psi(0)|\hat{U}_{t,0}^{\dagger}\hat{U}_{t,0}|\psi(0)\rangle + \int_0^t dt_1 \sum_{k_1}\langle\psi(0)|\hat{U}_{t_1,0}^{\dagger}\hat{S}_{k_1}^{\dagger}\hat{U}_{t,t_1}^{\dagger}\hat{U}_{t,t_1}\hat{S}_{k_1}\hat{U}_{t_1,0}|\psi(0)\rangle + \cdots \\
&\quad + \sum_{k_1,\cdots,k_n}\int_0^t dt_n\cdots\int_0^{t_3} dt_2\int_0^{t_2} dt_1 \\
&\quad \times \langle\psi(0)|\hat{U}_{t_1,0}^{\dagger}\hat{S}_{k_1}^{\dagger}\hat{U}_{t_2,t_1}^{\dagger}\hat{S}_{k_2}^{\dagger}\cdots\hat{S}_{k_n}^{\dagger}\hat{U}_{t,t_n}^{\dagger}\hat{U}_{t,t_n}\hat{S}_{k_n}\cdots\hat{S}_{k_2}\hat{U}_{t_2,t_1}\hat{S}_{k_1}\hat{U}_{t_1,0}|\psi(0)\rangle + \cdots \quad (3.87)
\end{aligned}
$$

The first term in Eq. 3.87 can be identified as the probability that no jumps will occur in the interval $[0,t]$. The second term can be identified as the probability that exactly one jump will occur in the interval $[0,t]$, and likewise, the $(n+1)$th term can be identified as the probability that n jumps will occur in the interval $[0,t]$.

In the $(n+1)$th term, the sum over k_i is a sum over all of the possible jump operators that could be applied in the trajectory, $\hat{U}_{t,t_{i-1}}\hat{S}_{k_{i-1}}\cdots\hat{S}_{k_2}\hat{U}_{t_2,t_1}\hat{S}_{k_1}\hat{U}_{t_1,0}|\psi(0)\rangle$. Furthermore, the integral over dt_i is an integral over all the possible times that the ith jump operator is applied. Therefore, the quantity,

$$P_{(t_1,k_1;t_2,k_2;\cdots;t_n,k_n)} \equiv \langle\psi(0)| \hat{U}_{t_1,0}^\dagger \hat{S}_{k_1}^\dagger \hat{U}_{t_2,t_1}^\dagger \hat{S}_{k_2}^\dagger \cdots \hat{S}_{k_n}^\dagger \hat{U}_{t,t_n}^\dagger \hat{U}_{t,t_n} \hat{S}_{k_n} \cdots \hat{S}_{k_2} \hat{U}_{t_2,t_1} \hat{S}_{k_1} \hat{U}_{t_1,0} |\psi(0)\rangle \quad (3.88)$$

can be interpreted as the probability of the specific jumps $\{\hat{S}_{k_1}, \hat{S}_{k_2}, \cdots, \hat{S}_{k_n}\}$ occurring at the specific times $\{t_1, t_2, \cdots, t_n\}$ in the interval $[0, t]$.

Because of this, Eq. 3.85 is rewritten as

$$
\begin{aligned}
|\psi_{t_1,k_1;t_2,k_2;\cdots;t_n,k_n}(t)\rangle &= \sqrt{\langle\psi(0)| \hat{U}_{t_1,0}^\dagger \hat{S}_{k_1}^\dagger \hat{U}_{t_2,t_1}^\dagger \hat{S}_{k_2}^\dagger \cdots \hat{S}_{k_n}^\dagger \hat{U}_{t,t_n}^\dagger \cdots \hat{S}_{k_2} \hat{U}_{t_2,t_1} \hat{S}_{k_1} \hat{U}_{t_1,0} |\psi(0)\rangle} \\
&\times \frac{\hat{U}_{t,t_n} \hat{S}_{k_n} \hat{U}_{t_n,t_{n-1}} \hat{S}_{k_{n-1}} \cdots \hat{S}_{k_2} \hat{U}_{t_2,t_1} \hat{S}_{k_1} \hat{U}_{t_1,0} |\psi(0)\rangle}{\sqrt{\langle\psi(0)| \hat{U}_{t_1,0}^\dagger \hat{S}_{k_1}^\dagger \hat{U}_{t_2,t_1}^\dagger \hat{S}_{k_2}^\dagger \cdots \hat{S}_{k_n}^\dagger \hat{U}_{t,t_n}^\dagger \hat{U}_{t,t_n} \hat{S}_{k_n} \cdots \hat{S}_{k_2} \hat{U}_{t_2,t_1} \hat{S}_{k_1} \hat{U}_{t_1,0} |\psi(0)\rangle}} \\
&= \sqrt{P_{(t_1,k_1;t_2,k_2;\cdots;t_n,k_n)}} \frac{|\psi_{t_1,k_1;t_2,k_2;\cdots;t_n,k_n}(t)\rangle}{\sqrt{\langle\psi_{t_1,k_1;t_2,k_2;\cdots;t_n,k_n}(t)|\psi_{t_1,k_1;t_2,k_2;\cdots;t_n,k_n}(t)\rangle}}, \quad (3.89)
\end{aligned}
$$

Thus, we know the probability with which every single possible trajectory will come into the Dyson expansion of the master equation.

The probability of getting a specific trajectory can be split up into a product of the probabilities of intermediate steps. This can be seen by rewriting it as

$$
\begin{aligned}
P_{(t_1,k_1;t_2,k_2;\cdots;t_n,k_n)} &= \frac{\langle\psi(0)| \hat{U}_{t_1,0}^\dagger \hat{S}_{k_1}^\dagger \hat{U}_{t_2,t_1}^\dagger \hat{S}_{k_2}^\dagger \cdots \hat{S}_{k_n}^\dagger \hat{U}_{t,t_n}^\dagger \hat{U}_{t,t_n} \hat{S}_{k_n} \cdots \hat{S}_{k_2} \hat{U}_{t_2,t_1} \hat{S}_{k_1} \hat{U}_{t_1,0} |\psi(0)\rangle}{\langle\psi(0)| \hat{U}_{t_1,0}^\dagger \hat{S}_{k_1}^\dagger \hat{U}_{t_2,t_1}^\dagger \hat{S}_{k_2}^\dagger \cdots \hat{S}_{k_n}^\dagger \hat{S}_{k_n} \cdots \hat{S}_{k_2} \hat{U}_{t_2,t_1} \hat{S}_{k_1} \hat{U}_{t_1,0} |\psi(0)\rangle} \\
&\times \frac{\langle\psi(0)| \hat{U}_{t_1,0}^\dagger \hat{S}_{k_1}^\dagger \hat{U}_{t_2,t_1}^\dagger \hat{S}_{k_2}^\dagger \cdots \hat{S}_{k_n}^\dagger \hat{S}_{k_n} \cdots \hat{S}_{k_2} \hat{U}_{t_2,t_1} \hat{S}_{k_1} \hat{U}_{t_1,0} |\psi(0)\rangle}{\langle\psi(0)| \hat{U}_{t_1,0}^\dagger \hat{S}_{k_1}^\dagger \hat{U}_{t_2,t_1}^\dagger \hat{S}_{k_2}^\dagger \cdots \hat{S}_{k_{n-1}}^\dagger \hat{S}_{k_{n-1}} \cdots \hat{S}_{k_2} \hat{U}_{t_2,t_1} \hat{S}_{k_1} \hat{U}_{t_1,0} |\psi(0)\rangle} \\
&\times \cdots \\
&\times \frac{\langle\psi(0)| \hat{U}_{t_1,0}^\dagger \hat{S}_{k_1}^\dagger \hat{U}_{t_2,t_1}^\dagger \hat{S}_{k_2}^\dagger \hat{S}_{k_2} \hat{U}_{t_2,t_1} \hat{S}_{k_1} \hat{U}_{t_1,0} |\psi(0)\rangle}{\langle\psi(0)| \hat{U}_{t_1,0}^\dagger \hat{S}_{k_1}^\dagger \hat{S}_{k_1} \hat{U}_{t_1,0} |\psi(0)\rangle} \\
&\times \frac{\langle\psi(0)| \hat{U}_{t_1,0}^\dagger \hat{S}_{k_1}^\dagger \hat{S}_{k_1} \hat{U}_{t_1,0} |\psi(0)\rangle}{\langle\psi(0)|\psi(0)\rangle} \quad (3.90)
\end{aligned}
$$

Therefore, a trajectory with the record $(t_1, k_1; t_2, k_2; \cdots; t_n, k_n)$ can be constructed in a piecewise fashion, one time evolution and jump at time. It is beneficial to construct a trajectory this way, since it is fairly easy to obtain the probability distribution for getting the record $\{t_1, k_1; \cdots; t_i, k_i\}$ conditioned upon having gotten the record $\{t_1, k_1; \cdots; t_{i-1}, k_{i-1}\}$.

To find this, it is noted that for a small time interval $[0, \tau]$, the probability that an emission occurs at time τ should be related to the probability that no emission occurs on the interval. The

equation of motion for the norm of $|\psi(\tau)\rangle$ is

$$
\begin{aligned}
\frac{d}{dt}\langle\psi(\tau)|\psi(\tau)\rangle &= \frac{d\langle\psi(\tau)|}{dt}|\psi(\tau)\rangle + \langle\psi(\tau)|\frac{d|\psi(\tau)\rangle}{dt} \\
&= \langle\psi(\tau)|\left(-\frac{1}{\imath\hbar}\hat{H}_{eff}^{\dagger}\right)|\psi(\tau)\rangle + \langle\psi(\tau)|\left(\frac{1}{\imath\hbar}\hat{H}_{eff}\right)|\psi(\tau)\rangle \\
&= \langle\psi(\tau)|\left(-\frac{1}{\imath\hbar}\hat{H}_{eff}^{\dagger}\right) + \left(\frac{1}{\imath\hbar}\hat{H}_{eff}\right)|\psi(\tau)\rangle \\
&= \langle\psi(\tau)| -\frac{1}{\imath\hbar}\left(\hat{H}_0 + \frac{\imath\hbar}{2}\sum_k \hat{S}_k^{\dagger}\hat{S}_k\right) + \frac{1}{\imath\hbar}\left(\hat{H}_0 - \frac{\imath\hbar}{2}\sum_k \hat{S}_k^{\dagger}\hat{S}_k\right)|\psi(\tau)\rangle \\
&= -\sum_k \langle\psi(\tau)|\hat{S}_k^{\dagger}\hat{S}_k|\psi(\tau)\rangle .
\end{aligned}
\tag{3.91}
$$

Integrating both sides from $t'=0$ to $t'=\tau$,

$$
\langle\psi(\tau)|\psi(\tau)\rangle - \langle\psi(0)|\psi(0)\rangle = -\int_0^{\tau} dt' \sum_k \langle\psi(t')|\hat{S}_k^{\dagger}\hat{S}_k|\psi(t')\rangle ,
\tag{3.92}
$$

or since $\langle\psi(0)|\psi(0)\rangle = 1$,

$$
\int_0^{\tau} dt' \sum_k \langle\psi(t')|\hat{S}_k^{\dagger}\hat{S}_k|\psi(t')\rangle + \langle\psi(\tau)|\psi(\tau)\rangle = 1.
\tag{3.93}
$$

The above equation says that the loss of norm of $|\psi(\tau)\rangle$, produced by evolving with $\hat{H}_{eff}$, is taken up by the set of states $\left\{\hat{S}_k|\psi(\tau)\rangle\right\}$, and that the sum of the norm of both is equal to one.

3.4.4   The Quantum Jumps Algorithm

We are now in a position to describe the quantum Monte Carlo algorithm that simulates the Dyson expansion of the master equation. This algorithm can be performed as follows:

(1) Start in the state $|\psi_i\rangle$ at time t_i.

(2) Pick a random number r_1 in the interval $[0,1]$.

(3) Evolve $|\psi_i\rangle$ under $\hat{H}_{eff}$,

$$
|\psi(t)\rangle = e^{-\frac{\imath}{\hbar}\hat{H}_{eff}(t-t_i)}|\psi_i\rangle ,
\tag{3.94}
$$

until $\langle\psi(t)|\psi(t)\rangle = r_1$, and call this time t_{i+1}.

(4) Choose another random number r_2 on the interval $[0,1]$.

(5) Set r_2 equal to the cumulative distribution function of the conditional probabilities of a decay into mode k at time t_{i+1},

$$r_2 = \frac{\sum_{k=0}^{k=k_i} \langle \psi(t_{i+1})| \hat{S}_k^\dagger \hat{S}_k |\psi(t_{i+1})\rangle}{\sum_k \langle \psi(t_{i+1})| \hat{S}_k^\dagger \hat{S}_k |\psi(t_{i+1})\rangle}, \tag{3.95}$$

and solve for k_i, the ith random mode of decay.

(6) Apply the jump operator corresponding to k_i to the state $|\psi(t_{i+1})\rangle$, normalize, and call this new state

$$|\psi_{i+1}\rangle = \frac{\hat{S}_{k_i} |\psi(t_{i+1})\rangle}{\langle \psi(t_{i+1})| \hat{S}_{k_i}^\dagger \hat{S}_{k_i} |\psi(t_{i+1})\rangle}. \tag{3.96}$$

(7) Repeat steps 1-6 until t $\geq$ T, the time at which the experiment ends, keeping track of the pieces of the trajectory $|\psi_i\rangle$ and construct a trajectory out of these pieces,

$$|\psi_R\rangle = \begin{cases} |\psi_1\rangle & 0 \leq t < t_1 \\ |\psi_2\rangle & t_1 \leq t < t_2 \\ \vdots \\ |\psi_n\rangle & t_{n-1} \leq t < t_n, \end{cases} \tag{3.97}$$

where $R = \{t_1, k_1; t_2, k_2; \cdots ; t_n, k_n\}$, is the record of the random times and modes of decay of the trajectory.

(8) The simulation the Dyson expansion of the master equation, and hence the full time evolution of the density operator under the master equation, is given by repeating steps 1-7 N times, and forming,

$$\hat{\rho}(t) = \lim_{N \to \infty} \frac{1}{N} \sum_{m=1}^{N} \frac{|\psi_R\rangle_m \langle\psi_R|_m}{\langle\psi_R|_m |\psi_R\rangle_m}, \tag{3.98}$$

where $|\psi_R\rangle_m$ is the mth trajectory constructed by repeating steps 1-6 N times. The expectation value of any observable $\hat{\mathcal{O}}$ can be found by,

$$tr[\hat{\mathcal{O}}\hat{\rho}(t)] = \lim_{N \to \infty} \frac{1}{N} \sum_{m=1}^{N} \frac{\langle\psi_R|_m \hat{\mathcal{O}} |\psi_R\rangle_m}{\langle\psi_R|_m |\psi_R\rangle_m}. \tag{3.99}$$

3.4.5   Computer Simulation of Quantum Jumps

Although analytical solutions exist for simple systems, such as the damped harmonic oscillator, for more complex systems, for instance where multiple atoms are coupled to a cavity field, analytic solutions do not exist. To treat these more complex systems, the numerical solution methods must be relied on. Even so, it will be advantageous to demonstrate these methods for the simple systems since they are easily extended to more complicated systems.

In Fig. 3.1, the results of a computer simulation which implements the quantum jumps algorithm for the damped harmonic oscillator is shown. We consider the average number of excitation $\langle \hat{a}^\dagger(t)\hat{a}(t) \rangle$ in the damped mode with $\bar{n} = 1$ as a function of t/κ . For reference, the analytical solution for $\langle \hat{a}^\dagger(t)\hat{a}(t) \rangle$, Eq. 3.45, can be seen in black. In a single trajectory, which is shown in blue, there is a precise number of excitations until a random jump occurs at a random time. Then, the number of excitations is increased or decreased by one, depending on which jump operator was randomly chosen. When many of these random trajectories are averaged together, the correct evolution for $\langle \hat{a}^\dagger(t)\hat{a}(t) \rangle$ is approached, which is demonstrated in red, where 1000 random trajectories are averaged over.

3.5   Quantum State Diffusion

The unraveling of the master equation into quantum jumps is only one of many possible unravelings. It corresponds to a measurement scheme in which light from the system is directly detected on a photodetector. Another possible measurement scheme is homodyne detection, in which the light coming from the system is mixed with a strong laser called the local oscillator. An unraveling of the master equation that corresponds to homodyne detection yields the quantum state diffusion equation. It is basically the limit of the quantum jump method in which the mixed light from the system and local oscillator has an infinite number of infinitesimally small jumps.
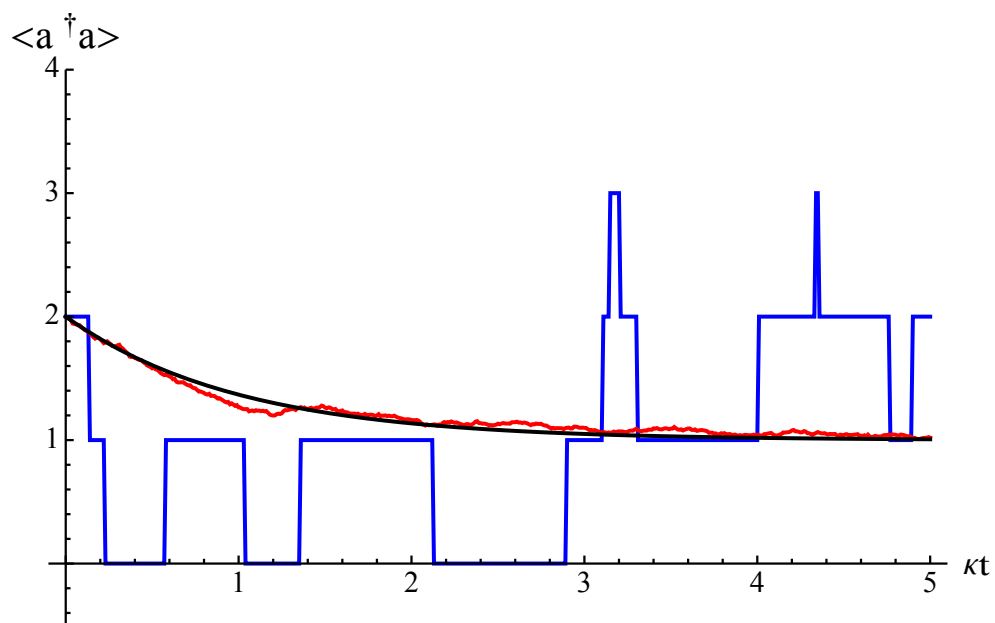
Figure 3.1: The quantum jumps algorithm is used to find $\langle \hat{a}^\dagger(t)\hat{a}(t)\rangle$ for a damped harmonic oscillator with $\bar{n} = 1$, and $\alpha(0) = 2$. The analytic expression for $\langle \hat{a}^\dagger(t)\hat{a}(t)\rangle$ is shown in black, a single trajectory is shown in blue, and 1000 trajectories is shown in red.

3.5.1 Master Equation of a Homodyne System

Consider the master equation for a damped single mode cavity field of linewidth κ,

$$\frac{d}{dt}\hat{\rho}(t) = -\frac{\kappa}{2}\left\{\hat{a}^{\dagger}\hat{a}\hat{\rho}(t) + \hat{\rho}(t)\hat{a}^{\dagger}\hat{a} - 2\hat{a}\hat{\rho}(t)\hat{a}^{\dagger}\right\}. \tag{3.100}$$

Where $\hat{a}$ is the annihilation operator of the mode, and $\hat{\rho}(t)$ is the system's density operator. If this damped cavity field is mixed with strong local oscillator of amplitude β through a beam splitter with high transmittivity, the amplitude of the resulting field that is incident on a detector is given by,

$$\hat{C} = \sqrt{\kappa}\left(\hat{a} + \beta\right), \tag{3.101}$$

where we have assumed that the phase of the local oscillator is zero. In an interaction picture that rotates at the frequency of the cavity field, the master equation describing this system is of the form of Eq. 3.63 with $\hat{S}_k \to \hat{C}$ and $\hat{H}_0$ dropped,

$$
\begin{aligned}
\frac{d}{dt}\hat{\rho}(t) &= -\frac{1}{2}\left\{\hat{C}^{\dagger}\hat{C}\hat{\rho}(t) + \hat{\rho}(t)\hat{C}^{\dagger}\hat{C} - 2\hat{C}\hat{\rho}(t)\hat{C}^{\dagger}\right\} \\
&= \hat{\mathscr{L}}_0\hat{\rho}(t) + \hat{\mathscr{L}}_J\hat{\rho}(t),
\end{aligned}
\tag{3.102}
$$

where,

$$\hat{\mathscr{L}}_0\hat{\rho}(t) = -\frac{\imath}{\hbar}\left(\hat{H}_{eff}\hat{\rho}(t) - \hat{\rho}(t)\hat{H}^{\dagger}_{eff}\right), \tag{3.103}$$

with

$$\hat{H}_{eff} = -\frac{\imath\hbar}{2}\hat{C}^{\dagger}\hat{C}, \tag{3.104}$$

and

$$\hat{\mathscr{L}}_J\hat{\rho}(t) = \hat{C}\hat{\rho}(t)\hat{C}^{\dagger}. \tag{3.105}$$

The Dyson expansion of Eq. 3.102 has the same form as Eq. 3.76, so that the analysis of the previous section carries over directly into this section.

In a time interval Δt, the photon flux that reaches the photodetector is

$$
\begin{aligned}
\left\langle \hat{C}^{\dagger}\hat{C}\right\rangle \Delta t &= \kappa\Delta t\left\langle \hat{a}^{\dagger} + \beta\right\rangle\left\langle \hat{a} + \beta\right\rangle \\
&\approx \kappa\Delta t\left(\beta\left\langle \hat{a}^{\dagger} + \hat{a}\right\rangle + \beta^2\right),
\end{aligned}
\tag{3.106}
$$

where $\langle \hat{a}^\dagger \hat{a} \rangle$ has been dropped since β is large. We assume $\kappa \Delta t \sim \beta^{-3/2}$, so that for large β, the number of photodetections $n = \kappa \Delta t \beta^2 \sim \beta^{1/2}$ is large, while the change of the system $\kappa \Delta t \beta \langle \hat{a}^\dagger + \hat{a} \rangle \sim \beta^{-1/2}$ is small.

By Eq. 3.87, the probability that n jumps occur in a time interval Δt, is given by

$$
\begin{aligned}
P_n(\Delta t) &= \int_0^{\Delta t} dt_n \cdots \int_0^{t_3} dt_2 \int_0^{t_2} dt_1 \\
&\quad \langle \psi(0) | \hat{U}_{t_1,0}^\dagger \hat{C}^\dagger \hat{U}_{t_2,t_1}^\dagger \hat{C}^\dagger \cdots \hat{C}^\dagger \hat{U}_{\Delta t,t_n}^\dagger \hat{U}_{\Delta t,t_n} \hat{C} \cdots \hat{C} \hat{U}_{t_2,t_1} \hat{C} \hat{U}_{t_1,0} | \psi(0) \rangle, \quad (3.107)
\end{aligned}
$$

where,

$$
\begin{aligned}
\hat{U}_{t_i,t_{i-1}} &= e^{-\frac{i}{\hbar} \hat{H}_{eff}(t_i - t_{i-1})} \\
&= e^{-\frac{1}{2} \hat{C}^\dagger \hat{C}(t_i - t_{i-1})}. \quad (3.108)
\end{aligned}
$$

To order $\mathcal{O}(\beta^{-3/2})$, $\hat{U}_{t_i,t_{i-1}}$ and $\hat{C}$ commute, so that,

$$
P_n(\Delta t) = \frac{t^n}{n!} \langle \psi(0) | \hat{U}_{\Delta t,0}^\dagger \left(\hat{C}^\dagger \hat{C} \right)^n \hat{U}_{t,0} | \psi(0) \rangle. \quad (3.109)
$$

After substitution of Eqns. 3.101 and 3.108, Eq. 3.109 becomes,

$$
P_n(\Delta t) = e^{-(\kappa \Delta t \beta^2)} \frac{(\kappa \Delta t \beta^2)^n}{n!} \left(1 + (n - (\kappa \Delta t \beta^2)) 2x \beta^{-1} + \mathcal{O}(\beta^{-3/2}) \right), \quad (3.110)
$$

where $x = \langle \psi(0) | (\hat{a}^\dagger + \hat{a})/2 | \psi(0) \rangle$. From Eq. 3.110, it can be shown [87] that the random variable n corresponding to this probability distribution can be approximated by a Gaussian random variable of the form,

$$
n = \kappa \Delta t \beta^2 \left(1 + 2x \beta^{-1} + \mathcal{O}(\beta^{-3/2}) \right) + \sqrt{\kappa} \Delta W \beta \left(1 + \mathcal{O}(\beta^{-1/2}) \right), \quad (3.111)
$$

where ΔW is a Wiener increment [34] which satisfies $\langle \Delta W \rangle_{avg}^2 = \Delta t$.

The state of a specific trajectory after a time interval Δt, is given by Eq. 3.85 which now takes the form,

$$
| \psi_R(\Delta t) \rangle = \hat{U}_{\Delta t,t_n} \hat{C} \hat{U}_{t_n,t_{n-1}} \hat{C} \cdots \hat{C} \hat{U}_{t_2,t_1} \hat{C} \hat{U}_{t_1,0} | \psi(0) \rangle, \quad (3.112)
$$

where the subscript R denotes a specific record of jump at times $R = \{t_1, t_2, \cdots, t_n\}$. To order

$\mathcal{O}(\beta^{-3/2})$, $\hat{U}_{t_i,t_{i-1}}$ and $\hat{C}$ commute, so that Eq. 3.112 can be rewritten,

$$
\begin{aligned}
|\psi_R(\Delta t)\rangle &= \hat{U}_{\Delta t,0}\hat{C}^n |\psi(0)\rangle \\
&= e^{-\frac{\kappa}{2}(\hat{a}^\dagger+\beta)(\hat{a}+\beta)\Delta t} \left(\sqrt{\kappa}(\hat{a}+\beta)\right)^n |\psi(0)\rangle .
\end{aligned}
\tag{3.113}
$$

Finally, Eq. 3.113 is expanded to $\mathcal{O}(\beta^{-3/2})$, Eq. 3.111 is substituted for n, and the limit of $\beta \to 0$ is taken, resulting in the quantum state diffusion equation for a trajectory corresponding to homodyne measurement,

$$
|\psi_R(t+\Delta t)\rangle = \left\{1 + \kappa\Delta t\left(-\frac{1}{2}\hat{a}^\dagger\hat{a} + 2x(t)\hat{a}\right) + \sqrt{\kappa}\Delta W(t)\hat{a}\right\} |\psi_R(t)\rangle .
\tag{3.114}
$$

In numerical simulations, Eq. 3.114 must be normalized after each time step. The density operator is then reconstructed by simulating N random trajectories, and forming,

$$
\hat{\rho}(t) = \lim_{N\to\infty} \frac{1}{N}\sum_{m=1}^{N} \frac{|\psi_R\rangle_m \langle\psi_R|_m}{\langle\psi_R|_m |\psi_R\rangle_m},
\tag{3.115}
$$

The expectation value of any observable $\hat{\mathcal{O}}$ can be found by,

$$
tr[\hat{\mathcal{O}}\hat{\rho}(t)] = \lim_{N\to\infty} \frac{1}{N}\sum_{m=1}^{N} \frac{\langle\psi_R|_m \hat{\mathcal{O}} |\psi_R\rangle_m}{\langle\psi_R|_m |\psi_R\rangle_m}.
\tag{3.116}
$$

3.5.2 Computer Simulation of the Quantum State Diffusion Equation

In Fig. 3.2, the results of a computer simulation which solves the quantum state diffusion equation for random trajectories, for the damped harmonic oscillator is shown. We consider the average number of excitation $\langle\hat{a}^\dagger(t)\hat{a}(t)\rangle$ in the damped mode with $\bar{n}=1$ as a function of t/κ. For reference, the analytical solution for $\langle\hat{a}^\dagger(t)\hat{a}(t)\rangle$, Eq. 3.45, can be seen in black. In a single trajectory, which is shown in blue, there are many very small jumps, so that the number of excitations randomly diffuses in time. When many of these random trajectories are averaged together, the correct evolution for $\langle\hat{a}^\dagger(t)\hat{a}(t)\rangle$ is approached, which is demonstrated in red, where 1000 random trajectories are averaged over.
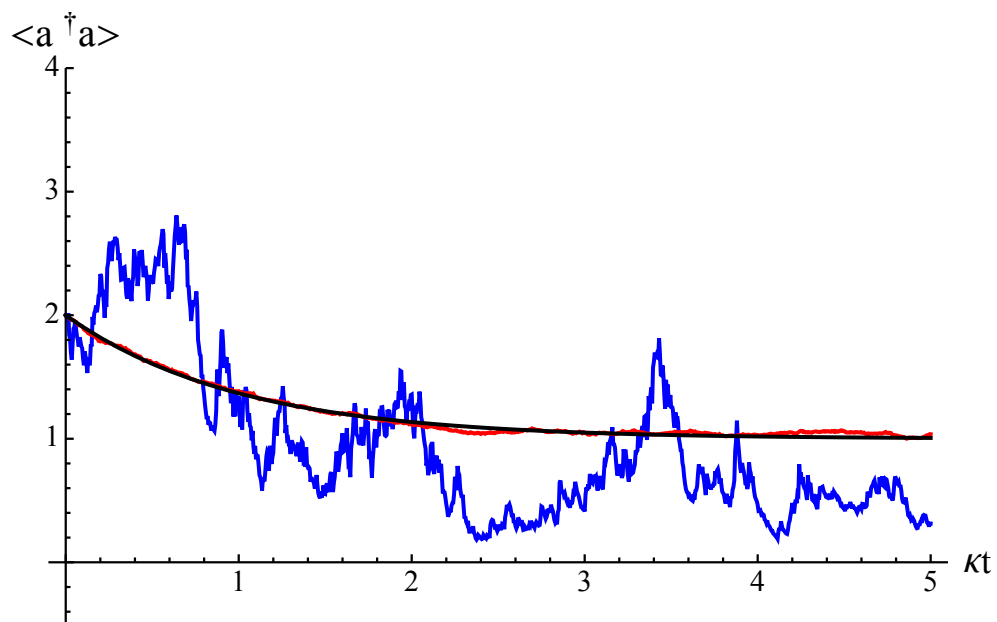
Figure 3.2: The quantum state diffusion equation is solved for random trajectories which are used to find $\langle \hat{a}^\dagger(t)\hat{a}(t) \rangle$ for a damped harmonic oscillator with $\bar{n} = 1$, and $\alpha(0) = 2$. The analytic expression for $\langle \hat{a}^\dagger(t)\hat{a}(t) \rangle$ is shown in black, a single trajectory is shown in blue, and 1000 trajectories is shown in red.

3.6   The Master Equation for a General Cavity QED System

In a cavity QED system, in which energy is re-supplied to the atoms, energy can not be supplied directly at the frequency of the considered transition. Otherwise, when a large number of atoms become excited, stimulated emission would occur, and the inversion would never become positive. However, if a higher third level is repumped, and this level spontaneously decays down, the system can achieve positive inversion. This repumping process can be thought of as reverse spontaneous emission, and can be modeled with the master equation for a two level atom with $\gamma \to w$, $\hat{\sigma}^+ \to \hat{\sigma}^-$, and $\hat{\sigma}^- \to \hat{\sigma}^+$, where w is now the repumping rate.

In addition to the damping of the excited state population due to spontaneous emission, it is also possible that decoherence of the phase between excited and ground states can occur. This dephasing can occur, for instance, due to elastic collisions in an atomic cloud. It can be modeled by a system reservoir coupling Hamiltonian $\hat{H}_{SR}$ of the form,

$$\hat{H}_{SR} = \hbar \sum_j \left(\lambda_j \hat{\sigma}^z \hat{r}_j + \lambda_j^* \hat{\sigma}^z \hat{r}_j^\dagger \right), \tag{3.117}$$

where $\hat{r}_j$ is the annihilation operator of the jth mode in the reservoir Hilbert space, λ_j is coupling rate between the system and the jth mode of the reservoir, and $\hat{\sigma}^z$ is a Pauli operator, which obeys Eqns. 3.58. This form of $\hat{H}_{SR}$ models the dephasing between excited and ground states, since the action of the operator $\hat{\sigma}^z$ is to change the relative phase between the excited and ground state by π. Eq. 3.117 is the same as Eq. 3.57 with $\hat{\sigma}^+ \to \hat{\sigma}^z$. Therefore the derivation is preformed in the same way as in Sec. 3.3, with $\gamma \to 1/2T_2$, where $1/T_2$ is the dephasing rate. Then, the master equation describing atomic dephasing is given by,

$$\begin{aligned}
\frac{d}{dt}\tilde{\rho}(t) &= -\frac{1}{4T_2}\left(\bar{n}+1\right)\left(\hat{\sigma}^z\hat{\sigma}^z\tilde{\rho}(t) + \tilde{\rho}(t)\hat{\sigma}^z\hat{\sigma}^z - 2\hat{\sigma}^z\tilde{\rho}(t)\hat{\sigma}^z\right) \\
&\quad -\frac{1}{4T_2}\bar{n}\left(\hat{\sigma}^z\hat{\sigma}^z\tilde{\rho}(t) + \tilde{\rho}(t)\hat{\sigma}^z\hat{\sigma}^z - 2\hat{\sigma}^z\tilde{\rho}(t)\hat{\sigma}^z\right) \\
&= \frac{1}{2T_2}\left(\bar{n}+1\right)\left(\hat{\sigma}^z\tilde{\rho}(t)\hat{\sigma}^z - \tilde{\rho}(t)\right)\frac{1}{2T_2}\bar{n}\left(\hat{\sigma}^z\tilde{\rho}(t)\hat{\sigma}^z - \tilde{\rho}(t)\right).
\end{aligned} \tag{3.118}$$

Many cavity QED experiments are done at close to zero temperature, so that average number of thermal excitations $\bar{n} = 0$. Putting it all together, the master equation for N two level atoms

of frequency ω_a, decay rate γ, repumping rate w, and dephasing rate $\frac{1}{2T_2}$, coupled with rate g to a single mode cavity of decay rate κ is given by,

$$\frac{d}{dt}\hat{\rho} = -\frac{\imath}{\hbar}\left[\hat{H},\hat{\rho}\right] - \frac{\kappa}{2}\left\{\hat{a}^\dagger\hat{a}\hat{\rho} + \hat{\rho}\hat{a}^\dagger\hat{a} - 2\hat{a}\hat{\rho}\hat{a}^\dagger\right\} - \frac{\gamma}{2}\sum_{j=1}^{N}\left\{\hat{\sigma}_j^+\hat{\sigma}_j^-\hat{\rho} + \hat{\rho}\hat{\sigma}_j^+\hat{\sigma}_j^- - 2\hat{\sigma}_j^-\hat{\rho}\hat{\sigma}_j^+\right\}$$

$$- \frac{w}{2}\sum_{j=1}^{N}\left\{\hat{\sigma}_j^-\hat{\sigma}_j^+\hat{\rho} + \hat{\rho}\hat{\sigma}_j^-\hat{\sigma}_j^+ - 2\hat{\sigma}_j^+\hat{\rho}\hat{\sigma}_j^-\right\} + \frac{1}{2T_2}\sum_{j=1}^{N}\left\{\hat{\sigma}_j^z\hat{\rho}\hat{\sigma}_j^z - \hat{\rho}\right\}, \tag{3.119}$$

with,

$$\hat{H} = \frac{\hbar\omega_a}{2}\sum_{j=1}^{N}\hat{\sigma}_j^z + \hbar\omega_c\hat{a}^\dagger\hat{a} + \frac{\hbar g}{2}\sum_{j=1}^{N}\left(\hat{\sigma}_j^-\hat{a}^\dagger + \hat{\sigma}_j^+\hat{a}\right), \tag{3.120}$$

where $\hat{\rho}$ is the system density operator, and $\hat{a}$ is the annihilation operator for the cavity mode. The jth atom is described by the operators,

$$\hat{\sigma}_j^- = |g\rangle_j\langle e|_j$$

$$\hat{\sigma}_j^+ = |e\rangle_j\langle g|_j$$

$$\hat{\sigma}_j^z = |e\rangle_j\langle e|_j - |g\rangle_j\langle g|_j$$

$$\hat{\mathbb{1}}_j = |e\rangle_j\langle e|_j + |g\rangle_j\langle g|_j, \tag{3.121}$$

where $|e\rangle_j$ is the excited state, $|g\rangle_j$ is the ground state, and $\hat{\mathbb{1}}_j$ is the identity operator for the jth atom. Then we can use the fact that $|e\rangle_j$ and $|g\rangle_j$ are orthonormal, i.e. $\langle e|_i|g\rangle_i = 0$, and $\langle e|_i|e\rangle_i = \langle g|_i|g\rangle_i = 1$, to simplify calculations. The commutation relations between the atomic operators are,

$$\left[\hat{\sigma}_i^+, \hat{\sigma}_j^-\right] = \hat{\sigma}_i^z\delta_{ij}$$

$$\left[\hat{\sigma}_i^z, \hat{\sigma}_j^+\right] = 2\hat{\sigma}_i^+\delta_{ij}$$

$$\left[\hat{\sigma}_i^-, \hat{\sigma}_j^-\right] = 2\hat{\sigma}_i^-\delta_{ij}, \tag{3.122}$$

where δ_{ij} is the Kronecker delta.

3.7 Cumulant Expansion to Second Order

The quantum jumps and quantum state diffusion methods are only able to describe very small systems, with atom numbers $N \sim 10$. This is because the basis used to describe the system

scales with atom number N as 2^N. Many experiments done today have atom numbers $N \sim 10^5$ or higher, and in order to describe these larger systems, approximation methods must be employed. The cumulant expansion is one such approximate method that allows large systems to be described. In this method, equations for expectation values of observables of interest will be derived. These equations will couple to higher order moments, which will in turn couple to even higher order moments. We choose to factorize all moments higher that second order, using the cumulant expansion [56]. This will allow a closed set of equations for expectation values to be derived. With the help of the quantum regression theorem, and again using the cumulant expansion, equations for two-time expectation values can also be derived.

3.7.1   Closed Set of One-Time Expectation Values

We begin by deriving the equation of motion for $\langle \hat{\sigma}_1^z \rangle$, the inversion for a single atom of the atomic ensemble. Using Eq. 3.119,

$$
\begin{aligned}
\frac{d}{dt} \langle \hat{\sigma}_1^z \rangle &= tr[\hat{\sigma}_1^z \frac{d}{dt} \hat{\rho}] \\
&= -\frac{\imath \omega_a}{2} \sum_{j=1}^{N} tr \left[\hat{\sigma}_1^z \hat{\sigma}_j^z \hat{\rho} - \hat{\sigma}_j^z \hat{\sigma}_1^z \hat{\rho} \right] - \frac{\imath g}{2} \sum_{j=1}^{N} tr \left[\hat{\sigma}_1^z \left(\hat{\sigma}_j^- \hat{a}^\dagger + \hat{\sigma}_j^+ \hat{a} \right) \hat{\rho} - \left(\hat{\sigma}_j^- \hat{a}^\dagger + \hat{\sigma}_j^+ \hat{a} \right) \hat{\sigma}_1^z \hat{\rho} \right] \\
&\quad -\frac{\gamma}{2} \sum_{j=1}^{N} tr \left[\hat{\sigma}_1^z \hat{\sigma}_j^+ \hat{\sigma}_j^- \hat{\rho} + \hat{\sigma}_j^+ \hat{\sigma}_j^- \hat{\sigma}_1^z \hat{\rho} - 2 \hat{\sigma}_j^+ \hat{\sigma}_1^z \hat{\sigma}_j^- \hat{\rho} \right] \\
&\quad -\frac{w}{2} \sum_{j=1}^{N} tr \left[\hat{\sigma}_1^z \hat{\sigma}_j^- \hat{\sigma}_j^+ \hat{\rho} + \hat{\sigma}_j^- \hat{\sigma}_j^+ \hat{\sigma}_1^z \hat{\rho} - 2 \hat{\sigma}_j^- \hat{\sigma}_1^z \hat{\sigma}_j^+ \hat{\rho} \right] \\
&\quad +\frac{1}{2T_2} \sum_{j=1}^{N} tr \left[\hat{\sigma}_j^z \hat{\sigma}_1^z \hat{\sigma}_j^z \hat{\rho} - \hat{\sigma}_1^z \hat{\rho} \right],
\end{aligned}
\tag{3.123}
$$

where the cyclic property of the trace has been used. After using Eq. 3.121 to simplify, Eq. 3.123 becomes,

$$
\begin{aligned}
\frac{d}{dt}\left\langle \hat{\sigma}_1^z \right\rangle &= -\frac{\imath g}{2} tr\left[-\hat{\sigma}_j^- \hat{a}^\dagger + \hat{\sigma}_j^+ \hat{a}\hat{\rho} - \hat{\sigma}_j^- \hat{a}^\dagger + \hat{\sigma}_j^+ \hat{a} \right] \\
&\quad -\frac{\gamma}{2} tr\left[\hat{\sigma}_1^+ \hat{\sigma}_1^- \hat{\rho} + \hat{\sigma}_1^+ \hat{\sigma}_1^- \hat{\rho} + 2\hat{\sigma}_1^+ \hat{\sigma}_1^- \hat{\rho} \right] \\
&\quad -\frac{w}{2} tr\left[-\hat{\sigma}_1^- \hat{\sigma}_1^+ \hat{\rho} - \hat{\sigma}_1^- \hat{\sigma}_1^+ \hat{\rho} - 2\hat{\sigma}_1^- \hat{\sigma}_1^+ \hat{\rho} \right] \\
&= \imath g \left(\left\langle \hat{a}^\dagger \hat{\sigma}_1^- \right\rangle - \left\langle \hat{a}\hat{\sigma}_1^+ \right\rangle \right) - (w+\gamma)\left(\langle \hat{\sigma}_1^z \rangle - d_0 \right),
\end{aligned}
\tag{3.124}
$$

where $d_0 \equiv \frac{w-\gamma}{w+\gamma}$. Since $\left\langle \hat{a}^\dagger \hat{\sigma}_1^- \right\rangle$ couples into Eq. 3.124, its equation must also be calculated. Eq. 3.119 is used again to find,

$$
\begin{aligned}
\frac{d}{dt}\left\langle \hat{a}^\dagger \hat{\sigma}_1^- \right\rangle &= tr[\hat{a}^\dagger \hat{\sigma}_1^- \frac{d}{dt}\hat{\rho}] \\
&= -\frac{\imath \omega_a}{2} \sum_{j=1}^{N} tr\left[\hat{a}^\dagger \hat{\sigma}_1^- \hat{\sigma}_j^z \hat{\rho} - \hat{\sigma}_j^z \hat{a}^\dagger \hat{\sigma}_1^- \hat{\rho} \right] - \frac{\imath \omega_c}{2} tr\left[\hat{a}^\dagger \hat{\sigma}_1^- \hat{a}^\dagger \hat{a}\hat{\rho} - \hat{a}^\dagger \hat{a}\hat{a}^\dagger \hat{\sigma}_1^- \hat{\rho} \right] \\
&\quad -\frac{\imath g}{2} \sum_{j=1}^{N} tr\left[\hat{a}^\dagger \hat{\sigma}_1^- \left(\hat{\sigma}_j^- \hat{a}^\dagger + \hat{\sigma}_j^+ \hat{a} \right)\hat{\rho} - \left(\hat{\sigma}_j^- \hat{a}^\dagger + \hat{\sigma}_j^+ \hat{a} \right) \hat{a}^\dagger \hat{\sigma}_1^- \hat{\rho} \right] \\
&\quad -\frac{\kappa}{2} tr\left[\hat{a}^\dagger \hat{\sigma}_1^- \hat{a}^\dagger \hat{a}\hat{\rho} + \hat{a}^\dagger \hat{a}\hat{a}^\dagger \hat{\sigma}_1^- \hat{\rho} - 2\hat{a}^\dagger \hat{a}^\dagger \hat{\sigma}_1^- \hat{a}\hat{\rho} \right] \\
&\quad -\frac{\gamma}{2} \sum_{j=1}^{N} tr\left[\hat{a}^\dagger \hat{\sigma}_1^- \hat{\sigma}_j^+ \hat{\sigma}_j^- \hat{\rho} + \hat{\sigma}_j^+ \hat{\sigma}_j^- \hat{a}^\dagger \hat{\sigma}_1^- \hat{\rho} - 2\hat{\sigma}_j^+ \hat{a}^\dagger \hat{\sigma}_1^- \hat{\sigma}_j^- \hat{\rho} \right] \\
&\quad -\frac{w}{2} \sum_{j=1}^{N} tr\left[\hat{a}^\dagger \hat{\sigma}_1^- \hat{\sigma}_j^- \hat{\sigma}_j^+ \hat{\rho} + \hat{\sigma}_j^- \hat{\sigma}_j^+ \hat{a}^\dagger \hat{\sigma}_1^- \hat{\rho} - 2\hat{\sigma}_j^- \hat{a}^\dagger \hat{\sigma}_1^- \hat{\sigma}_j^+ \hat{\rho} \right] \\
&\quad +\frac{1}{2T_2} \sum_{j=1}^{N} tr\left[\hat{\sigma}_j^z \hat{a}^\dagger \hat{\sigma}_1^- \hat{\sigma}_j^z \hat{\rho} - \hat{a}^\dagger \hat{\sigma}_1^- \hat{\rho} \right].
\end{aligned}
\tag{3.125}
$$

With the use of the commutation relations for creation and annihilation operators, Eq. 3.43, and with the help of Eqns. 3.121, Eq. 3.125 becomes,

$$
\begin{aligned}
\frac{d}{dt}\left\langle \hat{a}^\dagger \hat{\sigma}_1^- \right\rangle &= -\frac{\imath \omega_a}{2} tr\left[\hat{a}^\dagger \hat{\sigma}_1^- \hat{\rho} + \hat{a}^\dagger \hat{\sigma}_1^- \hat{\rho} \right] + \imath \omega_c tr\left[\hat{a}^\dagger \hat{\sigma}_1^- \hat{\rho} \right] \\
&\quad -\frac{\imath g}{2} \sum_{j=1}^{N} tr\left[\hat{a}^\dagger \hat{a}\hat{\sigma}_1^- \hat{\sigma}_j^+ \hat{\rho} - \hat{a}\hat{a}^\dagger \hat{\sigma}_j^+ \hat{\sigma}_1^- \hat{\rho} \right] \\
&\quad -\frac{\kappa}{2} tr\left[\hat{a}^\dagger \hat{\sigma}_1^- \hat{\rho} \right] - \frac{\gamma}{2} tr\left[\hat{a}^\dagger \hat{\sigma}_1^- \hat{\rho} \right] - \frac{w}{2} tr\left[\hat{a}^\dagger \hat{\sigma}_1^- \hat{\rho} \right] - \frac{1}{T_2} tr\left[\hat{a}^\dagger \hat{\sigma}_1^- \hat{\rho} \right].
\end{aligned}
\tag{3.126}
$$

The coupling term requires closer attention, since here, the $j \neq 1$ terms in the sum are not zero:

$$
\begin{aligned}
\frac{d}{dt} \left\langle \hat{a}^\dagger \hat{\sigma}_1^- \right\rangle &= \left(-\imath \omega_a + \imath \omega_c - \frac{\kappa}{2} - \frac{\gamma}{2} - \frac{w}{2} - \frac{1}{T_2} \right) \left\langle \hat{a}^\dagger \hat{\sigma}_1^- \right\rangle \\
&\quad - \frac{\imath g}{2} tr \left[\hat{a}^\dagger \hat{a} \hat{\sigma}_1^- \hat{\sigma}_1^+ \hat{\rho} - \hat{a} \hat{a}^\dagger \hat{\sigma}_1^+ \hat{\sigma}_1^- \hat{\rho} \right] - \frac{\imath g}{2} \sum_{j \neq 1}^{N} tr \left[\hat{a}^\dagger \hat{a} \hat{\sigma}_1^- \hat{\sigma}_j^+ \hat{\rho} - \hat{a} \hat{a}^\dagger \hat{\sigma}_j^+ \hat{\sigma}_1^- \hat{\rho} \right] \\
&= \left(-\imath \delta - \frac{\kappa}{2} - \frac{\gamma}{2} - \frac{w}{2} - \frac{1}{T_2} \right) \left\langle \hat{a}^\dagger \hat{\sigma}_1^- \right\rangle \\
&\quad + \frac{\imath g}{2} \left(\left\langle \hat{a}^\dagger \hat{a} \hat{\sigma}_1^z \right\rangle + \frac{1}{2} \left(1 + \langle \hat{\sigma}_1^z \rangle \right) \right) + \frac{\imath g}{2} (N-1) \left\langle \hat{\sigma}_1^+ \hat{\sigma}_2^- \right\rangle ,
\end{aligned}
\tag{3.127}
$$

where $\delta \equiv \omega_a - \omega_c$, and the identical atom assumption has been invoked in the last term. It is clear now that it is the coupling term that causes nth order moments to couple to $(n+1)$th order moments. We therefore use the cumulant expansion [56], dropping cumulants higher than second order. Applying this to $\left\langle \hat{a}^\dagger \hat{a} \hat{\sigma}_1^z \right\rangle$ yields,

$$
\begin{aligned}
\left\langle \hat{a}^\dagger \hat{a} \hat{\sigma}_1^z \right\rangle &= \left\langle \hat{a}^\dagger \hat{a} \right\rangle \langle \hat{\sigma}_1^z \rangle + \left\langle \hat{a}^\dagger \hat{\sigma}_1^z \right\rangle \langle \hat{a} \rangle + \langle \hat{a} \hat{\sigma}_1^z \rangle \left\langle \hat{a}^\dagger \right\rangle - 2 \left\langle \hat{a}^\dagger \right\rangle \langle \hat{a} \rangle \langle \hat{\sigma}_1^z \rangle \\
&= \left\langle \hat{a}^\dagger \hat{a} \right\rangle \langle \hat{\sigma}_1^z \rangle ,
\end{aligned}
\tag{3.128}
$$

where the last line follows from the fact that $\langle \hat{a} \rangle = 0$. Eq. 3.128 is substituted into Eq. 3.127 to obtain,

$$
\begin{aligned}
\frac{d}{dt} \left\langle \hat{a}^\dagger \hat{\sigma}_1^- \right\rangle &= \left(-\imath \omega_a + \imath \omega_c - \frac{\kappa}{2} - \frac{\gamma}{2} - \frac{w}{2} - \frac{1}{T_2} \right) \left\langle \hat{a}^\dagger \hat{\sigma}_1^- \right\rangle \\
&\quad + \frac{\imath g}{2} \left(\left\langle \hat{a}^\dagger \hat{a} \right\rangle \langle \hat{\sigma}_1^z \rangle + \frac{1}{2} \left(1 + \langle \hat{\sigma}_1^z \rangle \right) \right) + \frac{\imath g}{2} (N-1) \left\langle \hat{\sigma}_1^+ \hat{\sigma}_2^- \right\rangle .
\end{aligned}
\tag{3.129}
$$

The equations of motion of both $\langle \hat{a}^\dagger \hat{a} \rangle$ and $\langle \hat{\sigma}_1^+ \hat{\sigma}_2^- \rangle$ are now calculated, and the cumulant expansion is used to expand moments higher than second order, dropping all cumulants of higher than second order. Then, we arrive at the closed set of equations,

$$
\begin{aligned}
\frac{d}{dt} \langle \hat{\sigma}_1^z \rangle &= \imath g \left(\left\langle \hat{a}^\dagger \hat{\sigma}_1^- \right\rangle - \langle \hat{a} \hat{\sigma}_1^+ \rangle \right) - (w + \gamma) \left(\langle \hat{\sigma}_1^z \rangle - d_0 \right) \\
\frac{d}{dt} \left\langle \hat{a}^\dagger \hat{\sigma}_1^- \right\rangle &= \left(-\imath \delta - \frac{\kappa}{2} - \frac{\gamma}{2} - \frac{w}{2} - \frac{1}{T_2} \right) \left\langle \hat{a}^\dagger \hat{\sigma}_1^- \right\rangle \\
&\quad + \frac{\imath g}{2} \left(\left\langle \hat{a}^\dagger \hat{a} \right\rangle \langle \hat{\sigma}_1^z \rangle + \frac{1}{2} \left(1 + \langle \hat{\sigma}_1^z \rangle \right) \right) + \frac{\imath g}{2} (N-1) \left\langle \hat{\sigma}_1^+ \hat{\sigma}_2^- \right\rangle \\
\frac{d}{dt} \langle \hat{\sigma}_1^+ \hat{\sigma}_2^- \rangle &= - \left(w + \gamma + \frac{2}{T_2} \right) \langle \hat{\sigma}_1^+ \hat{\sigma}_2^- \rangle - \frac{\imath g}{2} \langle \hat{\sigma}_1^z \rangle \left(\left\langle \hat{a}^\dagger \hat{\sigma}_1^- \right\rangle - \langle \hat{a} \hat{\sigma}_1^+ \rangle \right) \\
\frac{d}{dt} \left\langle \hat{a}^\dagger \hat{a} \right\rangle &= -\kappa \left\langle \hat{a}^\dagger \hat{a} \right\rangle - \frac{\imath N g}{2} \left(\left\langle \hat{a}^\dagger \hat{\sigma}_1^- \right\rangle - \langle \hat{a} \hat{\sigma}_1^+ \rangle \right) ,
\end{aligned}
\tag{3.130}
$$

with $d_0 \equiv \frac{w-\gamma}{w+\gamma}$. Eqns. 3.130 can be solved on a computer with a numerical differential equation solver in fractions of a second. Even so, for most purposes we are only interested in the steady state solution, which can be found by setting the time derivatives to zero, and solving the resulting algebraic equations. These algebraic equations can also be easily solved on a computer, which is what is typically done in practice. However, for a broad strokes understanding of the physics, simple analytic solutions are desirable, and can be obtained in the limit of large N. We set $\delta = \frac{1}{T_2} = \gamma = 0$, for simplicity, and combine Eqns. 3.130 with the time derivatives set to zero,

$$
\begin{aligned}
0 &= \imath g \left(\left\langle \hat{a}^\dagger \hat{\sigma}_1^- \right\rangle - \left\langle \hat{a} \hat{\sigma}_1^+ \right\rangle \right) - w \left(\langle \hat{\sigma}_1^z \rangle - d_0 \right), \\
0 &= \left(-\frac{\kappa}{2} - \frac{w}{2} \right) \left\langle \hat{a}^\dagger \hat{\sigma}_1^- \right\rangle + \frac{\imath g}{2} \left(\left\langle \hat{a}^\dagger \hat{a} \right\rangle \langle \hat{\sigma}_1^z \rangle + \frac{1}{2} \left(1 + \langle \hat{\sigma}_1^z \rangle \right) \right) + \frac{\imath g}{2} (N-1) \left\langle \hat{\sigma}_1^+ \hat{\sigma}_2^- \right\rangle \\
0 &= -w \left\langle \hat{\sigma}_1^+ \hat{\sigma}_2^- \right\rangle - \frac{\imath g}{2} \langle \hat{\sigma}_1^z \rangle \left(\left\langle \hat{a}^\dagger \hat{\sigma}_1^- \right\rangle - \left\langle \hat{a} \hat{\sigma}_1^+ \right\rangle \right) \\
0 &= -\kappa \left\langle \hat{a}^\dagger \hat{a} \right\rangle - \frac{\imath N g}{2} \left(\left\langle \hat{a}^\dagger \hat{\sigma}_1^- \right\rangle - \left\langle \hat{a} \hat{\sigma}_1^+ \right\rangle \right).
\end{aligned}
\tag{3.131}
$$

Then, after defining,

$$
C \equiv \frac{N g^2}{w + \kappa} \qquad \epsilon \equiv \frac{\kappa}{N(w + \kappa)}, \tag{3.132}
$$

we arrive at the quadratic,

$$
0 = C \left(1 - \epsilon \right) \left(1 - \langle \hat{\sigma}_1^z \rangle \right)^2 + \left(1 - C + 2\epsilon C \right) \left(1 - \langle \hat{\sigma}_1^z \rangle \right) - 2\epsilon C. \tag{3.133}
$$

For $\epsilon = 0$, $(1 - \langle \hat{\sigma}_1^z \rangle) = 1 - \frac{1}{C}$, so for $\epsilon \ll 1$, we add the quantity ξ to this,

$$
(1 - \langle \hat{\sigma}_1^z \rangle) = 1 - \frac{1}{C} + \xi \tag{3.134}
$$

where ξ is of order ϵ. Eq. 3.134 is substituted into Eq. 3.133, and only first order terms in ϵ are kept. In this way, ξ is found to be,

$$
\xi = \frac{\epsilon}{C} \frac{C^2 + 1}{C - 1}, \tag{3.135}
$$

From Eqns. 3.131, the rest of the steady state observables are easily solved for. All together, they

are,

$$\langle \hat{\sigma}_1^z \rangle = \frac{1}{C} - \frac{\epsilon}{C}\frac{(C^2+1)}{(C-1)}$$

$$\langle \hat{\sigma}_1^+ \hat{\sigma}_2^- \rangle = \frac{1}{2}\langle \hat{\sigma}_1^z \rangle (1 - \langle \hat{\sigma}_1^z \rangle)$$

$$\langle \hat{a}^\dagger \hat{a} \rangle = \frac{Nw}{2\kappa}(1 - \langle \hat{\sigma}_1^z \rangle)$$

$$\langle \hat{a}^\dagger \hat{\sigma}_1^- \rangle = \frac{iw}{2g}(1 - \langle \hat{\sigma}_1^z \rangle). \tag{3.136}$$

The optimum repumping value $w = w_{opt}$, at which the maximum photon number is achieved, is found by setting $\frac{d}{dw}\langle \hat{a}^\dagger \hat{a} \rangle = 0$ and solving for the w at which this occurs. Doing this, it is found,

$$0 = \frac{d}{dw}\langle \hat{a}^\dagger \hat{a} \rangle = \frac{N}{2\kappa} - \frac{w_{opt}}{g^2} \tag{3.137}$$

so that

$$w_{opt} = \frac{Ng^2}{2\kappa}. \tag{3.138}$$

Substituting Eq. 3.138 into Eqns. 3.136 yields,

$$\langle \hat{\sigma}_1^z \rangle_{opt} = \frac{1}{2} \qquad \langle \hat{\sigma}_1^+ \hat{\sigma}_2^- \rangle_{opt} = \frac{1}{8}$$

$$\langle \hat{a}^\dagger \hat{a} \rangle_{opt} = \frac{N^2 g^2}{8\kappa^2} \qquad \langle \hat{a}^\dagger \hat{\sigma}_1^- \rangle_{opt} = \frac{iNg}{8\kappa}. \tag{3.139}$$

3.7.2 Closed Set of Two-Time Expectation Values

The cumulant expansion method can also be used to calculate $\langle \hat{a}^\dagger(t+\tau)\hat{a}(t) \rangle$ using the quantum regression theorem demonstrated in Sec. 3.2.3. With $\hat{A} \to \hat{a}^\dagger$ and $\hat{B} \to \hat{a}$ in Eq. 3.49, and noting now that $\hat{S}(\tau) = e^{-\frac{i}{\hbar}\hat{H}\tau}\hat{a}\hat{\rho}e^{\frac{i}{\hbar}\hat{H}\tau}$, we arrive at,

$$\frac{d}{d\tau}\langle \hat{a}^\dagger(t+\tau)\hat{a}(t) \rangle = tr\left[\left(\frac{d}{d\tau}\hat{S}(\tau)\right)\hat{a}^\dagger\right]$$

$$= -i\omega_c tr\left[\hat{a}^\dagger \hat{a}^\dagger \hat{a}\hat{S}(\tau) - \hat{a}^\dagger \hat{a}\hat{a}^\dagger \hat{S}(\tau)\right]$$

$$-\frac{ig}{2}\sum_{j=1}^N tr\left[\hat{a}^\dagger\left(\hat{\sigma}_j^- \hat{a}^\dagger + \hat{\sigma}_j^+ \hat{a}\right)\hat{S}(\tau) - \left(\hat{\sigma}_j^- \hat{a}^\dagger + \hat{\sigma}_j^+ \hat{a}\right)\hat{a}^\dagger\hat{S}(\tau)\right]$$

$$-\frac{\kappa}{2}tr\left[\hat{a}^\dagger \hat{a}^\dagger \hat{a}\hat{\rho} + \hat{a}^\dagger \hat{a}\hat{a}^\dagger \hat{\rho} - 2\hat{a}^\dagger \hat{a}^\dagger \hat{a}\hat{\rho}\right], \tag{3.140}$$

where the cyclic property of the trace has been used. The commutation relations for creation and annihilation operators, Eq. 3.43, are used to simplify,

$$
\begin{aligned}
\frac{d}{d\tau}\left\langle \hat{a}^\dagger(t+\tau)\hat{a}(t)\right\rangle &= \imath\omega_c tr\left[\hat{a}^\dagger \hat{S}(\tau)\right] - \frac{\kappa}{2}tr\left[\hat{a}^\dagger \hat{S}(\tau)\right] + \frac{\imath g}{2}\sum_{j=1}^{N} tr\left[\hat{\sigma}_j^+ \hat{S}(\tau)\right] \\
&= \left(\imath\omega_c - \frac{\kappa}{2}\right)\left\langle \hat{a}^\dagger(t+\tau)\hat{a}(t)\right\rangle + \frac{\imath g N}{2}\left\langle \hat{\sigma}_j^+(t+\tau)\hat{a}(t)\right\rangle, \qquad (3.141)
\end{aligned}
$$

where we have assumed identical atoms in the last line. Since $\left\langle \hat{\sigma}_1^+(t+\tau)\hat{a}(t)\right\rangle$ couples into Eq. 3.141, its equation of motion must also be found. We therefore calculate,

$$
\begin{aligned}
\frac{d}{d\tau}\left\langle \hat{\sigma}_1^+(t+\tau)\hat{a}(t)\right\rangle &= tr\left[\left(\frac{d}{d\tau}\hat{S}(\tau)\right)\hat{\sigma}_1^+\right] \\
&= -\frac{\imath\omega_a}{2}\sum_{j=1}^{N} tr\left[\hat{\sigma}_1^+\hat{\sigma}_j^z \hat{S}(\tau) - \hat{\sigma}_j^z\hat{\sigma}_1^+ \hat{S}(\tau)\right] \\
&\quad -\frac{\imath g}{2}\sum_{j=1}^{N} tr\left[\hat{\sigma}_1^+\left(\hat{\sigma}_j^-\hat{a}^\dagger + \hat{\sigma}_j^+\hat{a}\right)\hat{S}(\tau) - \left(\hat{\sigma}_j^-\hat{a}^\dagger + \hat{\sigma}_j^+\hat{a}\right)\hat{\sigma}_1^+\hat{S}(\tau)\right] \\
&\quad -\frac{\gamma}{2}\sum_{j=1}^{N} tr\left[\hat{\sigma}_1^+\hat{\sigma}_j^+\hat{\sigma}_j^- \hat{S}(\tau) + \hat{\sigma}_j^+\hat{\sigma}_j^-\hat{\sigma}_1^+\hat{S}(\tau) - 2\hat{\sigma}_j^+\hat{\sigma}_1^+\hat{\sigma}_j^-\hat{S}(\tau)\right] \\
&\quad -\frac{w}{2}\sum_{j=1}^{N} tr\left[\hat{\sigma}_1^+\hat{\sigma}_j^-\hat{\sigma}_j^+ \hat{S}(\tau) + \hat{\sigma}_j^-\hat{\sigma}_j^+\hat{\sigma}_1^+\hat{S}(\tau) - 2\hat{\sigma}_j^-\hat{\sigma}_1^+\hat{\sigma}_j^+\hat{S}(\tau)\right] \\
&\quad +\frac{1}{2T_2}\sum_{j=1}^{N} tr\left[\hat{\sigma}_j^z\hat{\sigma}_1^+\hat{\sigma}_j^z \hat{S}(\tau) - \hat{\sigma}_1^+ \hat{S}(\tau)\right], \qquad (3.142)
\end{aligned}
$$

where the cyclic property of the trace has been used. After simplifying using Eq. 3.121, Eq. 3.142 becomes,

$$
\begin{aligned}
\frac{d}{d\tau}\left\langle \hat{\sigma}_1^+(t+\tau)\hat{a}(t)\right\rangle &= \imath\omega_a tr\left[\hat{\sigma}_1^+\hat{S}(\tau)\right] - \frac{\imath g}{2}tr\left[\hat{a}^\dagger\left(\hat{\sigma}_1^+\hat{\sigma}_1^- - \hat{\sigma}_1^-\hat{\sigma}_1^+\right)\hat{S}(\tau)\right] \\
&\quad -\frac{\gamma}{2}tr\left[\hat{\sigma}_1^+\hat{S}(\tau)\right] - \frac{w}{2}tr\left[\hat{\sigma}_1^+\hat{\sigma}_j^-\hat{\sigma}_j^+\hat{S}(\tau)\right] - \frac{1}{T_2}tr\left[\hat{\sigma}_1^+\hat{S}(\tau)\right] \\
&= \left(\imath\omega_a - \frac{\gamma}{2} - \frac{w}{2} - \frac{1}{T_2}\right)\left\langle \hat{\sigma}_1^+\hat{S}(\tau)\right\rangle - \frac{\imath g}{2}\left\langle \hat{a}^\dagger\hat{\sigma}_1^z\hat{S}(\tau)\right\rangle \\
&= \left(\imath\omega_a - \frac{\gamma}{2} - \frac{w}{2} - \frac{1}{T_2}\right)\left\langle \hat{\sigma}_1^+(t+\tau)\hat{a}(t)\right\rangle - \frac{\imath g}{2}\left\langle \hat{a}^\dagger(t+\tau)\hat{\sigma}_1^z(t+\tau)\hat{a}(t)\right\rangle.
\end{aligned}
$$

$$(3.143)$$

To be consistent with the approximations of Sec. 3.7.1, the third order moment in Eq. 3.143 is factorized and the third order cumulant is dropped, which yields,

$$
\begin{aligned}
\left\langle \hat{a}^\dagger(t+\tau)\hat{\sigma}_1^z(t+\tau)\hat{a}(t) \right\rangle &= \left\langle \hat{a}^\dagger \hat{a} \right\rangle \langle \hat{\sigma}_1^z \rangle + \left\langle \hat{a}^\dagger \hat{\sigma}_1^z \right\rangle \langle \hat{a} \rangle + \langle \hat{a}\hat{\sigma}_1^z \rangle \left\langle \hat{a}^\dagger \right\rangle - 2\left\langle \hat{a}^\dagger \right\rangle \langle \hat{a} \rangle \langle \hat{\sigma}_1^z \rangle \\
&= \langle \hat{\sigma}_1^z(t+\tau) \rangle \left\langle \hat{a}^\dagger(t+\tau)\hat{a}(t) \right\rangle.
\end{aligned}
\tag{3.144}
$$

Putting it all together, in an interaction picture that rotates at ω_a, defined by,

$$
\tilde{\hat{a}}(t) = e^{-i\omega_a t}\hat{a}(t) \qquad \tilde{\hat{\sigma}}_1^-(t) = e^{-i\omega_a t}\hat{\sigma}_1^-(t),
\tag{3.145}
$$

we have,

$$
\begin{aligned}
\frac{d}{d\tau}\left\langle \hat{a}^\dagger(t+\tau)\hat{a}(t) \right\rangle &= -\left(i\delta + \frac{\kappa}{2}\right)\left\langle \hat{a}^\dagger(t+\tau)\hat{a}(t) \right\rangle + \frac{igN}{2}\left\langle \hat{\sigma}_j^+(t+\tau)\hat{a}(t) \right\rangle \\
\frac{d}{d\tau}\left\langle \hat{\sigma}_1^+(t+\tau)\hat{a}(t) \right\rangle &= -\frac{ig}{2}\langle \hat{\sigma}_1^z(t+\tau) \rangle \left\langle \hat{a}^\dagger(t+\tau)\hat{a}(t) \right\rangle \\
&\quad - \left(\frac{\gamma}{2} + \frac{w}{2} + \frac{1}{T_2}\right)\langle \hat{\sigma}_1^+(t+\tau)\hat{a}(t) \rangle,
\end{aligned}
\tag{3.146}
$$

where $\delta \equiv \omega_a - \omega_c$.

To solve Eqns. 3.146, we note that they are of the form,

$$
\begin{aligned}
\frac{d}{d\tau}A(\tau) &= c_1 A(\tau) + c_2 B(\tau) \\
\frac{d}{d\tau}B(\tau) &= c_3 A(\tau) + c_4 B(\tau),
\end{aligned}
\tag{3.147}
$$

which can be solved by taking the Laplace transform of both sides,

$$
\begin{aligned}
\int_0^\infty d\tau e^{-s\tau}\left\{\frac{d}{d\tau}A(\tau)\right\} &= \int_0^\infty d\tau e^{-s\tau}\left\{c_1 A(\tau) + c_2 B(\tau)\right\} \\
\int_0^\infty d\tau e^{-s\tau}\left\{\frac{d}{d\tau}B(\tau)\right\} &= \int_0^\infty d\tau e^{-s\tau}\left\{c_3 A(\tau) + c_4 B(\tau)\right\}.
\end{aligned}
\tag{3.148}
$$

After integrating the left hand sides by parts, and defining,

$$
\begin{aligned}
\mathcal{A}(s) &= \int_0^\infty d\tau e^{-s\tau}A(\tau) \\
\mathcal{B}(s) &= \int_0^\infty d\tau e^{-s\tau}B(\tau),
\end{aligned}
\tag{3.149}
$$

Eq. 3.148 becomes,

$$-A(0) + s\mathcal{A}(s) = c_1\mathcal{A}(s) + c_2\mathcal{B}(s)$$

$$-B(0) + s\mathcal{B}(s) = c_3\mathcal{A}(s) + c_4\mathcal{B}(s). \tag{3.150}$$

Eq. 3.150 is algebraically solved for $\mathcal{A}(s)$, yielding,

$$\begin{aligned} \mathcal{A}(s) &= \frac{(s - c_4) A(0) + c_2 B(0)}{s^2 - (c_1 + c_4) s + (c_1 c_4 - c_2 c_3)} \\ &= \frac{(s - c_4) A(0) + c_2 B(0)}{\left(s - \frac{\Delta\nu_+}{2}\right)\left(s - \frac{\Delta\nu_-}{2}\right)}, \end{aligned} \tag{3.151}$$

where,

$$\begin{aligned} \Delta\nu_\pm &= -(c_1 + c_4) \mp \sqrt{(c_1 + c_4)^2 - 4(c_1 c_4 - c_2 c_3)} \\ &= \frac{1}{2}(\kappa + w) \mp \frac{1}{2}\sqrt{(-\kappa + w)^2 - 4Ng^2\langle\hat{\sigma}_1^z\rangle}. \end{aligned} \tag{3.152}$$

By the method of partial fractions, Eq. 3.151 can be put into the form,

$$\mathcal{A}(s) = \frac{X}{\left(s - \frac{\Delta\nu_+}{2}\right)} + \frac{Y}{\left(s - \frac{\Delta\nu_-}{2}\right)}, \tag{3.153}$$

so that taking the inverse Laplace transform yields

$$\left\langle \hat{a}^\dagger(t + \tau)\hat{a}(t)\right\rangle = A(\tau) = Xe^{-\frac{\Delta\nu_+\tau}{2}} + Ye^{-\frac{\Delta\nu_-\tau}{2}}. \tag{3.154}$$

Since $\Delta\nu_+ \ll \Delta\nu_-$, the second term decays fast to zero, so that the first term dominates. Then, since the Fourier transform of an exponential with decay rate $\Delta\nu$ is a Lorentzian with a full width half maximum linewidth $\Delta\nu$, the steady state linewidth $\Delta\nu$ of a system described by Eq. 3.119 is given by,

$$\Delta\nu = \frac{1}{2}(\kappa + w) - \frac{1}{2}\sqrt{(-\kappa + w)^2 - 4Ng^2\langle\hat{\sigma}_1^z\rangle}. \tag{3.155}$$

By plugging Eq. 3.136 into Eq. 5.50, and again assuming $N \gg \frac{\kappa}{w+\kappa}$, we find a simple expression for the linewidth,

$$\Delta\nu = \frac{C^2 + 1}{C(C - 1)}\frac{\Omega^2\kappa}{(w + \kappa)^2}. \tag{3.156}$$

3.8   Conclusion

We have seen that an open quantum system can be described by coupling it to a large reservoir, and evolving the combined system and reservoir to second order in perturbation theory. Then, after taking the partial trace over the reservoir Hilbert space, and making the Markov approximation, the master equation was obtained. For simple systems, such as the damped harmonic oscillator, the master equation can be used to derive exact analytical solutions for expectation values. With the help of the quantum regression theorem, analytical solutions for two-time expectation values can also be derived. We also introduced the quantum jumps and quantum state diffusion methods which can be used to solve the master equation using a computer. The quantum jumps method unravels the master equation into random trajectories, which correspond to the random measurement record of photons leaving the system and being detected. The quantum state diffusion method unravels the master equation into random trajectories, which correspond to a randomly fluctuating homodyne photocurrent that results from mixing the photons from the system with a strong local oscillator. In both cases, the random trajectories are averaged over to obtain the correct evolution in the ensemble sense. Computer simulations using both of these methods were demonstrated in the system of the damped harmonic oscillator. For systems with a large number of atoms, the quantum jumps and quantum state diffusion methods are not possible, since the size of the Liouville space grows exponentially with atom number. For very large systems, approximate methods such as the cumulant expansion method must be employed. We derived a closed set of equations for expectation values by factorizing all moments higher than second order that appear in the equations. With the help of the quantum regression theorem, equations for two-time expectation values were also derived.

Chapter 4

Langevin Equations

Another way to incorporate dissipation into quantum mechanics is through the quantum Langevin equations. This formalism is completely equivalent to the master equation approach, but instead of the time dependence being on the state of the system, it is put on the operators themselves. Thus, the Langevin equations are in the Heisenberg picture of quantum mechanics, while the master equation is in the Schrödinger picture. In analogy to the master equation approach, dissipation occurs in the Langevin approach due to the coupling of the small system to a large reservoir.

The quantum Langevin equations are operator equations, which are cumbersome and not easily simulated on a computer. Therefore, for solutions methods that do not make approximations, the quantum master equation is a better starting point. However, the quantum Langevin equations can be used to derive approximate equations that can describe large systems, where exact solution methods are not possible. Therefore, after the quantum Langevin equations are derived from first principles, the Fokker-Planck equation for a quazi-probability distribution which describes the quantum system, is derived. With the aid of stochastic calculus, this Fokker-Planck equation will be shown to be equivalent to a set of c-number Langevin equations, which can be used to describe large systems, and are easily simulated on a computer.

Once this correspondence between quantum operator Langevin equations and c-number Langevin equations is demonstrated, a more practical route to obtain the c-number Langevin equations is given.

4.1   Derivation of the Quantum Langevin Equations

We will begin by deriving the quantum Langevin equations [67] for N two level atoms coupled to a single cavity mode. The derivation will focus on the decay of the cavity only, for simplicity. However, in analogy to the master equation derivation, the incoherent decay and repumping of the atoms is derived in an almost identical manner as presented here. The Hamiltonian $\hat{H}$ of the combined system and reservoir is given by,

$$\hat{H} = \frac{\hbar\omega_a}{2}\hat{J}_z + \hbar\omega_c\hat{a}^\dagger\hat{a} + \frac{\hbar g}{2}\left(\hat{J}_-\hat{a}^\dagger + \hat{J}_+\hat{a}\right) + \hbar\sum_k \nu_k\hat{b}_k^\dagger\hat{b}_k + \hbar\sum_k \lambda_k\left(\hat{b}_k^\dagger\hat{a} + \hat{b}_k\hat{a}^\dagger\right), \qquad (4.1)$$

which describes N two level atoms of frequency ω_a coupled with frequency g to a single mode cavity of frequency ω_c, which is coupled with rates λ_k to a large reservoir of other harmonic oscillators of frequency ν_k. The cavity mode is described by the annihilation operator $\hat{a}$, and the reservoir is described by the annihilation operators $\hat{b}_k$, while the N two level atoms are described by,

$$\hat{J}_z = \sum_{j=1}^{N}\sigma_j^z,$$

$$\hat{J}_\pm = \sum_{j=1}^{N}\sigma_j^\pm,$$

where $\sigma_j^-, \sigma_j^+, \sigma_j^z$ are the Pauli matricies for the jth atom.

In the Heisenberg picture, the equation of motion of $\hat{a}$ is given by,

$$\begin{aligned}
\dot{\hat{a}} &= \frac{i}{\hbar}\left[\hat{H}, \hat{a}\right] \\
&= i\left[\left(\omega_c\hat{a}^\dagger\hat{a} + \frac{g}{2}\hat{J}_-\hat{a}^\dagger + \sum_k \lambda_k\hat{b}_k\hat{a}^\dagger\right), \hat{a}\right] \\
&= i\omega_c\left[\hat{a}^\dagger\hat{a}, \hat{a}\right] + i\frac{g}{2}\left[\hat{a}^\dagger, \hat{a}\right]\hat{J}_- + i\left[\hat{a}^\dagger, \hat{a}\right]\sum_k \lambda_k\hat{b}_k \\
&= -i\omega_c\hat{a} - i\frac{g}{2}\hat{J}_- - i\sum_k \lambda_k\hat{b}_k, \qquad (4.2)
\end{aligned}$$

and the equation of motion of $\hat{b}_k$ is given by,

$$
\begin{aligned}
\dot{\hat{b}}_k &= \frac{i}{\hbar}\left[\hat{H},\hat{b}_k\right] \\
&= i\left[\left(\sum_l \nu_l \hat{b}_l^\dagger \hat{b}_l + \sum_l \lambda_l \hat{b}_l^\dagger \hat{a}\right),\hat{b}_k\right] \\
&= i\sum_l \nu_l\left[\hat{b}_l^\dagger \hat{b}_l,\hat{b}_k\right] + i\hat{a}\sum_l \lambda_l\left[\hat{b}_l^\dagger,\hat{b}_k\right] \\
&= -i\nu_k\hat{b}_k - i\lambda_k\hat{a}.
\end{aligned}
\tag{4.3}
$$

As an aside, it is now apparent that if the decay of the atoms was accounted for, it would not change the form of Eq. 4.2 or Eq. 4.3, but would change the equations associated with the atoms.

Eq. 4.3 is now integrated,

$$
\hat{b}_k(t) = \hat{b}_k(0)e^{-i\nu_k t} - i\lambda_k\int_0^t dt'\, e^{-i\nu_k(t-t')}\hat{a}(t'),
\tag{4.4}
$$

and substituted into Eq. 4.2 to obtain,

$$
\begin{aligned}
\dot{\hat{a}} &= -i\omega_c\hat{a} - i\frac{g}{2}\hat{J}_- - i\sum_k \lambda_k\left(\hat{b}_k(0)e^{-i\nu_k t} - i\lambda_k\int_0^t dt'\, e^{-i\nu_k(t-t')}\hat{a}(t')\right) \\
&= -i\omega_c\hat{a} - i\frac{g}{2}\hat{J}_- - \sum_k \lambda_k^2\int_0^t dt'\, e^{-i\nu_k(t-t')}\hat{a}(t') - i\sum_k \lambda_k\hat{b}_k(0)e^{-i\nu_k t}.
\end{aligned}
\tag{4.5}
$$

An interaction picture is defined by,

$$
\begin{aligned}
\tilde{\hat{a}} &= e^{i\omega_c t}\hat{a}, \\
\tilde{\hat{J}}_- &= e^{i\omega_c t}\hat{J}_-,
\end{aligned}
$$

so that in this interaction picture, Eq. 4.5 becomes,

$$
\dot{\tilde{\hat{a}}} = -i\frac{g}{2}\tilde{\hat{J}}_- - \sum_k \lambda_k^2\int_0^t dt'\, e^{-i(\nu_k-\omega_c)(t-t')}\tilde{\hat{a}}(t') + \tilde{\hat{F}},
\tag{4.6}
$$

where,

$$
\tilde{\hat{F}} = -i\sum_k \lambda_k\hat{b}_k(0)e^{-i(\nu_k-\omega_c)t}.
\tag{4.7}
$$

In the second term on the right hand side of Eq. 4.6, the sum over k is changed to an integral over ν by including a density of states,

$$
\begin{aligned}
\sum_k \lambda_k^2 \int_0^t dt' e^{-i(\nu_k - \omega_c)(t - t')} \hat{a}(t') &= \sum_k \Delta k \lambda_k^2 \int_0^t dt' e^{-i(\nu_k - \omega_c)(t - t')} \hat{a}(t') \\
&= \int_0^B d\nu \mathcal{D}(\nu) \left| \lambda(\nu) \right|^2 \int_0^t dt' e^{-i(\nu - \omega_c)(t - t')} \hat{a}(t') \\
&= \int_0^B d\nu \mathcal{D}(\nu) \left| \lambda(\nu) \right|^2 \int_0^t d\tau e^{-i(\nu - \omega_c)\tau} \hat{a}(t - \tau).
\end{aligned}
\tag{4.8}
$$

In analogy to the derivation of the master equation, it is assumed that the reservoir has a very large bandwidth B, so that the reservoir relaxation rate $\frac{1}{\tau_R}$ will be much larger than the systems relaxation rate $\frac{1}{\tau_S}$. Then, for $\tau << \tau_S$, $\hat{a}(t - \tau)$ will be approximately constant, so that it can be evaluated at $\tau = 0$ and factored outside of the integral. The resulting integral of exponentials will then destructively interfere when $\tau >> \tau_R$, resulting in it averaging to zero. Therefore the upper limit of that integral can be extended to $\tau = \infty$ with minimal error. In this Markov approximation, Eq. 4.8 becomes,

$$
\begin{aligned}
\sum_k \lambda_k^2 \int_0^t dt' e^{-i\nu_k(t - t')} \tilde{\hat{a}}(t') &= \int_0^\infty d\nu \mathcal{D}(\nu) \left| \lambda(\nu) \right|^2 \hat{a}(\tau) \int_0^\infty d\tau e^{-i(\nu - \omega_c)\tau} \\
&= \lim_{\eta \to 0} \int_0^\infty d\nu \mathcal{D}(\nu) \left| \lambda(\nu) \right|^2 \hat{a}(t) \int_0^\infty d\tau e^{-i(\nu - \omega_c - i\eta)\tau} \\
&= \int_0^\infty d\nu \mathcal{D}(\nu) \left| \lambda(\nu) \right|^2 \hat{a}(t) \left[\pi \delta(\nu - \omega_c) + i \mathcal{P} \left(\frac{1}{\nu - \omega_c} \right) \right].
\end{aligned}
\tag{4.9}
$$

where $\mathcal{D}(\nu)$ is a density of states, and Eq. 3.35 has been again used. Neglecting the principal part of Eq. 4.9, which leads to a small frequency shift related to the Lamb shift, and substituting it into Eq. 4.6 results in,

$$
\dot{\tilde{\hat{a}}} = -i \frac{g}{2} \tilde{\hat{J}}_- - \frac{\kappa}{2} \tilde{\hat{a}} + \tilde{\hat{F}},
\tag{4.10}
$$

where,

$$
\kappa = 2\pi \mathcal{D}(\omega_c) \left| \lambda(\omega_c) \right|^2.
\tag{4.11}
$$

For use in later calculations, using Eq. 4.7, we calculate,

$$
\begin{aligned}
\left\langle \tilde{\hat{F}} \right\rangle &= -i \sum_k \lambda_k \left\langle \tilde{\hat{b}}_k(0) \right\rangle e^{-i(\nu_k - \omega_c)t} \\
&= 0,
\end{aligned}
\tag{4.12}
$$

since $\left\langle \tilde{\tilde{b}}_k(0) \right\rangle = 0$, because it is the trace of an annihilation operator. We also calculate,

$$
\begin{aligned}
\left\langle \tilde{\tilde{F}}^\dagger(t) \tilde{\tilde{F}}(t') \right\rangle &= \sum_k \sum_{k'} \lambda_k^* \lambda_{k'} \left\langle \tilde{\tilde{b}}_k^\dagger(0) \tilde{\tilde{b}}_k(0) \right\rangle e^{i(\nu_k - \omega_c)t} e^{-i(\nu_{k'} - \omega_c)t'} \\
&= \sum_k |\lambda_k|^2 \, \bar{n}_k e^{i(\nu_k - \omega_c)(t - t')} \\
&\approx \mathcal{D}(\omega_c) |\lambda(\omega_c)|^2 \, \bar{n}(\omega_c) \int_{-\infty}^{\infty} d\nu e^{i(\nu_k - \omega_c)(t - t')} \\
&= \kappa \bar{n}(\omega_c) \delta(t - t'),
\end{aligned}
\tag{4.13}
$$

where the discrete sum has again been approximated as an integral over a density of states, and the slowly varying variables have been pulled outside the integral, which is valid under the Markov approximation described above. Also, the fact that,

$$
\int_{-\infty}^{\infty} d\nu e^{i(\nu_k - \omega_c)(t - t')} = 2\pi \delta(t - t'),
\tag{4.14}
$$

has been employed. In the same way, it can be shown that,

$$
\left\langle \tilde{\tilde{F}}(t) \tilde{\tilde{F}}^\dagger(t') \right\rangle = \kappa \left(\bar{n}(\omega_c) + 1 \right) \delta(t - t'),
\tag{4.15}
$$

and

$$
\left\langle \tilde{\tilde{F}}(t) \tilde{\tilde{F}}(t') \right\rangle = \left\langle \tilde{\tilde{F}}^\dagger(t) \tilde{\tilde{F}}^\dagger(t') \right\rangle = 0.
\tag{4.16}
$$

The quantities defined in Eqns. 4.13, 4.15 and 4.16 are called the diffusion coefficients, and are needed to characterize the system, as we will see later.

4.2   Adiabatic Elimination and the Superradiance Master Equation

As a brief aside, we are now in a position to derive the superradiance master equation. This is done by first integrating Eq. 4.10, obtaining,

$$
\begin{aligned}
\tilde{a}(t) &= \tilde{a}(0)e^{-\frac{\kappa}{2}t} + \int_0^t dt' e^{-\frac{\kappa}{2}(t - t')} \left(-i\frac{g}{2}\tilde{J}_- + \tilde{F} \right) \\
&= \tilde{a}(0)e^{-\frac{\kappa}{2}t} - i\frac{g}{2} \int_0^t dt' e^{-\frac{\kappa}{2}(t - t')} \tilde{J}_- + \int_0^t dt' e^{-\frac{\kappa}{2}(t - t')} \tilde{F}.
\end{aligned}
\tag{4.17}
$$

Assuming the system is in the steady state, t is large enough so that $e^{-\frac{\kappa}{2}t} \to 0$. This allows the first term in Eq. 4.17 to be dropped, but not the other terms because they have exponentials

that depend on $t - t'$ which can be small. The second term in Eq. 4.17 is now integrated by parts multiple times, and under the steady state assumption,

$$\int_0^t dt' e^{-\frac{\kappa}{2}(t-t')} \tilde{\hat{J}}_- = \frac{2}{\kappa} \tilde{\hat{J}}_- - \left(\frac{2}{\kappa}\right)^2 \frac{d}{dt} \tilde{\hat{J}}_- + \cdots \tag{4.18}$$

Eq. 4.18 tells us that if,

$$\left| \tilde{\hat{J}}_- \right| >> \frac{1}{\kappa} \left| \frac{d}{dt} \tilde{\hat{J}}_- \right|, \tag{4.19}$$

it is valid to make the adiabatic approximation, keeping only the first order term in Eq. 4.18. Under this approximation, Eq. 4.17 becomes

$$\tilde{\hat{a}}(t) = -i \frac{g}{\kappa} \tilde{\hat{J}}_- + \tilde{\hat{G}}, \tag{4.20}$$

where

$$\tilde{\hat{G}} = \int_0^t dt' e^{-\frac{\kappa}{2}(t-t')} \tilde{\hat{F}}. \tag{4.21}$$

An upper limit on the adiabatic condition, Eq. 4.19, in terms of the parameters of the problem can be obtained by finding the equation of motion for $\tilde{\hat{J}}_-$,

$$\begin{aligned}
\dot{\tilde{\hat{J}}}_- &= i \frac{g}{2} \tilde{\hat{a}} \left[\tilde{\hat{J}}_+, \tilde{\hat{J}}_- \right] \\
&= ig\tilde{\hat{a}}\tilde{\hat{J}}_z \\
&= ig \left(-i \frac{g}{\kappa} \tilde{\hat{J}}_- + \tilde{\hat{G}} \right) \tilde{\hat{J}}_z \\
&= \frac{g^2}{\kappa} \tilde{\hat{J}}_- \tilde{\hat{J}}_z + ig\tilde{\hat{G}}\tilde{\hat{J}}_z,
\end{aligned} \tag{4.22}$$

substituting this into Eq. 4.19, and noting that the largest value of $\left| \tilde{\hat{J}}_z \right|$ occurs when the Bloch vector points to one of the poles, having the value N. Eq. 4.19 then says,

$$\kappa >> NC\gamma, \tag{4.23}$$

where

$$C = \frac{g^2}{\kappa\gamma}. \tag{4.24}$$

The master equation for a system of atoms interacting with a damped cavity mode, which has been adiabatically eliminated is then given by inserting Eq. 4.20 into Eq. 3.119. Since the master

equation is course grain averaged over the timescale of the reservoir, it is valid to set $\hat{\tilde{G}} \to \left\langle \hat{\tilde{G}} \right\rangle_R$ in Eq. 4.20 before inserting it into Eq. 3.119, and still consistent with the approximations of the master equation. The expectation value $\left\langle \hat{\tilde{G}}(t) \right\rangle_R$ is given by,

$$
\begin{aligned}
\left\langle \hat{\tilde{G}}(t) \right\rangle_R &= \int_0^t dt' e^{-\frac{\kappa}{2}(t-t')} \left\langle \hat{\tilde{F}}(t') \right\rangle \\
&= 0.
\end{aligned}
\tag{4.25}
$$

Therefore, we arrive at the superradiance master equation,

$$
\begin{aligned}
\frac{d}{dt}\tilde{\rho} &= -\frac{C\gamma}{2}\left\{ \tilde{\hat{J}}_+ \tilde{\hat{J}}_- \tilde{\rho} + \tilde{\rho}\tilde{\hat{J}}_+ \tilde{\hat{J}}_- - 2\tilde{\hat{J}}_- \tilde{\rho}\tilde{\hat{J}}_+ \right\} \\
&\quad -\frac{\gamma}{2}\sum_{j=1}^{N}\left\{ \hat{\sigma}_j^+ \hat{\sigma}_j^- \tilde{\rho} + \tilde{\rho}\hat{\sigma}_j^+ \hat{\sigma}_j^- - 2\hat{\sigma}_j^- \tilde{\rho}\hat{\sigma}_j^+ \right\} \\
&\quad -\frac{w}{2}\sum_{j=1}^{N}\left\{ \hat{\sigma}_j^- \hat{\sigma}_j^+ \tilde{\rho} + \tilde{\rho}\hat{\sigma}_j^- \hat{\sigma}_j^+ - 2\hat{\sigma}_j^+ \tilde{\rho}\hat{\sigma}_j^- \right\}.
\end{aligned}
\tag{4.26}
$$

4.3   Fokker-Planck Equations for the P Function

Since Eq. 4.10 is an equation of quantum operators, it cannot simply be used in numerical simulations. We therefore seek a method that can be used for numerical simulation. To this end, the Fokker-Planck equation for a quazi-probability distribution describing the system is derived from the master equation. It is then demonstrated that the resulting Fokker-Planck equation can be equivalently described in terms of a set of c-number Langevin equations, which can be easily solved using numerical simulations. The method is demonstrated for the damped harmonic oscillator.

The master equation for the damped harmonic oscillator is,

$$
\begin{aligned}
\dot{\rho} &= -\imath\omega_0\left[\hat{a}^\dagger\hat{a}, \hat{\rho}\right] + \frac{\gamma}{2}(\bar{n}+1)\left(2\hat{a}\hat{\rho}\hat{a}^\dagger - \hat{a}^\dagger\hat{a}\hat{\rho} - \hat{\rho}\hat{a}^\dagger\hat{a}\right) + \frac{\gamma}{2}\bar{n}\left(2\hat{a}^\dagger\hat{\rho}\hat{a} - \hat{a}\hat{a}^\dagger\hat{\rho} - \hat{\rho}\hat{a}\hat{a}^\dagger\right) \\
&= -\imath\omega_0\left[\hat{a}^\dagger\hat{a}, \hat{\rho}\right] + \frac{\gamma}{2}\left(2\hat{a}\hat{\rho}\hat{a}^\dagger - \hat{a}^\dagger\hat{a}\hat{\rho} - \hat{\rho}\hat{a}^\dagger\hat{a}\right) + \gamma\bar{n}\left(\hat{a}\hat{\rho}\hat{a}^\dagger + \hat{a}^\dagger\hat{\rho}\hat{a} - \hat{a}^\dagger\hat{a}\hat{\rho} - \hat{\rho}\hat{a}\hat{a}^\dagger\right). \tag{4.27}
\end{aligned}
$$

It is assumed that $\hat{\rho}$ can be expanded as,

$$
\hat{\rho} = \int d^2\alpha P(\alpha, t)\left|\alpha\right\rangle\left\langle\alpha\right|,
\tag{4.28}
$$

where $P(\alpha, t)$ is a quazi-probability function called the P function, and $|\alpha\rangle$ is a coherent state. Eq. 4.28 is substituted into Eq. 4.27, yielding,

$$
\begin{aligned}
\int d^2\alpha \, |\alpha\rangle \langle\alpha| \frac{\partial}{\partial t} P(\alpha, t) &= \int d^2\alpha P(\alpha, t) \Big\{ - \imath\omega_0 \left(\hat{a}^\dagger \hat{a} \, |\alpha\rangle \langle\alpha| - |\alpha\rangle \langle\alpha| \, \hat{a}^\dagger \hat{a} \right) \\
&\quad + \frac{\gamma}{2} \left(2\hat{a} \, |\alpha\rangle \langle\alpha| \, \hat{a}^\dagger - \hat{a}^\dagger \hat{a} \, |\alpha\rangle \langle\alpha| - |\alpha\rangle \langle\alpha| \, \hat{a}^\dagger \hat{a} \right) \\
&\quad + \gamma\bar{n} \left(\hat{a} \, |\alpha\rangle \langle\alpha| \, \hat{a}^\dagger + \hat{a}^\dagger \, |\alpha\rangle \langle\alpha| \, \hat{a} - \hat{a}^\dagger \hat{a} \, |\alpha\rangle \langle\alpha| - |\alpha\rangle \langle\alpha| \, \hat{a}\hat{a}^\dagger \right) \Big\}.
\end{aligned}
$$

$$(4.29)$$

To simplify Eq. 4.29, the fact that,

$$
|\alpha\rangle = e^{-\frac{1}{2}|\alpha|^2} e^{\alpha \hat{a}^\dagger} |0\rangle,
$$

$$(4.30)$$

is used to show that,

$$
\begin{aligned}
\frac{\partial}{\partial\alpha} |\alpha\rangle \langle\alpha| &= \frac{\partial}{\partial\alpha} \left(e^{-|\alpha|^2} e^{\alpha \hat{a}^\dagger} |0\rangle \langle 0| \, e^{\alpha^* \hat{a}} \right) \\
&= \left(\hat{a}^\dagger - \alpha^* \right) |\alpha\rangle \langle\alpha|,
\end{aligned}
$$

$$(4.31)$$

and that also,

$$
\begin{aligned}
\frac{\partial}{\partial\alpha^*} |\alpha\rangle \langle\alpha| &= \frac{\partial}{\partial\alpha^*} \left(e^{-|\alpha|^2} e^{\alpha \hat{a}^\dagger} |0\rangle \langle 0| \, e^{\alpha^* \hat{a}} \right) \\
&= |\alpha\rangle \langle\alpha| \left(\hat{a} - \alpha \right).
\end{aligned}
$$

$$(4.32)$$

Eqns. 4.31 and 4.32 can then be used to simplify the various terms in Eq. 4.29, which then becomes,

$$
\begin{aligned}
\int d^2\alpha \, |\alpha\rangle \langle\alpha| \frac{\partial}{\partial t} P(\alpha, t) &= \int d^2\alpha P(\alpha, t) \Big\{ - \left(\frac{\gamma}{2} + \imath\omega_0 \right) \alpha \frac{\partial}{\partial\alpha} \\
&\quad - \left(\frac{\gamma}{2} - \imath\omega_0 \right) \alpha^* \frac{\partial}{\partial\alpha^*} + \gamma\bar{n} \frac{\partial^2}{\partial\alpha\partial\alpha^*} \Big\} |\alpha\rangle \langle\alpha|.
\end{aligned}
$$

$$(4.33)$$

Eq. 4.33 is now integrated by parts, assuming that $P(\alpha, t)$ vanishes sufficiently rapidly at infinity so that the surface terms can be dropped. Then,

$$
\begin{aligned}
\int d^2\alpha \, |\alpha\rangle \langle\alpha| \frac{\partial}{\partial t} P(\alpha, t) &= \int d^2\alpha \, |\alpha\rangle \langle\alpha| \Big\{ \left(\frac{\gamma}{2} + \imath\omega_0 \right) \frac{\partial}{\partial\alpha} \alpha \\
&\quad + \left(\frac{\gamma}{2} - \imath\omega_0 \right) \frac{\partial}{\partial\alpha^*} \alpha^* + \gamma\bar{n} \frac{\partial^2}{\partial\alpha\partial\alpha^*} \Big\} P(\alpha, t).
\end{aligned}
$$

$$(4.34)$$

Eq. 4.34 implies that,

$$\frac{\partial}{\partial t}P(\alpha,t) = \left\{ \left(\frac{\gamma}{2}+\imath\omega_0\right)\frac{\partial}{\partial\alpha}\alpha + \left(\frac{\gamma}{2}-\imath\omega_0\right)\frac{\partial}{\partial\alpha^*}\alpha^* + \gamma\bar{n}\frac{\partial^2}{\partial\alpha\partial\alpha^*} \right\}P(\alpha,t). \tag{4.35}$$

This is the Fokker-Planck equation for the damped harmonic oscillator in the P representation.

Eq. 4.35 can be put into a more convenient form by defining $\alpha = x + \imath y$ and substituting,

$$\frac{\partial}{\partial t}P(\alpha,t) = \left\{ \frac{\gamma}{2}\left(\frac{\partial}{\partial x}x + \frac{\partial}{\partial y}y\right) + \omega_0\left(\frac{\partial}{\partial x}y - \frac{\partial}{\partial y}x\right) + \frac{\bar{n}}{2}\left(\frac{\partial^2}{\partial x^2} + \frac{\partial^2}{\partial x^2}\right) \right\}P(\alpha,t). \tag{4.36}$$

4.4   Equivalence of Langevin and Fokker-Planck Equations

It is now demonstrated a Fokker-Planck equation for a probability distribution has an equivalent Langevin equation for the random variable of that probability distribution. To do this, we will need to take a brief aside into Stochastic calculus [34].

A Langevin equation is a stochastic differential equation of the form,

$$\frac{dx}{dt} = a(x,t) + b(x,t)\xi(t), \tag{4.37}$$

where $\xi(t)$ is a rapidly fluctuating random function of time. We assume that $\xi(t)$ is idealized in the sense that we assume that $\xi(t)$ and $\xi(t')$ are statistically independent. Mathematically this is the statement that the time average of $\xi(t)$ and $\xi(t')$ are delta correlated,

$$\langle\xi(t)\xi(t')\rangle = \delta(t-t'). \tag{4.38}$$

We also assume that

$$\langle\xi(t)\rangle = 0, \tag{4.39}$$

since any non-zero mean can be absorbed into the definition of $a(x,t)$. This idealized random process is called white noise.

It can be shown that

$$\int_0^t dt'\xi(t') = W(t), \tag{4.40}$$

where $W(t)$ is the Wiener process. Since the Wiener process is not differentiable, Eq. 4.37 does not actually exist. However, the integral equation

$$\begin{aligned}
x(t) - x(0) &= \int_0^t dt' a(x, t') + \int_0^t \xi(t') dt' b(x, t') \\
&= \int_0^t dt' a(x, t') + \int_0^t dW(t') b(x, t'),
\end{aligned} \tag{4.41}$$

where

$$dW(t) \equiv dW(t + dt) - dW(t) = \xi(t) dt \tag{4.42}$$

does exist, but comes with its own difficulties, namely that the last term is not well defined. This can be seen by looking at the integral before dt is allowed to be come infinitesimal. Consider

$$S_n = \sum_{i=1}^n G(\tau_i) \left\{ W(t_i) - W(t_{i-1}) \right\}, \tag{4.43}$$

where τ_i is some value between t_i and t_{i-1}. The crux of the whole situation is that the value of S_n is dependent on the value of τ_i that we choose. This issue, which does not occur with an ordinary Riemann sum defined integral, is caused by the discontinuous nature of $W(t)$. The choice $\tau_i = t_{i-1}$, defines what is known as the Ito stochastic integral. Other choices, such as $\tau_i = \frac{1}{2}(t_i + t_{i-1})$, which defines the Stratonovich stochastic integral, will not be considered here. By using the definition of the Ito integral, it can be shown that in the Ito interpretation of a stochastic integral,

$$\begin{aligned}
dW(t)^2 &= dt, \\
dW(t)^{2+N} &= 0,
\end{aligned}$$

where N is a positive integer. This causes the chain rule from ordinary calculus not to hold. To find the Ito calculus chain rule, consider the differential of a function $f(x(t))$ of a stochastic variable $x(t)$,

$$\begin{aligned}
df[x(t)] &= f[x(t) + dx(t)] - f[x(t)] \\
&= f'[x(t)] dx(t) + \frac{1}{2} f''[x(t)] dx(t)^2 + \dots \\
&= f'[x(t)] \left\{ a(x, t) dt + b(x, t) dW(t) \right\} \\
&\quad + \frac{1}{2} f''[x(t)] \left\{ a(x, t) dt + b(x, t) dW(t) \right\}^2 + \dots
\end{aligned} \tag{4.44}$$

To first order in dt, this gives,

$$
\begin{aligned}
df[x(t)] &= f'[x(t)]\{a(x,t)dt + b(x,t)dW(t)\} + \frac{1}{2}f''[x(t)]b(x,t)dW(t)^2 \\
&= f'[x(t)]\{a(x,t)dt + b(x,t)dW(t)\} + \frac{1}{2}f''[x(t)]b(x,t)dt. \quad (4.45)
\end{aligned}
$$

This is known as Ito's formula.

The equivalence between a stochastic differential for a stochastic variable $x(t)$ and a Fokker-Planck equation for the stochastic variable's probability distribution $P(x(t))$ can now be demonstrated. Consider the time development of the average value of an arbitrary function $f(x(t))$,

$$
\begin{aligned}
\frac{d}{dt}\langle f(x(t))\rangle &= \frac{\langle df(x(t))\rangle}{dt} \\
&= \left\langle f'[x(t)]a(x,t) + \frac{1}{2}f''[x(t)]b(x,t)\right\rangle, \quad (4.46)
\end{aligned}
$$

where the average value of the term multiplied by $dW(t)$ is zero because $dW(t) = \xi(t)dt$ and $\langle\xi(t)\rangle = 0$. The average value of a stochastic variable is found by integrating the stochastic variable multiplied by its conditional probability density $P(x', t'|x_0, t_0)$ from time x_0 to x. Following this procedure, Eq. 4.46 becomes,

$$
\frac{d}{dt}\langle f(x(t))\rangle = \int dx \left\{ f'(x)a(x,t) + \frac{1}{2}f''(x)b(x,t)\right\} P(x,t|x_0,t_0). \quad (4.47)
$$

Integrating by parts and discarding the surface terms results in,

$$
\frac{d}{dt}\langle f(x(t))\rangle = \int dx f(x)\left\{ -\frac{d}{dx}[a(x,t)P(x,t|x_0,t_0)] + \frac{1}{2}\frac{d^2}{dx^2}[b(x,t)^2 P(x,t|x_0,t_0)]\right\}. \quad (4.48)
$$

The time development of the average value of an arbitrary function $f(x(t))$ can also be written as

$$
\frac{d}{dt}\langle f(x(t))\rangle = \int dx f(x)\frac{d}{dt}P(x,t|x_0,t_0). \quad (4.49)
$$

Equating Eqns. 4.48 and 4.49 and remembering that $f(x)$ is an arbitrary function of x results in,

$$
\frac{d}{dt}P(x,t|x_0,t_0) = -\frac{d}{dx}[a(x,t)P(x,t|x_0,t_0)] + \frac{1}{2}\frac{d^2}{dx^2}[b(x,t)^2 P(x,t|x_0,t_0)]. \quad (4.50)
$$

Eq. 4.50 is the Fokker-Planck equation for the conditional probability density $P(x,t|x_0,t_0)$ for the stochastic variable $x(t)$. This shows the equivalence between a stochastic differential equation, Eq. 4.37, for a stochastic variable $x(t)$ and a Fokker-Planck equation for the probability distribution of that variable.

4.5   C-number Langevin Equations For Coherent State Amplitudes

Eq. 4.50 is now used to find the stochastic differential equations for $\alpha(t)$ that is equivalent to Eq. 4.36. Since $P(\alpha, t)$ is complex, there are two stochastic equations; one for the real part of $P(\alpha, t)$,

$$dx = -\left(\frac{\gamma}{2}x + \omega_0 y\right)dt + \sqrt{\frac{\bar{n}}{2}}dW_1(t), \tag{4.51}$$

and one for the imaginary part of $P(\alpha, t)$,

$$dy = -\left(\frac{\gamma}{2}y - \omega_0 x\right)dt + \sqrt{\frac{\bar{n}}{2}}dW_2(t). \tag{4.52}$$

These equations can be rewritten as one complex Langevin equation as

$$d\alpha = -\left(\frac{\gamma}{2} + \imath\omega_0\right)\alpha dt + \sqrt{\bar{n}}d\eta(t), \tag{4.53}$$

where

$$d\eta(t) = \frac{(dW_1(t) + \imath dW_2(t))}{\sqrt{2}}.$$

Eq. 4.53 can be used to generate trajectories for α. These trajectories can then be used to calculate various expectation values of interest, even n time expectation values because,

$$\langle(\hat{a}^\dagger(t_1)\cdots\hat{a}^\dagger(t_m)\hat{a}(t_{m+1})\cdots\hat{a}(t_n)\rangle = \int d^2\alpha P(\alpha)\{\alpha^*(t_1)\cdots\alpha^*(t_m)\alpha(t_{m+1})\cdots\alpha(t_n)\}$$

$$= \frac{1}{N}\sum_{i=1}^N \alpha_i^*(t_1)\cdots\alpha_i^*(t_m)\alpha_i(t_{m+1})\cdots\alpha_i(t_n), \tag{4.54}$$

where $\alpha_i(t)$ is a single trajectory, and N is the number of trajectories.

The results of a computer simulation that solves Eq. 4.53 and uses Eq. 4.102 to find $\langle\hat{a}^\dagger(t)\hat{a}(t)\rangle$ and $g^{(1)}(\tau) = Re\left[\langle\hat{a}^\dagger(t_{ss} + \tau)\hat{a}(t_{ss})\rangle\right]$ are shown in Fig. 4.1 and Fig. 4.2, respectively, where t_{ss} is the time in which the system reaches steady state.

In both figures, the analytical solutions, Eqns. 3.45 and 3.55 are shown in black. In a single trajectory, which are shown in blue in both figures, the system is undergoing a random walk, so that the number of excitations randomly diffuses in time. When many of these random trajectories

are averaged together, the correct evolution for $\left\langle \hat{a}^\dagger(t)\hat{a}(t) \right\rangle$ and $g^{(1)}(\tau)$ are approached, which is shown in red, where 1000 random trajectories are averaged over. The figures show good agreement between the analytical results and the numerical results from the above Langevin method.

4.6   A More Practical Derivation of Quantum Langevin Equations

In theory, the quantum Langevin equations, along with the corresponding diffusion coefficients, for an arbitrarily complicated system can be derived as they were in section 4.1. In practice, however, there is a much simpler way to derive them, which proves very valuable with increasing system complexity. Langevin equations consist of two separate terms, called drift and diffusion terms. The drift terms consist of the Hamiltonian dynamics, and the decay due to the coupling of the system to a large reservoir. The diffusion terms contain the fluctuations caused by the coupling of the system to a large reservoir. The generalized Einstein relations provide a way to obtain the diffusion terms if the drift terms and all of the second order moments are known. The drift terms, and the second order moments can be calculated using the master equation that describes the system. Then, the diffusion terms can be found using the Einstein relations. We begin by deriving the generalized Einstein relations.

4.6.1   The Generalized Einstein Relations

Consider the Langevin equations for a general system described by the operators $\hat{A}_\mu$,

$$\frac{d}{dt}\hat{A}_\mu(t) = \hat{D}_\mu(t) + \hat{F}_\mu(t), \tag{4.55}$$

where $\hat{D}_\mu(t)$ are the drift terms and $\hat{F}_\mu(t)$ are the diffusion terms, or noise operators. We assume that the noise operators obey

$$\left\langle \hat{F}_\mu(t) \right\rangle = 0, \tag{4.56}$$

and

$$\left\langle \hat{F}_\mu(t)\hat{F}_\nu(t') \right\rangle = 2M_{\mu\nu}(t)\delta(t-t'), \tag{4.57}$$

where $M_{\mu\nu}(t)$ are called the diffusion coefficients.
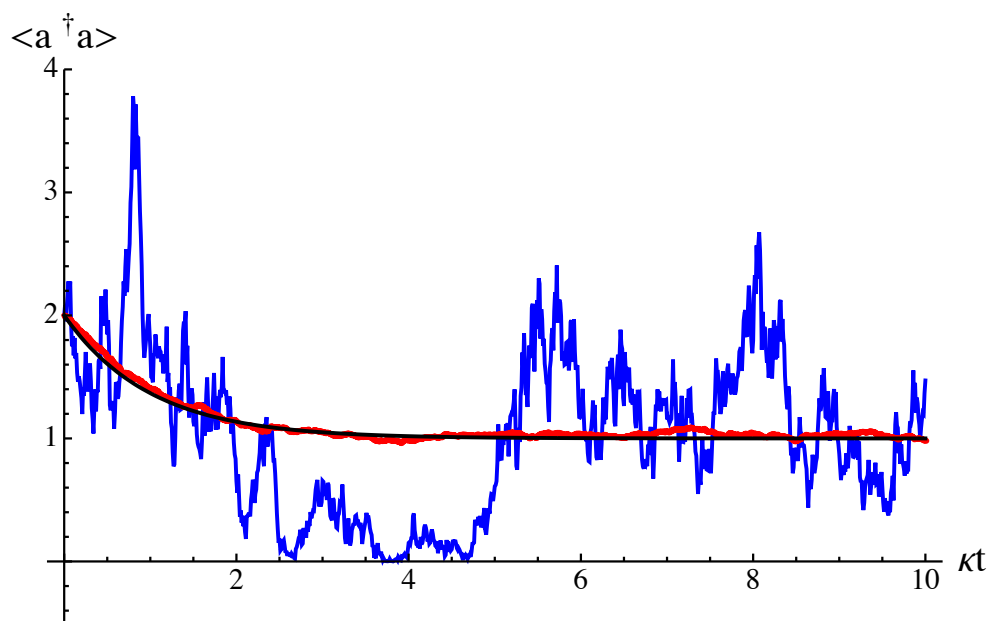
Figure 4.1: The c-number Langevin equations are used to find $\langle \hat{a}^\dagger(t)\hat{a}(t) \rangle$ for a damped harmonic oscillator with $\bar{n} = 1$, and $\alpha(0) = 2$. The analytic expression for $\langle \hat{a}^\dagger(t)\hat{a}(t) \rangle$ is shown in black, a single trajectory is shown in blue, and an average over 1000 trajectories is shown in red.
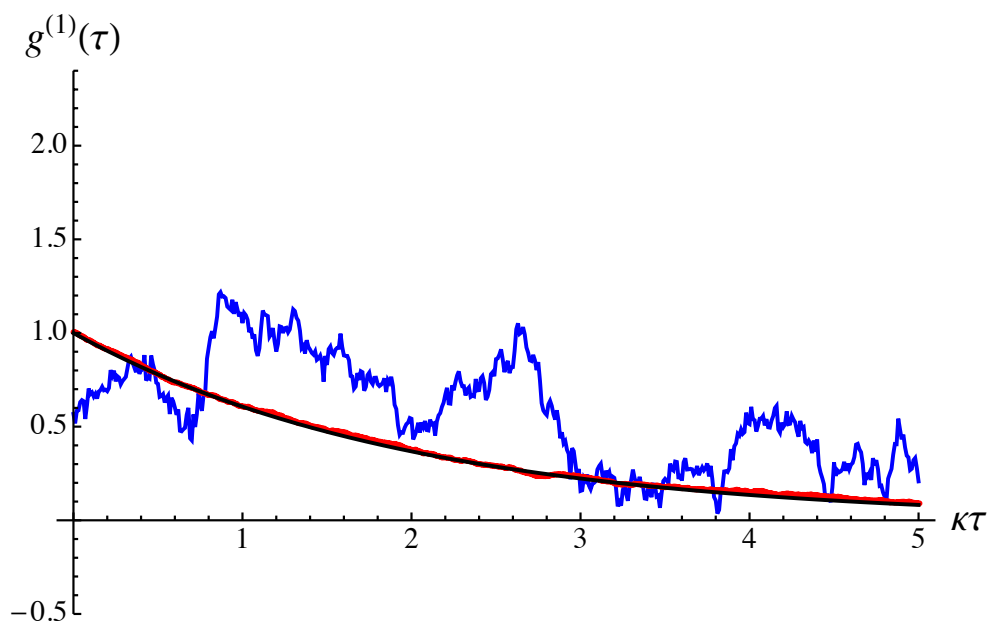
Figure 4.2: The c-number Langevin equations are used to find $g^{(1)}(\tau) = Re\left[\langle \hat{a}^\dagger(t_{ss} + \tau)\hat{a}(t_{ss})\rangle\right]$ for a damped harmonic oscillator with $\bar{n} = 1$, and $\alpha(0) = 2$, and t_{ss} is the time in which the system reaches steady state. The analytic expression for $g^{(1)}(\tau)$ is shown in black, a single trajectory is shown in blue, and an average over 1000 trajectories is shown in red.

We substitute Eq. 4.55 into the identity,

$$\hat{A}_\mu(t) = \hat{A}_\mu(t - \Delta t) + \int_{t-\Delta t}^{t} dt' \frac{d}{dt} \hat{A}_\mu(t'), \tag{4.58}$$

multiply by $\hat{F}_\nu(t)$ on the left, and then arrive at,

$$\left\langle \hat{A}_\mu(t)\hat{F}_\nu(t) \right\rangle = \left\langle \hat{A}_\mu(t - \Delta t)\hat{F}_\nu(t) \right\rangle + \int_{t-\Delta t}^{t} dt' \left\langle \hat{D}_\mu(t')\hat{F}_\nu(t) + \hat{F}_\mu(t')\hat{F}_\nu(t) \right\rangle. \tag{4.59}$$

The first term on the right hand side of Eq. 4.59 is zero on physical grounds. This is because a system operator at a given time can have no correlation with a reservoir operator at a later time, hence this term is factorizable, and $\left\langle \hat{F}_\mu(t) \right\rangle = 0$. A similar line of reasoning shows that $\left\langle \hat{D}_\mu(t')\hat{F}_\nu(t) \right\rangle = 0$, unless $t = t'$, so the lower limit of integration on this term can be changed to t, and hence this term is zero. Then,

$$\left\langle \hat{A}_\mu(t)\hat{F}_\nu(t) \right\rangle = \int_{t-\Delta t}^{t} dt' \left\langle \hat{F}_\mu(t')\hat{F}_\nu(t) \right\rangle. \tag{4.60}$$

Using Eq. 4.57, combined with the fact that a delta function lying on one of the limits of integration causes the value of the integral to be half of what it would be otherwise, results in,

$$\left\langle \hat{A}_\mu(t)\hat{F}_\nu(t) \right\rangle = M_{\mu\nu}(t). \tag{4.61}$$

In an analogous manner to the method just described, it can be shown that,

$$\left\langle \hat{F}_\mu(t)\hat{A}_\nu(t) \right\rangle = M_{\mu\nu}(t). \tag{4.62}$$

Now consider,

$$\begin{aligned}
\frac{d}{dt}\left\langle \hat{A}_\mu(t)\hat{A}_\nu(t) \right\rangle &= \left\langle \frac{d}{dt}\left(\hat{A}_\mu(t)\right)\hat{A}_\nu(t) \right\rangle + \left\langle \hat{A}_\mu(t)\frac{d}{dt}\left(\hat{A}_\nu(t)\right) \right\rangle \\
&= \left\langle \hat{D}_\mu(t)\hat{A}_\nu(t) \right\rangle + \left\langle \hat{A}_\mu(t)\hat{D}_\nu(t) \right\rangle + \left\langle \hat{F}_\mu(t)\hat{A}_\nu(t) \right\rangle + \left\langle \hat{A}_\mu(t)\hat{F}_\nu(t) \right\rangle, (4.63)
\end{aligned}$$

$$\tag{4.64}$$

where in the last line Eq. 4.55 and linearity has been used. Substituting Eqns. 4.61 and 4.62 into Eq. 4.64 and solving for $M_{\mu\nu}(t)$, results in,

$$2M_{\mu\nu}(t) = \frac{d}{dt}\left\langle \hat{A}_\mu(t)\hat{A}_\nu(t) \right\rangle - \left\langle \hat{A}_\mu(t)\hat{D}_\nu(t) \right\rangle - \left\langle \hat{D}_\mu(t)\hat{A}_\nu(t) \right\rangle. \tag{4.65}$$

Eq. 4.65 is called the generalized Einstein relation. It shows how to calculate the diffusion coefficients $M_{\mu\nu}(t)$ if the drift terms and the equations of motion for $\left\langle \hat{A}_\mu(t)\hat{A}_\nu(t) \right\rangle$ are known. The generalized Einstein relation proves invaluable when the system under consideration is complex and the exact form of the noise operators is unknown.

4.6.2   Obtaining the Drift Terms

We specialize to the system of N damped two level atoms with decay rate γ and frequency ω_a at zero temperature, driven by a strong classical field that couples to the atoms with Rabi frequency Ω. By Eq. 3.119, this system is described by,

$$\frac{d}{dt}\hat{\rho}(t) = -\frac{\imath}{\hbar}\left[\hat{H},\hat{\rho}(t)\right] - \frac{\gamma}{2}\sum_{j=1}^{N}\left(\hat{\sigma}_j^+\hat{\sigma}_j^-\,\hat{\rho}(t) + \hat{\rho}(t)\hat{\sigma}_j^+\hat{\sigma}_j^- - 2\hat{\sigma}_j^-\hat{\rho}(t)\hat{\sigma}_j^+\right),\tag{4.66}$$

with

$$\hat{H} = \frac{\hbar\omega_a}{2}\sum_{j=1}^{N}\hat{\sigma}_j^z + \frac{\hbar\Omega}{2}\sum_{j=1}^{N}(\hat{\sigma}_j^- e^{\imath\omega_c t} + \hat{\sigma}_j^+ e^{-\imath\omega_c t}),\tag{4.67}$$

where,

$$\hat{J}_z = \sum_{j=1}^{N}\hat{\sigma}_j^z,$$

$$\hat{J}_\pm = \sum_{j=1}^{N}\hat{\sigma}_j^\pm,$$

where $\hat{\sigma}_j^-,\hat{\sigma}_j^+,\hat{\sigma}_j^z$ are the Pauli matricies for the jth atom.

We seek equations for $\hat{J}_-,\hat{J}_+,\hat{J}_z$ that are of the form of Eq. 4.55,

$$\frac{d}{dt}\hat{J}_\mu(t) = \hat{D}_\mu(t) + \hat{F}_\mu(t),\tag{4.68}$$

where $\mu = \{-,+,z\}$. From Eq 4.56, the drift terms are,

$$\left\langle \hat{D}_\mu(t) \right\rangle = \left\langle \frac{d}{dt}\hat{A}_\mu(t) \right\rangle$$
$$= tr\left\{\hat{A}_\mu\frac{d}{dt}\hat{\rho}(t)\right\},\tag{4.69}$$

where the last line is valid in the Schrödinger picture. Using Eq. 4.66 we find,

$$
\begin{aligned}
\left\langle \hat{\sigma}_j^- \frac{d}{dt} \hat{\rho}(t) \right\rangle &= tr\left\{ \hat{\sigma}_j^- \frac{d}{dt} \hat{\rho}(t) \right\} \\
&= \left(-\imath\omega_a - \frac{\gamma}{2}\right)\left\langle \hat{\sigma}_j^- \right\rangle + \frac{\imath\Omega}{2} e^{-\imath\omega_c t}\left\langle \hat{\sigma}_j^z \right\rangle,
\end{aligned}
\tag{4.70}
$$

so that,

$$
\begin{aligned}
\left\langle \hat{D}_-(t) \right\rangle &= \frac{1}{N}\sum_{j=1}^{N}\left\langle \hat{\sigma}_j^- \frac{d}{dt}\hat{\rho}(t) \right\rangle \\
&= \left\langle \left(-\imath\omega_a - \frac{\gamma}{2}\right)\hat{J}_- + \frac{\imath\Omega}{2} e^{-\imath\omega_c t}\hat{J}_z \right\rangle,
\end{aligned}
\tag{4.71}
$$

and therefore,

$$
\hat{D}_-(t) = \left(-\imath\omega_a - \frac{\gamma}{2}\right)\hat{J}_- + \frac{\imath\Omega}{2} e^{-\imath\omega_c t}\hat{J}_z.
\tag{4.72}
$$

Likewise, it can be shown that,

$$
\begin{aligned}
\hat{D}_+(t) &= \left(\imath\omega_a - \frac{\gamma}{2}\right)\hat{J}_+ - \frac{\imath\Omega}{2} e^{\imath\omega_c t}\hat{J}_z, \tag{4.73}\\
\hat{D}_z(t) &= -\gamma\left(\hat{\mathbb{1}} + \hat{J}_z\right) + \imath\Omega\left(\hat{J}_- e^{\imath\omega_c t} - \hat{J}_+ e^{-\imath\omega_c t}\right), \tag{4.74}
\end{aligned}
$$

where,

$$
\hat{\mathbb{1}} = \frac{1}{N}\sum_{j=1}^{N}\hat{\mathbb{1}}_j.
\tag{4.75}
$$

We move into an interaction picture by defining,

$$
\begin{aligned}
\tilde{\hat{J}}_- &= e^{\imath\omega_c t}\hat{J}_-, \\
\tilde{\hat{J}}_+ &= e^{-\imath\omega_c t}\hat{J}_+,
\end{aligned}
\tag{4.76}
$$

and combine these with Eqns 4.72 – 4.74 to obtain,

$$
\begin{aligned}
\tilde{\hat{D}}_- &= \left(-\imath\delta - \frac{\gamma}{2}\right)\tilde{\hat{J}}_- + \frac{\imath\Omega}{2}\hat{J}_z, \\
\tilde{\hat{D}}_+ &= \left(\imath\delta - \frac{\gamma}{2}\right)\tilde{\hat{J}}_+ - \frac{\imath\Omega}{2}\hat{J}_z, \\
\tilde{\hat{D}}_z &= -\gamma\left(\hat{\mathbb{1}} + \hat{J}_z\right) + \imath\Omega\left(\tilde{\hat{J}}_- - \tilde{\hat{J}}_+\right),
\end{aligned}
\tag{4.77}
$$

where $\delta = \omega_a - \omega_c$.

4.6.3 Obtaining the Diffusion Coefficients

Now that the drift terms are known, Eq. 4.65 can be used to find the diffusion coefficients. We first find,

$$
\begin{aligned}
2\tilde{M}_{z+} &= \frac{d}{dt}\left\langle \hat{J}_z \tilde{\hat{J}}_+ \right\rangle - \left\langle \hat{J}_z \tilde{\hat{D}}_+ \right\rangle - \left\langle \tilde{\hat{D}}_z \hat{J}_+ \right\rangle \\
&= \frac{1}{N}\frac{d}{dt}\left\langle \tilde{\hat{J}}_+ \right\rangle - \left\langle \hat{J}_z\left(\left(\imath\delta - \frac{\gamma}{2}\right)\tilde{\hat{J}}_- - \frac{\imath\Omega}{2}\hat{J}_z\right)\right\rangle \\
&\quad - \left\langle \left(-\gamma\left(\hat{\mathbb{1}} + \hat{J}_z\right) + \imath\Omega\left(\tilde{\hat{J}}_- - \tilde{\hat{J}}_+\right)\right)\tilde{\hat{J}}_+ \right\rangle,
\end{aligned}
\tag{4.78}
$$

where Eqns. 4.77, and the fact that,

$$
\begin{aligned}
\hat{J}_z \tilde{\hat{J}}_+ &= \frac{1}{N^2}\sum_{i=1}^{N}\sum_{j=1}^{N}\hat{\sigma}_i^z \tilde{\sigma}_j^+ \\
&= \frac{1}{N^2}\sum_{j=1}^{N}\tilde{\sigma}_j^+ \\
&= \frac{1}{N}\tilde{\hat{J}}_+,
\end{aligned}
\tag{4.79}
$$

have been used. Also, to obtain Eq. 4.79, Eqns. 3.121 have been employed. From Eq. 4.68, it is easy to see that $\frac{d}{dt}\left\langle \tilde{\hat{J}}_+ \right\rangle = \left\langle \tilde{\hat{D}}_+ \right\rangle$, so that after substitution of Eq. 4.77, and further simplification, Eq. 4.78 becomes,

$$
\begin{aligned}
2\tilde{M}_{z+} &= \frac{1}{N}\left\langle \left(\imath\delta - \frac{\gamma}{2}\right)\tilde{\hat{J}}_- - \frac{\imath\Omega}{2}\hat{J}_z \right\rangle - \frac{1}{N}\left\langle \left(\left(\imath\delta - \frac{\gamma}{2}\right)\tilde{\hat{J}}_- - \frac{\imath\Omega}{2}\hat{\mathbb{1}}\right)\right\rangle \\
&\quad - \frac{1}{N}\left\langle \left(-\gamma\left(\tilde{\hat{J}}_+ + \tilde{\hat{J}}_+\right) + \frac{\imath\Omega}{2}\left(\hat{\mathbb{1}} - \hat{J}_z\right)\right)\right\rangle \\
&= \frac{2\gamma}{N}\left\langle \tilde{\hat{J}}_+ \right\rangle.
\end{aligned}
\tag{4.80}
$$

Likewise, it can be shown,

$$
\begin{aligned}
2\tilde{M}_{-z} &= \frac{2\gamma}{N}\left\langle \tilde{\hat{J}}_- \right\rangle, \\
2\tilde{M}_{zz} &= \frac{2\gamma}{N}\left(1 + \left\langle \tilde{\hat{J}}_z \right\rangle\right), \\
2\tilde{M}_{-+} &= \frac{\gamma}{N}.
\end{aligned}
\tag{4.81}
$$

Putting it all together, the quantum Langevin equations for N two level atoms driven by a strong classical field in an interaction picture that rotates at the field frequency are,

$$
\begin{aligned}
\frac{d}{dt}\tilde{\hat{J}}_- &= \left(-\imath\delta - \frac{\gamma}{2}\right)\tilde{\hat{J}}_- + \frac{\imath\Omega}{2}\hat{J}_z + \tilde{\hat{F}}_- \\
\frac{d}{dt}\tilde{\hat{J}}_+ &= \left(\imath\delta - \frac{\gamma}{2}\right)\tilde{\hat{J}}_+ - \frac{\imath\Omega}{2}\hat{J}_z + \tilde{\hat{F}}_+ \\
\frac{d}{dt}\hat{J}_z &= -\gamma\left(\hat{\mathbb{1}} + \hat{J}_z\right) + \imath\Omega\left(\tilde{\hat{J}}_- - \tilde{\hat{J}}_+\right) + \tilde{\hat{F}}_z,
\end{aligned}
\tag{4.82}
$$

where the noises are correlated according to,

$$
\left\langle \tilde{\hat{F}}_\mu(t)\tilde{\hat{F}}_\nu(t')\right\rangle = 2\tilde{M}_{\mu\nu}\delta(t - t'),
\tag{4.83}
$$

with,

$$
2\tilde{M}_{\mu\nu} = \begin{array}{c} - \\ + \\ z \end{array}
\begin{array}{c} \\ \end{array}
\overset{\displaystyle\begin{array}{ccc} - & + & z \end{array}}{\left(\begin{array}{ccc} 0 & \frac{\gamma}{N} & \frac{2\gamma}{N}\left\langle\tilde{\hat{J}}_-\right\rangle \\ 0 & 0 & 0 \\ 0 & \frac{2\gamma}{N}\left\langle\tilde{\hat{J}}_+\right\rangle & \frac{2\gamma}{N}\left(1 + \left\langle\tilde{\hat{J}}_z\right\rangle\right) \end{array}\right)}.
\tag{4.84}
$$

It will be convenient in the next section to work with real quantities, so we define,

$$
\begin{aligned}
\tilde{\hat{J}}_x &\equiv \tilde{\hat{J}}_+ + \tilde{\hat{J}}_- & \tilde{\hat{F}}_x &\equiv \tilde{\hat{F}}_+ + \tilde{\hat{F}}_- \\
\tilde{\hat{J}}_y &\equiv -i\left(\tilde{\hat{J}}_+ - \tilde{\hat{J}}_-\right) & \tilde{\hat{F}}_y &\equiv -i\left(\tilde{\hat{F}}_+ - \tilde{\hat{F}}_-\right).
\end{aligned}
\tag{4.85}
$$

Using these definitions, and Eqns. 4.82 and Eqns. 4.84, it is then trivial to show that,

$$
\begin{aligned}
\frac{d}{dt}\tilde{\hat{J}}_x &= -\frac{\gamma}{2}\tilde{\hat{J}}_x - \delta\tilde{\hat{J}}_y + \tilde{\hat{F}}_x, \\
\frac{d}{dt}\tilde{\hat{J}}_y &= \delta\tilde{\hat{J}}_x - \frac{\gamma}{2}\tilde{\hat{J}}_y - \Omega\hat{J}_z + \tilde{\hat{F}}_y, \\
\frac{d}{dt}\hat{J}_z &= -\gamma\left(\hat{\mathbb{1}} + \hat{J}_z\right) + \Omega\tilde{\hat{J}}_y + \tilde{\hat{F}}_z,
\end{aligned}
\tag{4.86}
$$

where the noises are correlated according to,

$$
\left\langle \tilde{\hat{F}}_\mu(t)\tilde{\hat{F}}_\nu(t')\right\rangle = 2\tilde{M}_{\mu\nu}\delta(t - t'),
\tag{4.87}
$$

with,

$$2\tilde{M}_{\mu\nu} = \begin{array}{c} \\ x \\ y \\ z \end{array} \begin{array}{ccc} x & y & z \\ \left(\begin{array}{ccc} \frac{\gamma}{N} & -\frac{i\gamma}{N} & \frac{\gamma}{N}\left(\left\langle\tilde{\hat{J}}_x\right\rangle - i\left\langle\tilde{\hat{J}}_y\right\rangle\right) \\ \frac{i\gamma}{N} & \frac{\gamma}{N} & \frac{i\gamma}{N}\left(\left\langle\tilde{\hat{J}}_x\right\rangle - i\left\langle\tilde{\hat{J}}_y\right\rangle\right) \\ \frac{\gamma}{N}\left(\left\langle\tilde{\hat{J}}_x\right\rangle + i\left\langle\tilde{\hat{J}}_y\right\rangle\right) & -\frac{i\gamma}{N}\left(\left\langle\tilde{\hat{J}}_x\right\rangle + i\left\langle\tilde{\hat{J}}_y\right\rangle\right) & \frac{2\gamma}{N}\left(1 + \left\langle\tilde{\hat{J}}_z\right\rangle\right) \end{array}\right) \end{array}. \tag{4.88}$$

4.7 A More Practical Derivation of the C-number Langevin Equations

4.7.1 Solving for the C-Number Diffusion Coefficients

There is also a more practical way to derive c-number Langevin equations than the method described in Sections 4.3 - 4.5. We assume that there exists a set of c-number equations that have a correspondence with the quantum Langevin equations,

$$\begin{aligned} \frac{d}{dt}\mathcal{J}_x &= -\frac{\gamma}{2}\mathcal{J}_x - \delta\mathcal{J}_y + \mathcal{F}_x, \\ \frac{d}{dt}\mathcal{J}_y &= \delta\mathcal{J}_x - \frac{\gamma}{2}\mathcal{J}_y - \Omega\mathcal{J}_z + \mathcal{F}_y, \\ \frac{d}{dt}\mathcal{J}_z &= -\gamma\left(1 + \mathcal{J}_z\right) + \Omega\mathcal{J}_y + \mathcal{F}_z, \end{aligned} \tag{4.89}$$

with,

$$\langle\mathcal{F}_\mu(t)\rangle = 0, \tag{4.90}$$

where $\mu = \{-, +, z\}$. Also the noises are correlated according to,

$$\langle\mathcal{F}_\mu(t)\mathcal{F}_\nu(t')\rangle = 2\mathcal{M}_{\mu\nu}(t)\delta(t - t'), \tag{4.91}$$

where $\mathcal{M}_{\mu\nu}$ is a 3×3 an unknown matrix of c-numbers, as a function of time. The entire problem thus boils down to finding the c-number diffusion matrix elements $\mathcal{M}_{\mu\nu}$ that make the c-number Langevin equation have a correspondence with the quantum Langevin equation. To make this correspondence, we force the second order moments from the quantum equations to be equal to the second order moments from the c-number equation. However, since c-numbers commute, and

quantum operators do not, we must choose an ordering for the quantum equations before the correspondence can be made.

To illustrate this point, consider the following c-number second order moment, constructed from Eq. 4.89,

$$
\begin{aligned}
\frac{d}{dt}\langle \mathcal{J}_x \mathcal{J}_y \rangle &= \left\langle \left(\frac{d}{dt}\mathcal{J}_x\right)\mathcal{J}_y \right\rangle + \left\langle \mathcal{J}_x\left(\frac{d}{dt}\mathcal{J}_y\right)\right\rangle \\
&= \left\langle \left(-\frac{\gamma}{2}\mathcal{J}_x - \delta\mathcal{J}_y + \mathcal{F}_x\right)\mathcal{J}_y\right\rangle + \left\langle \mathcal{J}_x\left(\delta\mathcal{J}_x - \frac{\gamma}{2}\mathcal{J}_y - \Omega\mathcal{J}_z + \mathcal{F}_y\right)\right\rangle \\
&= -\gamma\langle\mathcal{J}_x\mathcal{J}_y\rangle + \delta\left(-\langle\mathcal{J}_y\mathcal{J}_y\rangle + \langle\mathcal{J}_x\mathcal{J}_x\rangle\right) - \Omega\langle\mathcal{J}_x\mathcal{J}_z\rangle + 2\mathcal{M}_{xy}, \qquad (4.92)
\end{aligned}
$$

where $\mathcal{M}_{xy} = \left\langle \tilde{\hat{F}}_x \tilde{\hat{J}}_y \right\rangle = \left\langle \tilde{\hat{J}}_x \tilde{\hat{F}}_y \right\rangle$. Since c-numbers commute, and quantum operators do not, Eq. 4.92 can correspond with equal validity to the quantum second order moment,

$$
\begin{aligned}
\frac{d}{dt}\left\langle \tilde{\hat{J}}_x \tilde{\hat{J}}_y \right\rangle &= \left\langle \left(\frac{d}{dt}\tilde{\hat{J}}_x\right)\tilde{\hat{J}}_y \right\rangle + \left\langle \tilde{\hat{J}}_x\left(\frac{d}{dt}\tilde{\hat{J}}_y\right)\right\rangle \\
&= \left\langle \left(-\frac{\gamma}{2}\tilde{\hat{J}}_x - \delta\tilde{\hat{J}}_y + \tilde{\hat{F}}_x\right)\tilde{\hat{J}}_y\right\rangle + \left\langle \tilde{\hat{J}}_x\left(\delta\tilde{\hat{J}}_x - \frac{\gamma}{2}\tilde{\hat{J}}_y - \Omega\hat{J}_z + \tilde{\hat{F}}_y\right)\right\rangle \\
&= -\gamma\left\langle\tilde{\hat{J}}_x\tilde{\hat{J}}_y\right\rangle + \delta\left(-\left\langle\tilde{\hat{J}}_y\tilde{\hat{J}}_y\right\rangle + \left\langle\tilde{\hat{J}}_x\tilde{\hat{J}}_x\right\rangle\right) - \Omega\left\langle\tilde{\hat{J}}_x\hat{J}_z\right\rangle + 2\tilde{M}_{xy}, \qquad (4.93)
\end{aligned}
$$

or its anti-ordered counterpart,

$$
\begin{aligned}
\frac{d}{dt}\left\langle \tilde{\hat{J}}_y \tilde{\hat{J}}_x \right\rangle &= \left\langle \left(\frac{d}{dt}\tilde{\hat{J}}_y\right)\tilde{\hat{J}}_x \right\rangle + \left\langle \tilde{\hat{J}}_y\left(\frac{d}{dt}\tilde{\hat{J}}_x\right)\right\rangle \\
&= \left\langle \left(\delta\tilde{\hat{J}}_x - \frac{\gamma}{2}\tilde{\hat{J}}_y - \Omega\hat{J}_z + \tilde{\hat{F}}_y\right)\tilde{\hat{J}}_x\right\rangle + \left\langle \tilde{\hat{J}}_y\left(-\frac{\gamma}{2}\tilde{\hat{J}}_x - \delta\tilde{\hat{J}}_y + \tilde{\hat{F}}_x\right)\right\rangle \\
&= -\gamma\left\langle\tilde{\hat{J}}_y\tilde{\hat{J}}_x\right\rangle + \delta\left(-\left\langle\tilde{\hat{J}}_y\tilde{\hat{J}}_y\right\rangle + \left\langle\tilde{\hat{J}}_x\tilde{\hat{J}}_x\right\rangle\right) - \Omega\left\langle\tilde{\hat{J}}_z\hat{J}_x\right\rangle + 2\tilde{M}_{yx}, \qquad (4.94)
\end{aligned}
$$

or a symmetric combination of the two,

$$
\begin{aligned}
\frac{d}{dt}\left\langle \tilde{\hat{J}}_x \tilde{\hat{J}}_y \right\rangle_s &= \frac{d}{dt}\left(\frac{1}{2}\left\langle \tilde{\hat{J}}_x \tilde{\hat{J}}_y \right\rangle + \frac{1}{2}\left\langle \tilde{\hat{J}}_y \tilde{\hat{J}}_x \right\rangle\right) \\
&= -\gamma\left\langle\tilde{\hat{J}}_x\tilde{\hat{J}}_y\right\rangle_s + \delta\left(-\left\langle\tilde{\hat{J}}_y\tilde{\hat{J}}_y\right\rangle_s + \left\langle\tilde{\hat{J}}_x\tilde{\hat{J}}_x\right\rangle_s\right) - \Omega\left\langle\tilde{\hat{J}}_x\hat{J}_z\right\rangle_s + \tilde{M}_{xy} + \tilde{M}_{yx}. (4.95)
\end{aligned}
$$

Here, we choose to make the symmetric correspondence, so that,

$$
\begin{aligned}
2\mathcal{M}_{xy} &\equiv \tilde{M}_{xy} + \tilde{M}_{yx} \\
&= -\frac{i\gamma}{N} + \frac{i\gamma}{N} \\
&= 0. \qquad (4.96)
\end{aligned}
$$

We choose the symmetric correspondence for several reasons. First, in this case, and in many other cases, it allows for the simplest diffusion matrix $2\mathcal{M}_{\mu\nu}$. Second, in the symmetric correspondence, $2\mathcal{M}_{\mu\nu}$ is, by construction, automatically a symmetric matrix. This fact allows an easy algorithm to be performed to find the noises that reproduce $2\mathcal{M}_{\mu\nu}$ for numerical simulations. Finally, again by construction, there will not be any commutator pieces left to be absorbed into the diffusion coefficients when the symmetric correspondence is made. To demonstrate this, consider the following c-number second order moment,

$$
\begin{aligned}
\frac{d}{dt}\langle \mathcal{J}_y\mathcal{J}_y\rangle &= \left\langle \left(\frac{d}{dt}\mathcal{J}_y\right)\mathcal{J}_y\right\rangle + \left\langle \mathcal{J}_y\left(\frac{d}{dt}\mathcal{J}_y\right)\right\rangle \\
&= \left\langle \left(\delta\mathcal{J}_x - \frac{\gamma}{2}\mathcal{J}_y - \Omega\hat{J}_z + \mathcal{F}_y\right)\mathcal{J}_y\right\rangle + \left\langle \mathcal{J}_y\left(\delta\mathcal{J}_x - \frac{\gamma}{2}\mathcal{J}_y - \Omega\hat{J}_z + \mathcal{F}_y\right)\right\rangle \\
&= 2\delta\langle\mathcal{J}_x\mathcal{J}_y\rangle - \gamma\langle\mathcal{J}_y\mathcal{J}_y\rangle - 2\Omega\langle\mathcal{J}_z\mathcal{J}_y\rangle + 2\mathcal{M}_{yy},
\end{aligned}
\tag{4.97}
$$

and the following quantum second order moment,

$$
\begin{aligned}
\frac{d}{dt}\left\langle \tilde{\hat{J}}_y\tilde{\hat{J}}_y\right\rangle &= \left\langle \left(\frac{d}{dt}\tilde{\hat{J}}_y\right)\tilde{\hat{J}}_y\right\rangle + \left\langle \tilde{\hat{J}}_y\left(\frac{d}{dt}\tilde{\hat{J}}_y\right)\right\rangle \\
&= \left\langle \left(\delta\tilde{\hat{J}}_x - \frac{\gamma}{2}\tilde{\hat{J}}_y - \Omega\hat{J}_z + \tilde{\hat{F}}_y\right)\tilde{\hat{J}}_y\right\rangle + \left\langle \tilde{\hat{J}}_y\left(\delta\tilde{\hat{J}}_x - \frac{\gamma}{2}\tilde{\hat{J}}_y - \Omega\hat{J}_z + \tilde{\hat{F}}_y\right)\right\rangle \\
&= \delta\left\langle \tilde{\hat{J}}_x\tilde{\hat{J}}_y\right\rangle + \delta\left\langle \tilde{\hat{J}}_y\tilde{\hat{J}}_x\right\rangle - \gamma\left\langle \tilde{\hat{J}}_y\tilde{\hat{J}}_y\right\rangle - \Omega\left\langle \hat{J}_z\tilde{\hat{J}}_y\right\rangle - \Omega\left\langle \tilde{\hat{J}}_y\hat{J}_z\right\rangle + 2\tilde{M}_{yy}.
\end{aligned}
\tag{4.98}
$$

Since, for instance, $\langle\mathcal{J}_z\mathcal{J}_y\rangle$ can not correspond to both $\left\langle \tilde{\hat{J}}_y\hat{J}_z\right\rangle$ and $\left\langle \tilde{\hat{J}}_z\hat{J}_y\right\rangle$ simultaneously, commutation relations must be used to put Eq. 4.98 in terms of one or the other before a correspondence can be made. The resulting left over commutator piece will have to be absorbed into the definition of $2\mathcal{M}_{yy}$. However, in the symmetric correspondence, since,

$$
\frac{d}{dt}\left\langle \tilde{\hat{J}}_\mu\tilde{\hat{J}}_\nu\right\rangle_s = \frac{1}{2}\frac{d}{dt}\left\langle \tilde{\hat{J}}_\mu\tilde{\hat{J}}_\nu\right\rangle + \frac{1}{2}\frac{d}{dt}\left\langle \tilde{\hat{J}}_\nu\tilde{\hat{J}}_\mu\right\rangle,
\tag{4.99}
$$

every term will automatically have its symmetric counterpart, so that there will be no left over commutator pieces to absorb into $\mathcal{M}_{\mu\nu}$. Therefore, in the symmetric correspondence, we can automatically set,

$$
2\mathcal{M}_{\mu\nu} = \tilde{M}_{\mu\nu} + \tilde{M}_{\nu\mu}.
\tag{4.100}
$$

In the symmetric correspondence, therefore, the c-number diffusion matrix is,

$$
2\mathcal{M}_{\mu\nu} =
\begin{array}{c}
 \\
x \\
y \\
z
\end{array}
\begin{array}{ccc}
x & y & z \\
\left(\begin{array}{ccc}
\frac{\gamma}{N} & 0 & \frac{\gamma}{N}\langle\mathcal{J}_x\rangle \\
0 & \frac{\gamma}{N} & \frac{\gamma}{N}\langle\mathcal{J}_y\rangle \\
\frac{\gamma}{N}\langle\mathcal{J}_x\rangle & \frac{\gamma}{N}\langle\mathcal{J}_y\rangle & \frac{2\gamma}{N}\left(1+\langle\mathcal{J}_z\rangle\right)
\end{array}\right) .
\end{array}
\tag{4.101}
$$

Eqns. 4.89 and Eq. 4.101 are the c-number Langevin equations for N two level atoms driven by a strong field, corresponding to symmetric ordering. These c-number Langevin equations correspond to a Fokker-Planck equation for a Wigner quazi-probability distribution.

4.7.2   Numerical Simulation of C-number Langevin Equations

The final problem that must be overcome before a numerical simulation can take place is how to choose the noises in Eqns. 4.89 so that Eq. 4.101 is reproduced. Since Eq. 4.101 is symmetric, it is easy to diagonalize. In this diagonal basis, the noises are simply the square root of independent real Wiener processes. Then the inverse transformation is applied, and in the original basis, the noises will be linear combinations of the independent real Wiener processes, and they will reproduce Eq. 4.101.

Now that this final problem has been solved, Eqns. 4.89 with noises that satisfying Eq. 4.101 can be used to generate trajectories. These trajectories can then be used to calculate various symmetric expectation values of interest,

$$
\left\langle \hat{J}_\mu(t_1)\cdots\hat{J}_\nu(t_m)\right\rangle_s = \frac{1}{N}\sum_{i=1}^{N}\mathcal{J}_\mu(t_1)\cdots\mathcal{J}_\nu(t_m),
\tag{4.102}
$$

where $\mathcal{J}_\mu(t)$ is an operator for a single trajectory, and N is the number of trajectories.

The results of a computer simulation that solves Eqns. 4.89 subject to Eq. 4.101 to find $\left\langle\hat{J}_z(t)\right\rangle$ and $S(\omega)$, the normalized Fourier transform of $g^{(1)}(\tau) = Re\left[\left\langle\hat{J}_+(t_{ss}+\tau)\hat{J}_-(t_{ss})\right\rangle\right]$ are shown in Fig. 4.3 and Fig. 4.4, respectively. Here, t_{ss} is the time in which the system reaches steady state.
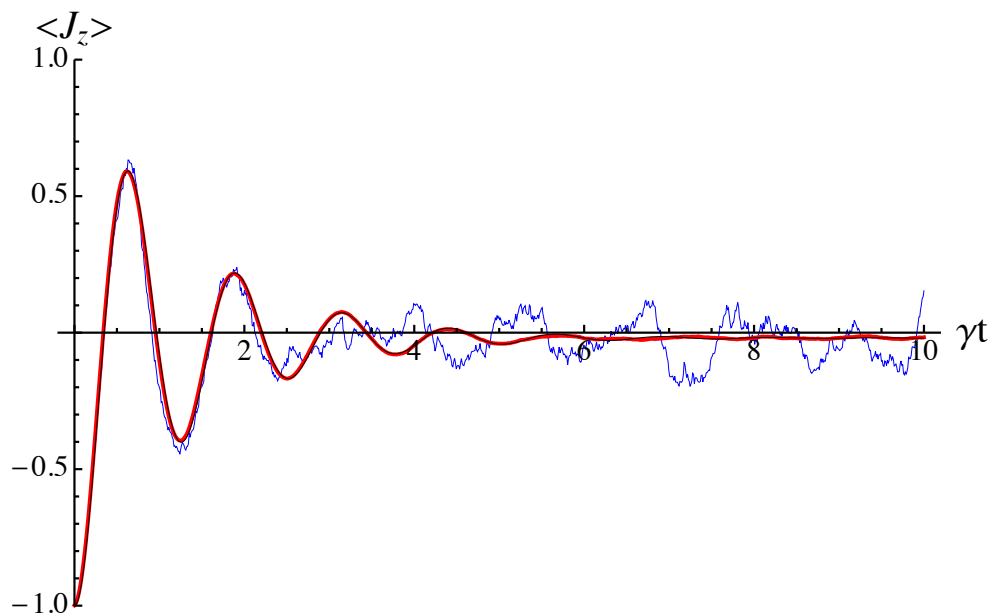
Figure 4.3: The c-number Langevin equations for symmetric ordering are used to find the inversion $\left\langle \hat{J}_z(t) \right\rangle$ for resonance fluorescence for $N = 100$ atoms, with $\Omega = 5\gamma$ and $\delta = 0$. The analytic expression for $\left\langle \hat{J}_z(t) \right\rangle$ for $N = 1$ is shown in black, a single trajectory is shown in blue, and an average over 1000 trajectories is shown in red.
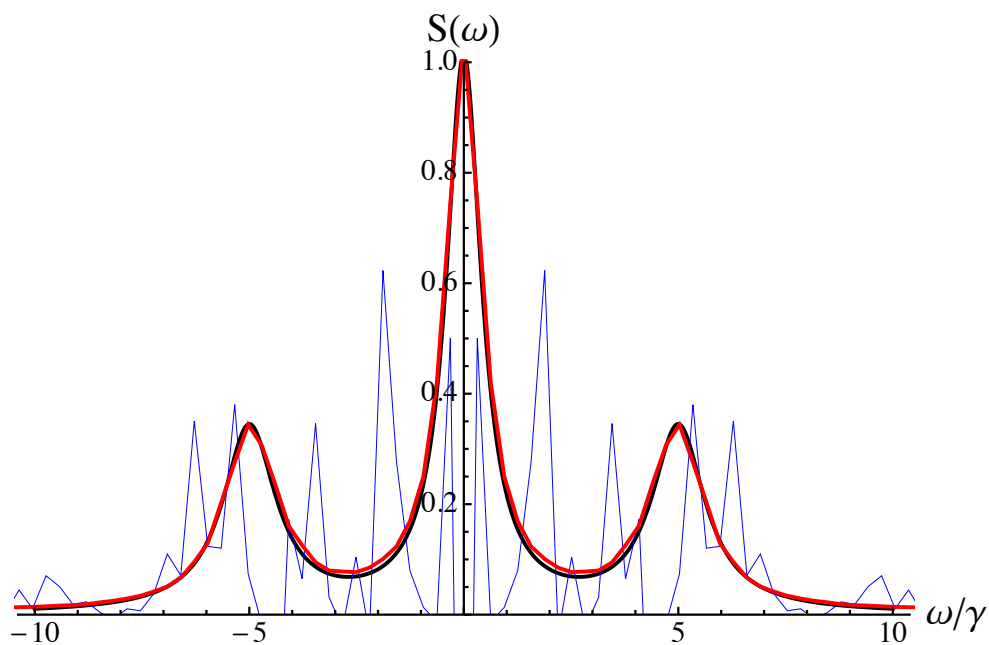
Figure 4.4: The c-number Langevin equations for symmetric ordering are used to find $S(\omega)$, the normalized Fourier transform of $g^{(1)}(\tau)$ for resonance fluorescence for $N = 100$ atoms, with $\Omega = 5\gamma$ and $\delta = 0$. The analytic expression for $S(\omega)$ for $N = 1$ is shown in black, a single trajectory is shown in blue, and an average over 1000 trajectories is shown in red.

In both figures, the analytical solutions for single atom resonance fluorescence [85] are shown in black. In a single trajectory, which are shown in blue in both figures, the system is undergoing a random walk, so that the number of excitations randomly diffuses in time. When many of these random trajectories are averaged together, the correct evolution for $\left\langle \hat{J}_z(t) \right\rangle$ and $S(\omega)$ are approached, which is shown in red, where 1000 random trajectories are averaged over.

4.8   Conclusion

We have seen how Langevin equations for quantum operators are derived. The approximations that go into this derivation are equivalent to the approximations used in the derivation of the master equation. In the superradiance limit, the cavity field described by the quantum Langevin equations can be adiabatically eliminated, and used to derive the superradiance master equation. Since Langevin equations of quantum operators are difficult to solve numerically, a Fokker-Planck equation for a quazi-probability distribution was derived. Here, we used the normal ordered quazi-probability distribution, called the P-function, which can be used to calculate normal ordered moments. This distribution was shown to be equivalent to a set of c-number Langevin equations by using methods of Ito stochastic calculus. These c-number Langevin equations were solved for many trajectories, which can be used to find general n-time expectation values. Since the derivation of the Fokker-Planck equation becomes quite complicated for systems of increasing complexity, a method to more practically derive c-number Langevin equations was described. This involved deriving the generalized Einstein relations, which allow the diffusion, or noise terms of a set of quantum Langevin equations to be known, if the diffusion terms are known. The drift terms and second ordered moments were found using a master equation, and the Einstein relations were then used to find the diffusion terms. Then, the method to find a correspondence to a set of c-number equations for a given ordering was described. We specialize here to use a symmetric correspondence, because in this ordering, the form of the equations are best suited for the numerical algorithm that we describe. Although this method may seem like unnecessary machinery to solve such a simple problem, it really proves worth its weight in gold when more complex systems are

analyzed involving large numbers of atoms.

Chapter 5

The Crossover from Lasing to Steady State Superradiance

The bulk of this chapter is being prepared for submission to Physical Review A. [81]

Since its first demonstration in 1960 [60], the laser has had a profound impact on fundamental science research and numerous areas of society. Lasers are integral to many fields of research and technological applications, ranging from atomic and molecular physics research, atomic clocks, the global positioning system, nuclear fusion research, biology research, medicine, and consumer electronics. Although many different types of lasers exist, with their characteristic parameters (such as intensity, power, linewidth, physical size) spanning many orders of magnitude, all lasers share a common conceptual foundation. A laser is a cavity quantum electrodynamics (QED) system consisting of a gain medium inside an optical cavity. We will oftentimes refer to the gain medium as "atoms" for brevity. Lasers typically operate in the good cavity regime of cavity QED where the linewidth of the cavity is much narrower than the bandwidth of the gain medium. The atoms generate a coherent electromagnetic field in the cavity by means of stimulated emission [73]. Stimulated emission is a quantum mechanical interference effect in which the presence of a large number of photons in a particular mode of a light field increases the probability that an atom will emit into that mode. The energy emitted into the cavity field has to be replenished by some repumping mechanism to achieve steady state operation. In a laser, the macroscopic phase information that is associated with the coherence of the generated radiation is encoded in the light field.

Around the same time as the laser was first demonstrated, the effect of superradiance was

predicted [19], and soon thereafter, experimentally demonstrated. Superradiance is a quantum mechanical interference effect in which correlations between atoms lead to collective emission. Superradiance has most commonly been considered as a pulsed phenomenon. Atoms in an ensemble are prepared in the excited state. Spontaneous emission into one or a few spatial modes is then enhanced via growth of atom-atom correlations. However, it has been known for some time that superradiance can also occur in steady state [66, 65, 64, 22] by placing the atomic ensemble inside a cavity. In contrast to lasers, superradiance in steady-state occurs in a cavity with a much broader linewidth than the atomic linewidth. This regime is referred to as the bad-cavity limit of cavity QED [84, 57, 14, 39, 40]. The radiation produced in steady state superradiance is also coherent. However, in contrast to a laser, the coherence is encoded in the atomic medium. Progress has recently been made towards the experimental verification [10, 9] of this proposal.

An important application of lasers is as a stable local oscillator for optical atomic clocks and precision spectroscopy. These lasers rely on stabilization against reference cavities. The most advanced such lasers reach linewidths of < 0.1Hz corresponding to quality factors of $Q > 10^{15}$ [16]. The principal limiting factor in the way of further improvement of these local oscillators is thermal vibrations of the dielectric coatings in the cavity mirrors [51]. To overcome this technical challenge, researchers have proposed an alternate approach using an active system based on steady state superradiance on a clock transition to create an even more stable light source [66, 14]. However, this proposal has challenges of its own. First of all, in spite of the enhancement that occurs due to superradiance, the produced intensity is orders of magnitude lower than for a conventional laser. Second of all, perturbations of atomic transition frequencies can potentially lead to phase and frequency perturbations in the generated field.

In this chapter we develop a unified theory for lasers and steady state superradiance. In this unified theory, lasers and steady state superradiance are the extreme limits of a continuous crossover and the theory continuously interpolates between the two. This allows us to directly compare and contrast lasers, steady state superradiant systems, and systems in the crossover region using the same language. Our analysis thus further clarifies the qualitative and quantitative differences

between lasing and steady state superradiance. From the perspective of applications the unified theory enables us to determine the optimal system for ultra stable local oscillators and precision measurement applications.

We analyze the model using different levels of approximation: An exact method using SU(4) operators, a semi-classical method based on c-number Langevin equations, a semi-classical method based on the cumulant expansion method, a quantum phase diffusion model for the field amplitude, and a mean field model. The different approaches provide insight into different aspects of the problem. Highly simplified models like the mean field equations and phase diffusion yield a qualitative understanding of the general characteristics of systems throughout the crossover. By comparison between the approximations we can differentiate between truly critical physical effects and less important details. We find that fluctuations and correlations are essential for the noise properties of the system (e.g. the linewidth of the generated light) but that the fluctuations and correlations can be modeled semi-classically. Comparison with the exact SU(4) method for small numbers of atoms shows that c-number Langevin equations provide an accurate description of the system. Due to their much smaller computational complexity, we are then able to use the c-number Langevin equations to quantitatively study much larger systems relevant for experiment.

The rest of this chapter is organized as follows. In section 5.1 we summarize the physical model upon which our analysis is based. In 5.2 we discuss several approximation methods. We compare the approximations with one another to determine their accuracy and to evaluate their ability to capture the various physical signatures. In section 5.3 we define a crossover parameter which characterizes the relative importance of stimulated emission to collective atomic effects in a cavity QED system. In section 5.4 we discuss our results on the crossover.

5.1 Model

We model our system as a collection of N two-level atoms inside a single mode optical cavity using the quantum Born-Markov master equation to describe the open quantum system,

$$\frac{d}{dt}\hat{\rho} = \frac{1}{i\hbar}\left[\hat{H},\hat{\rho}\right] + \hat{\mathcal{L}}\left[\hat{\rho}\right], \tag{5.1}$$

where,

$$\hat{H} = \frac{\hbar\omega_a}{2}\sum_{j=1}^{N}\hat{\sigma}_j^z + \hbar\omega_c\hat{a}^\dagger\hat{a} + \frac{\hbar\Omega}{2}\sum_{j=1}^{N}\left(\hat{a}^\dagger\hat{\sigma}_j^- + \hat{\sigma}_j^+\hat{a}\right), \tag{5.2}$$

and $\hat{\mathcal{L}}\left[\hat{\rho}\right]$ denotes the Liouvillian superoperator.

The Hamiltonian $\hat{H}$ describes the coherent evolution of the coupled atom cavity system, where ω_a is the frequency between the two levels of each of the atoms, and ω_c is the frequency of the cavity mode. The Pauli spin matrices for the atoms are $\hat{\sigma}_j^+$,$\hat{\sigma}_j^-$ and $\hat{\sigma}_j^z$, and $\hat{a}$ is the annihilation operator of the cavity mode. The atom-cavity coupling rate is Ω. That we take this to be the same for all items implies assumption of the equivalence of the atom-cavity coupling at the positions of all of the atoms. This could be achieved by strongly confining the ensemble in a optical lattice potential at the antinodes of the cavity modefunction.

The incoherent evolution is described by the Liouvillian $\hat{\mathcal{L}}\left[\hat{\rho}\right]$,

$$\begin{aligned}
\hat{\mathcal{L}}\left[\hat{\rho}\right] &= -\frac{\kappa}{2}\left(\hat{a}^\dagger\hat{a}\hat{\rho} + \hat{\rho}\hat{a}^\dagger\hat{a} - 2\hat{a}\hat{\rho}\hat{a}^\dagger\right) \\
&\quad -\frac{\gamma}{2}\sum_{j=1}^{N}\left(\hat{\sigma}_j^+\hat{\sigma}_j^-\hat{\rho} + \hat{\rho}\hat{\sigma}_j^+\hat{\sigma}_j^- - 2\hat{\sigma}_j^-\hat{\rho}\hat{\sigma}_j^+\right) \\
&\quad -\frac{w}{2}\sum_{j=1}^{N}\left(\hat{\sigma}_j^-\hat{\sigma}_j^+\hat{\rho} + \hat{\rho}\hat{\sigma}_j^-\hat{\sigma}_j^+ - 2\hat{\sigma}_j^+\hat{\rho}\hat{\sigma}_j^-\right), \\
&\quad +\frac{1}{2T_2}\sum_{j=1}^{N}\left(\hat{\sigma}_j^z\hat{\rho}\hat{\sigma}_j^z - \hat{\rho}\right),
\end{aligned} \tag{5.3}$$

where $\hat{\rho}$ is the system's density matrix, κ is the decay rate of the cavity, γ is the incoherent decay rate of the atoms, w is the incoherent repumping rate of the atoms, and $\frac{1}{T_2}$ is the inhomogeneous dephasing rate.

5.2   Solution Methods

Eq. 5.1 becomes increasingly complex with increasing atom number N, since the associated Hilbert space scales as 2^N. Exact simulation methods, such as the quantum jump and quantum state diffusion methods, are limited to $N \sim 10$ with the cavity field basis truncated to just a few photons.

The SU(4) solution method [43] [88] exploits an underlying permutation symmetry in Eq. 5.1 to drastically reduce the number of basis states needed to describe the problem, allowing systems with $N \sim 100$ to be treated. However to treat this many particles, the cavity field basis must also be truncated to just a few photons. In order to treat systems which have a larger number of photons, we combine the SU(4) method with the quantum jump method [17] [27] [69]. Even with the ability to describe problems with larger photon number, $N \sim 100$ is still too few particles to describe many realistic experimental situations.

We therefore also describe the c-number Langevin equation method [75, 55], which approximate the quantum Langevin equations that are equivalent to Eq. 5.1. These equations do not scale with N in the same way, and therefore can often be used to treat systems with large N where an exact treatment is not possible. Another method that does not scale with N in the same way is the mean field solutions of the quantum Langevin equations, along with an analytic solution for the linewidth of the power spectrum, which assumes Gaussian phase fluctuations and neglects amplitude fluctuations [39, 40]. Finally, the cumulant expansion method [56] does not scale exponentially with N, and can therefore also be used to treat large systems. These methods are now described in detail.

5.2.1   Langevin Theory

5.2.1.1   Quantum Langevin Equations

The Quantum Langevin equations that are equivalent to Eq. 5.1 are are derived using the method demonstrated in Chapter 4.6, and are given by,

$$\frac{d}{dt}\hat{a} = -\frac{1}{2}(\kappa + 2i\omega_c)\hat{a} - \frac{iN\Omega}{2}\hat{S}^- + \hat{F}^a, \tag{5.4}$$

$$\frac{d}{dt}\hat{S}^- = -\frac{1}{2}\left(\Gamma + 2i\omega_a\right)\hat{S}^- + \frac{i\Omega}{2}\hat{a}\hat{S}^z + \hat{F}^-, \tag{5.5}$$

$$\frac{d}{dt}\hat{S}^z = -(w+\gamma)\left(\hat{S}^z - d_0\right) + i\Omega\left(\hat{a}^\dagger\hat{S}^- - \hat{a}\hat{S}^+\right) + \hat{F}^z, \tag{5.6}$$

where $\delta = \omega_a - \omega_c$. We have defined the collective operators,

$$\hat{S}^- = \frac{1}{N}\sum_{k=1}^{N}\hat{\sigma}_k^-,$$

$$\hat{S}^z = \frac{1}{N}\sum_{k=1}^{N}\hat{\sigma}_k^z,$$

where $\Gamma \equiv w + \gamma + \frac{2}{T_2}$, $d_0 = \frac{w-\gamma}{w+\gamma}$ and where $\hat{S}^+$ and $\hat{S}^-$ are Hermitian conjugates of one another, $\hat{S}^+ = (\hat{S}^-)^\dagger$. The noise operators $\hat{F}^\mu$ have zero mean and their second order correlations are given by

$$\left\langle \hat{F}^\mu(t)\hat{F}^\nu(t')\right\rangle = 2D^{\mu\nu}\delta(t - t') . \tag{5.7}$$

The diffusion matrix elements $D^{\mu\nu}$ can be calculated using the Einstein relations [67],

$$2D^{aa^\dagger} = \kappa$$

$$2D^{+-} = \frac{1}{N}\left(w + \frac{1}{T_2}\left(1 + \left\langle\hat{S}^z\right\rangle\right)\right)$$

$$2D^{-+} = \frac{1}{N}\left(\gamma + \frac{1}{T_2}\left(1 - \left\langle\hat{S}^z\right\rangle\right)\right)$$

$$2D^{+z} = -\frac{2w}{N}\left\langle\hat{S}^+\right\rangle \qquad 2D^{z+} = \frac{2\gamma}{N}\left\langle\hat{S}^+\right\rangle$$

$$2D^{-z} = \frac{2\gamma}{N}\left\langle\hat{S}^-\right\rangle \qquad 2D^{z-} = -\frac{2w}{N}\left\langle\hat{S}^-\right\rangle$$

$$2D^{zz} = \frac{2\gamma}{N}\left(1 + \left\langle\hat{S}^z\right\rangle\right) + \frac{2w}{N}\left(1 - \left\langle\hat{S}^z\right\rangle\right). \tag{5.8}$$

5.2.1.2   *c*-number Langevin equations for numerical simulations

The quantum Langevin equation are operator valued stochastic differential equations. As such they are not suited for practical computations. To obtain practical equations we construct a semi-classical theory by replacing the operators in the quantum Langevin equations by *c*-numbers,

$$\frac{d}{dt}a = -\frac{1}{2}(\kappa + 2i\omega_c)a - \frac{iN\Omega}{2}S^- + F^a, \tag{5.9}$$

$$\frac{d}{dt}S^- = -\frac{1}{2}\left(\Gamma + 2i\omega_a\right)S^- + \frac{i\Omega}{2}aS^z + F^-, \tag{5.10}$$

$$\frac{d}{dt}S^z = -(w + \gamma)\left(S^z - d_0\right) + i\Omega\left(a^\dagger S^- - aS^+\right) + F^z, \tag{5.11}$$

where the omission of the hats over the variables signifies that they are *c*-numbers. The noise terms F^a, F^-, and F^z should be interpreted according to the rules of Ito calculus. The noises are correlated according to

$$\left\langle F^\mu(t)F^\nu(t')\right\rangle = 2\mathscr{D}^{\mu\nu}\delta(t - t') . \tag{5.12}$$

It is easier to construct the semi-classical equations by introducing real variables according to

$$\hat{q} = \frac{1}{2}\left(\hat{a}^\dagger + \hat{a}\right), \qquad \hat{p} = \frac{1}{2i}\left(\hat{a}^\dagger - \hat{a}\right), \tag{5.13}$$

$$\hat{S}^x = \frac{1}{2}\left(\hat{S}^+ + \hat{S}^-\right), \quad \hat{S}^y = \frac{1}{2i}\left(\hat{S}^+ - \hat{S}^-\right) . \tag{5.14}$$

The equations of motion in terms of these variables are

$$\frac{d}{dt}q = -\kappa q - 2\omega_c p - N\Omega S^y + F^q, \tag{5.15}$$

$$\frac{d}{dt}p = -\kappa p + 2\omega_c q + N\Omega S^x + F^p, \tag{5.16}$$

$$\frac{d}{dt}S^x = -\Gamma S^x - 2\omega_a S^y + \Omega p S^z + F^x, \tag{5.17}$$

$$\frac{d}{dt}S^y = -\Gamma S^y + 2\omega_a S^x - \Omega q S^z + F^y, \tag{5.18}$$

$$\frac{d}{dt}S^z = -(w + \gamma)\left(S^z - d_0\right) + 2\Omega\left(qS^y - pS^x\right) + F^z . $$

$$\tag{5.19}$$

The correspondence between the semi-classical and quantum mechanical Langevin equations is established by requiring that they produce identical equations for first and second moments of the system operators. Comparison of the first moments (i.e. the expectation values of the equations of motion) leads to

$$\langle F^q \rangle = \langle F^p \rangle = \langle F^x \rangle = \langle F^y \rangle = \langle F^z \rangle = 0 , \qquad (5.20)$$

Comparison of the second moments allows us to find the classical diffusion matrix elements $\mathscr{D}^{\mu\nu}$ from the quantum mechanical ones. To make this procedure well defined we have to choose a specific ordering of the quantum mechanical operators. We choose to make the correspondence using symmetric ordering defined by the symmetric expectation value

$$\left\langle \hat{A}^\mu \hat{A}^\nu \right\rangle_s = \frac{1}{2} \left(\left\langle \hat{A}^\mu \hat{A}^\nu \right\rangle + \left\langle \hat{A}^\nu \hat{A}^\mu \right\rangle \right) , \qquad (5.21)$$

where $\hat{A}^\mu$ and $\hat{A}^\nu$ are generic system operators. We point out that in this formulation, the classical Langevin equations are equivalent to a Fokker-Planck equation for the Wigner quasi-probability distribution. A tedious but straightforward calculation yields

$$
\begin{aligned}
2\mathscr{D}^{qq} &= \frac{\kappa}{4} & 2\mathscr{D}^{pp} &= \frac{\kappa}{4} \\
2\mathscr{D}^{xx} &= \frac{\Gamma}{4N} & 2\mathscr{D}^{yy} &= \frac{\Gamma}{4N} \\
2\mathscr{D}^{xz} &= 2\mathscr{D}^{zx} = \frac{-w+\gamma}{N} \left\langle \hat{S}^x \right\rangle \\
2\mathscr{D}^{yz} &= 2\mathscr{D}^{zy} = \frac{-w+\gamma}{N} \left\langle \hat{S}^y \right\rangle \\
2\mathscr{D}^{zz} &= \frac{2}{N} \left((w+\gamma) + (-w+\gamma) \left\langle \hat{S}^z \right\rangle \right) .
\end{aligned}
\qquad (5.22)
$$

We solve the stochastic differential equations (5.19) by means of the explicit second order weak scheme [52]. An ensemble of trajectories can be evolved simultaneously and the expectation values appearing in Eq. 5.22 can be calculated from the ensemble. This allows the additive form of the explicit second order weak scheme to be used, which is simpler than the general form.

The noises F^μ are found by means of

$$F^\mu = \sum_\nu \sqrt{\lambda_\nu} M_{\mu,\nu}^T f^\nu , \qquad (5.23)$$

where $M_{\mu,\nu}$ is the orthogonal matrix that diagonalizes the diffusion matrix, λ_ν are its eigenvalues, and f^ν are independent normalized Wiener processes. It was found empirically that the symmetrically ordered diffusion matrix is positive definite when the system is above the first threshold (defined in Sec. 5.2.1.3). Below this threshold, the symmetrically ordered diffusion matrix is not positive definite, and divergent trajectories can occur. Typically, an ensemble of 1000 trajectories can be used to achieve convergence to within a few percent.

5.2.1.3   Mean Field Equations

By taking expectation values of the semi-classical Eqns. 5.15–5.19 we obtain the so called mean field equations

$$\frac{d}{dt}a_0 = -\frac{1}{2}(\kappa + 2i(\omega_c - \omega))a_0 - \frac{iN\Omega}{2}S_0^-, \tag{5.24}$$

$$\frac{d}{dt}S_0^- = -\frac{1}{2}\left(\Gamma + 2i(\omega_a - \omega)\right)S_0^- + \frac{i\Omega}{2}a_0 S_0^z, \tag{5.25}$$

$$\frac{d}{dt}S_0^z = -(w + \gamma)\left(S_0^z - d_0\right) + i\Omega\left(a_0^* S_0^- - a_0 S_0^+\right) . \tag{5.26}$$

The noise terms drop out because they have zero mean. The mean field equations capture many of the most important features of the physical system because the noise terms scale as $\sqrt{N}$ while the expectation values scale as N. In the limit of large numbers of atoms the noise terms are therefore less important. Note that Eqns. 5.24–5.26 are written in the reference frame rotating at frequency ω.

Eqns. 5.24–5.26 can be written in steady-state by setting the left hand sides to zero and then solved in closed form. We find

$$S_0^z = \frac{(\kappa + 2i(\omega_c - \omega))(\Gamma + 2i(\omega_a - \omega))}{N\Omega^2} \tag{5.27}$$

for the steady state inversion. From this, the oscillation frequency of the atom-cavity coupled system w can be determined using the condition that S_0^z must be real, giving

$$\omega = \frac{\kappa\omega_a + \Gamma\omega_c}{\kappa + \Gamma} . \tag{5.28}$$

When $\delta = \omega_a - \omega_c \ll \Gamma, \kappa$ the inversion can be simplified to

$$S_0^z \approx \frac{1}{\mathcal{C}} \,, \tag{5.29}$$

where $\mathcal{C} \equiv \frac{N\Omega^2}{\kappa\Gamma}$ is the generalized many-atom cooperativity parameter (generalized since here the effective linewidth Γ includes the incoherent repumping w as well as the single atom linewidth γ and dephasing $1/T_2$).

In the same limit of small detuning we find for the steady state photon number

$$|a_0|^2 = \frac{N(w + \gamma)}{2\kappa}(d_0 - \frac{1}{\mathcal{C}}) \,. \tag{5.30}$$

The photon number has a maximum at

$$w = w_{\text{opt}} = \frac{N\Omega^2}{2\kappa} - \gamma - \frac{1}{T_2}. \tag{5.31}$$

In the limit where the collective decay rate $\mathcal{C}\Gamma$ is much larger than the single atom rates γ and $\frac{1}{T_2}$ we find a simple expression for the maximum photon number,

$$(|a_0|^2)_{\text{opt}} = \frac{N^2\Omega^2}{8\kappa^2} \,. \tag{5.32}$$

The zeros of the intra cavity photon number Eq. 5.30 determine the thresholds of the system. At the first threshold

$$w_1 = \gamma, \tag{5.33}$$

energy is supplied to the system at a high enough rate to sustain a macroscopic field amplitude in the cavity. The emergence of a coherent macroscopic field amplitude is accompanied by the formation of a collective atomic dipole. A second threshold occurs at

$$w_2 = \frac{N\Omega^2}{\kappa} \,. \tag{5.34}$$

At this point, S_0^z is close to unity, and the noise due to the strong repumping prevents the formation of either a macroscopic coherent state in the cavity or a macroscopic dipole in the atomic ensemble.

5.2.1.4   Phase Diffusion Linewidth

It is also possible to derive an analytic expression for the linewidth from the quantum Langevin equations, Eqns. 5.4 – 5.6 by assuming that only phase fluctuations of $\hat{a}$ are important, and neglecting amplitude fluctuations. To this end, we follow closely to the derivation done in [39, 40]. Eq. 5.4 is differentiated, and substituted into it Eqns. 5.4 – 5.5 and the integral of Eq. 5.6, to arrive at an equation for $\hat{a}$ alone,

$$\ddot{\hat{a}} = -\frac{1}{2}(\kappa + \Gamma)\dot{\hat{a}} - \frac{\kappa\Gamma}{4}\hat{a} + \frac{N\Omega^2}{4}\hat{a}\hat{S}^z + \hat{F},\tag{5.35}$$

where

$$\hat{S}^z = \int_0^t dt' e^{-(w+\gamma)(t-t')}\left((w+\gamma) + \hat{F}^z\right.$$
$$\left.-\frac{2}{N}\left(\frac{d}{dt}(\hat{a}^\dagger\hat{a}) + \kappa\hat{a}^\dagger\hat{a} - \hat{a}^\dagger\hat{F}^a - \hat{F}^{a\dagger}\hat{a}\right)\right),\tag{5.36}$$

and,

$$\hat{F} = \frac{\Gamma}{2}\hat{F}^a - \frac{iN\Omega}{2}\hat{F}^- + \dot{\hat{F}}^a.\tag{5.37}$$

The annihilation operator $\hat{a}$ is decomposed according to,

$$\hat{a} = (a_0 + \hat{\rho})e^{i\hat{\phi}}.\tag{5.38}$$

Above threshold, amplitude fluctuations are expected to be small, so that

$$\left\langle\hat{a}^\dagger(t)\hat{a}(0)\right\rangle = a_0^2\left\langle e^{i(\hat{\phi}(t)-\hat{\phi}(0))}\right\rangle.\tag{5.39}$$

After substituting Eq. 5.38 into Eq. 5.35, we take the imaginary part to first order in products of operators, and find,

$$\ddot{\hat{\phi}} = -\frac{1}{2}(\kappa + \Gamma)\dot{\hat{\phi}} + \frac{1}{a_0}\text{Im}[\hat{F}],\tag{5.40}$$

where a factor of $e^{-i\phi}$ has been absorbed into $\hat{F}$. Eq. 5.40 is then integrateed, assuming that $(\kappa+\Gamma)$ is large, to arrive at,

$$\hat{\phi}(t) - \hat{\phi}(0) = \frac{2}{a_0(\kappa+\Gamma)}\int_0^t dt'\text{Im}\left[\frac{\Gamma}{2}\hat{F}^a - \frac{iN\Omega}{2}\hat{F}^-\right].\tag{5.41}$$

Since $\hat{F}^a$ and $\hat{F}^-$ are Gaussian, we can use

$$\left\langle e^{i(\hat{\phi}(t)-\hat{\phi}(0))} \right\rangle = e^{-\frac{1}{2}\left\langle (\hat{\phi}(t)-\hat{\phi}(0))^2 \right\rangle}. \tag{5.42}$$

Therefore, we use Eq. 5.41, along with Eqns. 5.8 to find,

$$\left\langle (\hat{\phi}(t)-\hat{\phi}(0))^2 \right\rangle = \left(\frac{(C+1)}{2(Cd_0-1)} \frac{\Gamma}{(w+\gamma)} \frac{\Omega^2\kappa}{(\kappa+\Gamma)^2} \right) t, \tag{5.43}$$

so that the linewidth $\Delta\nu$ given by,

$$\Delta\nu = \frac{(C+1)}{2(Cd_0-1)} \frac{\Gamma}{(w+\gamma)} \frac{\Omega^2\kappa}{(\kappa+\Gamma)^2}. \tag{5.44}$$

5.2.2   2nd Order Cumulant Theory

The cumulant theory is derived in the same way as in Chapter 3.7. Eq. 5.1 is used to find

equations for expectation values of system observables, which are truncated to second order in a

cumulant expansion, resulting in the closed set of equations,

$$\frac{d}{dt}\langle\hat{\sigma}_1^z\rangle = -(w+\gamma)(\langle\hat{\sigma}_1^z\rangle - d_0) + i\Omega\left\{ \left\langle \hat{a}^\dagger\hat{\sigma}_1^- \right\rangle - \left\langle \hat{a}\hat{\sigma}_1^+ \right\rangle \right\} \tag{5.45}$$

$$\begin{aligned}
\frac{d}{dt}\left\langle \hat{a}^\dagger\hat{\sigma}_1^- \right\rangle &= -\frac{1}{2}(\Gamma+\kappa-2i\delta)\left\langle \hat{a}^\dagger\hat{\sigma}_1^- \right\rangle + \frac{i\Omega}{2}\left\{ \left\langle \hat{a}^\dagger\hat{a} \right\rangle \langle\hat{\sigma}_1^z\rangle \right. \\
&\quad \left. + \frac{1}{2}(\langle\hat{\sigma}_1^z\rangle + 1) + (N-1)\langle\hat{\sigma}_1^+\hat{\sigma}_2^-\rangle \right\}
\end{aligned} \tag{5.46}$$

$$\frac{d}{dt}\langle\hat{\sigma}_1^+\hat{\sigma}_2^-\rangle = -\Gamma\langle\hat{\sigma}_1^+\hat{\sigma}_2^-\rangle + \frac{\Omega}{2i}\langle\hat{\sigma}_1^z\rangle\left\{ \left\langle \hat{a}^\dagger\hat{\sigma}_1^- \right\rangle - \left\langle \hat{a}\hat{\sigma}_1^+ \right\rangle \right\} \tag{5.47}$$

$$\frac{d}{dt}\left\langle \hat{a}^\dagger\hat{a} \right\rangle = -\kappa\left\langle \hat{a}^\dagger\hat{a} \right\rangle + \frac{N\Omega}{2i}\left\{ \left\langle \hat{a}^\dagger\hat{\sigma}_1^- \right\rangle - \left\langle \hat{a}\hat{\sigma}_1^+ \right\rangle \right\}. \tag{5.48}$$

This second order cumulant expansion, along with the quantum regression theorem, can be used in

the same way as in chapter 3.7.2, to find a closed set of equations for two-time expectation values,

$$\frac{d}{d\tau}\begin{bmatrix} \left\langle \hat{a}^\dagger(\tau)\hat{a}(0) \right\rangle \\ \left\langle \hat{\sigma}_1^+(\tau)\hat{a}(0) \right\rangle \end{bmatrix} = \begin{bmatrix} -\frac{\kappa}{2}+i\delta & \frac{iN\Omega}{2} \\ -\frac{i\Omega\langle\hat{\sigma}_1^z\rangle}{2} & -\frac{\Gamma}{2} \end{bmatrix} \begin{bmatrix} \left\langle \hat{a}^\dagger(\tau)\hat{a}(0) \right\rangle \\ \left\langle \hat{\sigma}_1^+(\tau)\hat{a}(0) \right\rangle \end{bmatrix}. \tag{5.49}$$

These equations are written in a frame rotating at the atomic frequency. They are important, since

the Fourier transform of $\left\langle \hat{a}^\dagger(\tau)\hat{a}(0) \right\rangle$ is the spectrum of the light inside our cavity QED system.

By using Laplace transform methods, it is found that the solution of the $\langle \hat{a}^\dagger(\tau)\hat{a}(0)\rangle$ equation, of Eq. 5.49 is dominated by a single exponential with decay constant,

$$\Delta\nu = \frac{1}{2}(\kappa + \Gamma - 2i\delta) - \frac{1}{2}\sqrt{(-\kappa + \Gamma + 2i\delta)^2 + 4N\Omega^2\langle\hat{\sigma}_1^z\rangle}, \tag{5.50}$$

and hence the spectrum is a Lorentzian with linewidth given by Eq. 5.50.

5.3   Characterization of the Crossover

The crossover from superradiance to lasing is characterized by a transition from coherence encoded in an atomic ensemble to coherence encoded in the light field. The key parameter in identifying the regime is the ratio of the number of photons to the number of atoms when the system is operated at its most efficient point in terms of output intensity and spectral frequency width. With this motivation, we introduce a crossover parameter as

$$\xi \equiv \frac{(|a_0|^2)_{\text{opt}}}{N}, \tag{5.51}$$

that is, the dimensionless ratio of the intracavity photon number to the number of atoms. The parameter ξ quantifies the relative importance of stimulated emission to collective atomic spontaneous emission. If $\xi \ll 1$, the system is in the bad cavity or superradiant regime. If $\xi \gg 1$ the system is in the good cavity or laser regime. In the crossover or intermediate region, $\xi \sim 1$, and the system possesses features of both.

The mean field equations allow us to rewrite this expression in an alternate way that illuminates the role of the system parameters in determining the operating regime. From Eq. 5.32, which is applicable in the typical case where $w_{\text{opt}} \gg \gamma, 1/T_2$, Eq. 5.51 can be rewritten as an approximately equivalent definition

$$\xi \approx \frac{N\Omega^2}{8\kappa^2} \, . \tag{5.52}$$

The interpretation of this is that the crossover is also characterized by the ratio of the collective coupling between the many atom ensemble and the cavity mode, **i.e.** $N\Omega^2$, to the decay rate κ of the cavity mode.

5.4   Results

In this section we present numerical results for field intensity, inversion, line widths, and correlations throughout the crossover from lasing to superradiance. We begin by considering the different solution methods for small numbers of atoms were we can compare with the exact SU(4) Monte-Carlo results. This comparison shows that the semi-classical theory gives an accurate description of first and second moments of the system operators. This is an interesting result in itself besides verifying the semi-classical methods because it demonstrates that the system is not strongly correlated and we don't need to account for genuinely quantum fluctuations.

With the validity of the semi-classical method established we then consider systems with large numbers of atoms. These systems are experimentally relevant and allow us to more clearly understand the behavior of the system in the large N limit.

For simplicity, in all of these simulation results, we consider the parameter regime in which the single atom rates γ and $1/T_2$ are negligible compared to the cavity loss rate κ and use Eq. 5.52 to define ξ. The results of the c-number Langevin simulations are an average over 1000 trajectories. In each trajectory, the trajectory values were used in the diffusion matrix to compute the noise. This method is justified by its agreement to the method that uses expectation values in the diffusion matrix, and also by its agreement with the exact SU(4) results.

5.4.1   Simulations with small atom numbers

In order to determine the validity of the approximate solution methods, we begin by comparing them to the exact solutions. We use $N = 40$ atoms for the comparison. This is a small enough to still be tractable by exact SU(4) Monte-Carlo simulations and at the same time it is large enough to expect the approximate solution methods to be reasonably accurate.

Specifically, Fig. 5.1 shows several observables obtained using the mean field Langevin method, the phase diffusion method, the c-number Langevin method, the cumulant expansion method, and exact SU(4) Monte-Carlo simulations for three different values of the crossover parameter: $\xi = 0.2$,
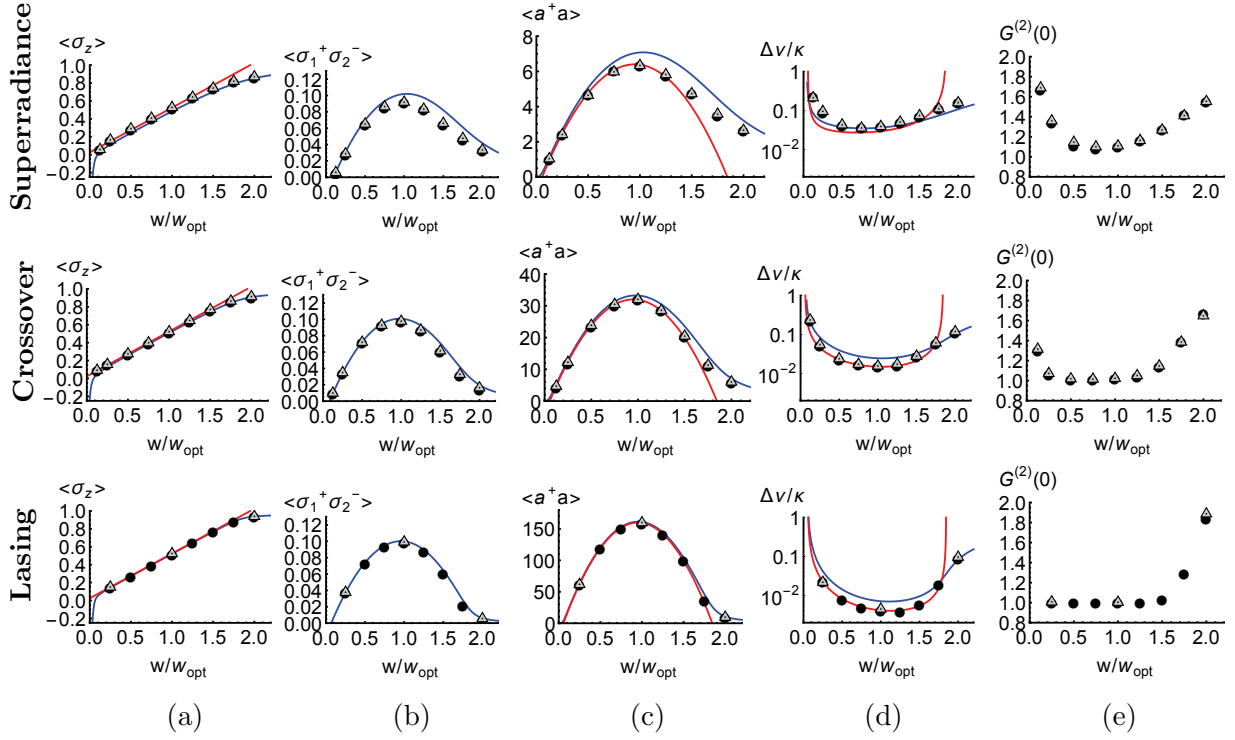
Figure 5.1: Comparison of the different solution methods in the superradiance ($\xi = 0.2$), crossover ($\xi = 1$), and lasing ($\xi = 5$) regions for $N = 40$ and $C = 1$. The analytic Langevin solution is shown in red (light gray), the 2nd order cumulant solution is shown in blue (dark gray), The exact SU(4) solution is shown by grey triangles, and the c-number Langevin simulation results are shown by black circles. The observables considered are (a) the inversion $\langle \hat{\sigma}^z \rangle$, (b) the correlation between atoms $\langle \hat{\sigma}_1^+ \hat{\sigma}_2^- \rangle$, (c) the intracavity photon number $\langle \hat{a}^\dagger \hat{a} \rangle$, (d) the linewidth $\Delta \nu$, and (e) the intensity correlation function $G^{(2)}(0)$.

$\xi = 1$, and $\xi = 5$. These values of ξ put the system in the superradiance, crossover, and lasing parameter regions, respectively. We note that the SU(4) method becomes more computationally intensive as ξ is increased, since there are more photons as ξ is increased, and hence more basis states need to be tracked. Therefore, for $\xi = 5$, we used a method that combines the SU(4) approach with the quantum jump method [81]. The results using this method that are shown are an average over 500 trajectories.

Fig. 5.1 shows excellent agreement between c-number Langevin and the exact SU(4) theory in all parameter regions for all of the considered observables. Therefore, the c-number Langevin theory can be relied upon for larger atom numbers inaccessible to direct numerical simulation.

Figures 5.1 (a) and (c) show that the mean field equations are accurate near the collective emission peak, $w/w_{\mathrm{opt}} = 1$, but they are less accurate outside that region. Figure 5.1 (d), shows that the phase diffusion model for the linewidth also agrees in the region around $w/w_{\mathrm{opt}} = 1$, but disagrees outside that region, where the phase diffusion approximation breaks down. Although they do not quantitatively agree with the exact SU(4) method, the analytic solutions obtained by the mean field and phase diffusion models capture the correct qualitative behavior of the system.

The 2nd order cumulant solution works well qualitatively in all parameter regions, but as seen in Fig. 5.1 (b) and (c) in the superradiance row, and in column (d), there is a quantitative disagreement between this theory and the SU(4) and c-number Langevin theories.

This quantitative disagreement is due to the fact that there is a difference between a Gaussian theory, one in which all moments factorize into products of no higher than second order moments, and a theory that uses Gaussian noise. This difference can be seen by considering the third order moment $\langle \hat{a}^\dagger \hat{a} \hat{\sigma}_i^z \rangle$. According to the cumulant theory, $\langle \hat{a}^\dagger \hat{a} \hat{\sigma}_i^z \rangle = \langle \hat{a}^\dagger \hat{a} \rangle \langle \hat{\sigma}_i^z \rangle$, a fact which was essential to use in deriving the closed the set of equations used to find the spectrum, Eqns. 5.49. In the Langevin theory, however, $\langle \hat{a}^\dagger \hat{a} \hat{\sigma}_i^z \rangle \neq \langle \hat{a}^\dagger \hat{a} \rangle \langle \hat{\sigma}_i^z \rangle$, a fact we have checked with our Langevin simulations. Even though the difference between $\langle \hat{a}^\dagger \hat{a} \hat{\sigma}_i^z \rangle$ and $\langle \hat{a}^\dagger \hat{a} \rangle \langle \hat{\sigma}_i^z \rangle$ decreases as $\frac{1}{N}$, it is precisely the $\frac{1}{N}$ terms that gives rise to the linewidth according to the cumulant theory.

The merit of the 2nd order cumulant theory lies in its simplicity. It is simple to derive the
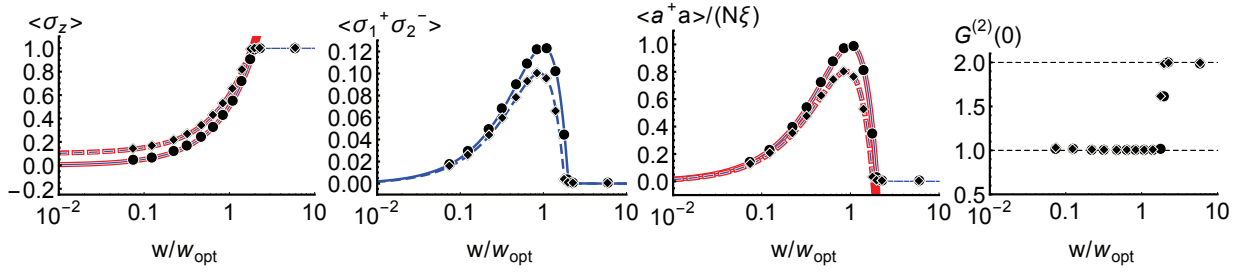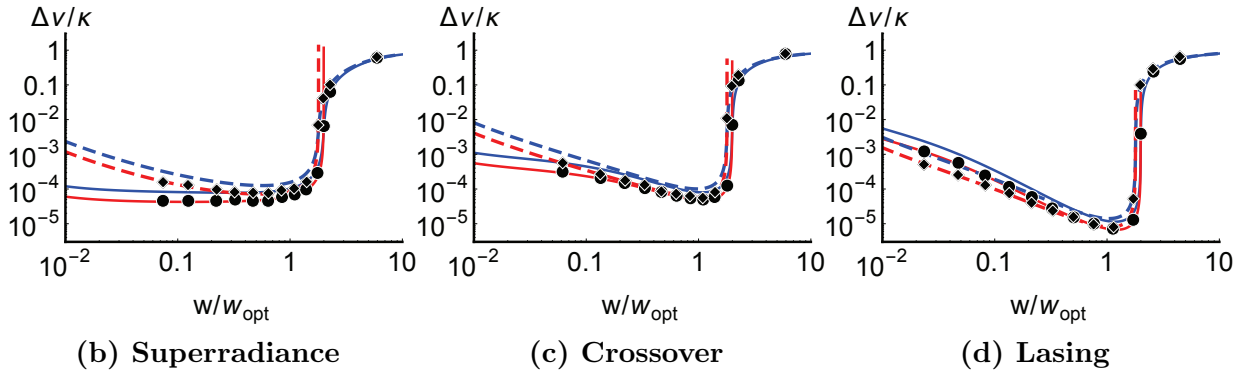
Figure 5.2: Solutions using the various methods in the superradiance ($\xi = 0.1$), crossover ($\xi = 1$), and lasing ($\xi = 10$) regions for N=10000 and $C = 0.1$. For $1/T_2 = 0$, the analytic Langevin solution is shown in solid red (solid light gray), the 2nd order cumulant solution is shown in solid blue (solid dark gray), and the c-number Langevin simulation results are shown by black circles. For $1/T_2 = \frac{1}{5}w_{opt}$, the analytic Langevin solution is shown in dashed red (dashed light gray), the 2nd order cumulant solution is shown in dashed blue (dashed dark gray), and the c-number Langevin simulation results are shown by black diamonds. (a) All observables considered except linewidth $\Delta\nu$ show universal behavior in the superradiance, crossover, and lasing regions, after appropriate scaling. The red (light gray) curves have been artificially widened in order to be seen underneath the blue curves. (b) $\Delta\nu/\kappa$ in the superradiance region (c) $\Delta\nu/\kappa$ in the crossover region, (d) $\Delta\nu/\kappa$ in the lasing region.

cumulant equations and it is not computationally intensive to solve them numerically, while the theory still captures the correct qualitative behavior of the system.

5.4.2   Simulations with large atom numbers

Now that an agreement between the c-number Langevin and exact SU(4) theories has been established, we study more experimentally realistic systems with $N = 10000$ using the semi-classical theory based on the c-number Langevin equations. We also include the mean field Langevin theory, the phase diffusion model for the linewidth. The results of these simulations are shown in Fig. 5.2. We consider both the case of vanishing inhomogeneous broadening, $1/T_2 = 0$, as well as $1/T_2 = w_{\mathrm{opt}}/5$.

As seen in Fig. 5.2 (a), when $1/T_2 = 0$, the inversion $\langle \hat{\sigma}^z \rangle$, the correlation between atoms $\langle \hat{\sigma}_1^+ \hat{\sigma}_2^- \rangle$, the intracavity photon number $\langle \hat{a}^\dagger \hat{a} \rangle$, and the intensity correlation function $G^{(2)}(0)$ all show universal behavior in the superradiance, crossover, and lasing regimes after appropriate scaling. For $1/T_2 = w_{\mathrm{opt}}/5$ these observables still show universal behavior after appropriate scaling, and the values do not change significantly from the $1/T_2 = 0$ case.

It is worth noting that, even though $\langle \hat{\sigma}_1^+ \hat{\sigma}_2^- \rangle$ has universal behavior throughout the crossover, typical lasers operate just above threshold in terms of the scaled quantities, i.e. $w \ll w_{\mathrm{opt}}$. Just above threshold the atom-atom correlations are typically very small,

$$\langle \hat{\sigma}_1^+ \hat{\sigma}_2^- \rangle_{opt} \ll 1 . \tag{5.53}$$

Thus atom-atom correlations are usually not important in lasers.

The linewidth $\Delta\nu$, however, does not show universal behavior in the superradiance, crossover, and lasing regimes. As seen in Fig. 5.2 (b), in the superradiance region, when $1/T_2 = 0$, $\Delta\nu/\kappa$ is flat in the region of $w/w_{\mathrm{opt}} < 1$. In contrast, the linewidth in the lasing regime, shown in Fig.5.2 (d), linearly decreases as w/w_{opt} increases towards unity. This is the typical Schawlow-Townes behavior, which can be seen by considering $\kappa/\langle \hat{a}^\dagger \hat{a} \rangle$ using Eq. 5.30. In the crossover region, shown in Fig. 5.2 (c), we see that for $w/w_{\mathrm{opt}} \ll 1$, $\Delta\nu/\kappa$ is flat, and as w/w_{opt} approaches unity, $\Delta\nu/\kappa$
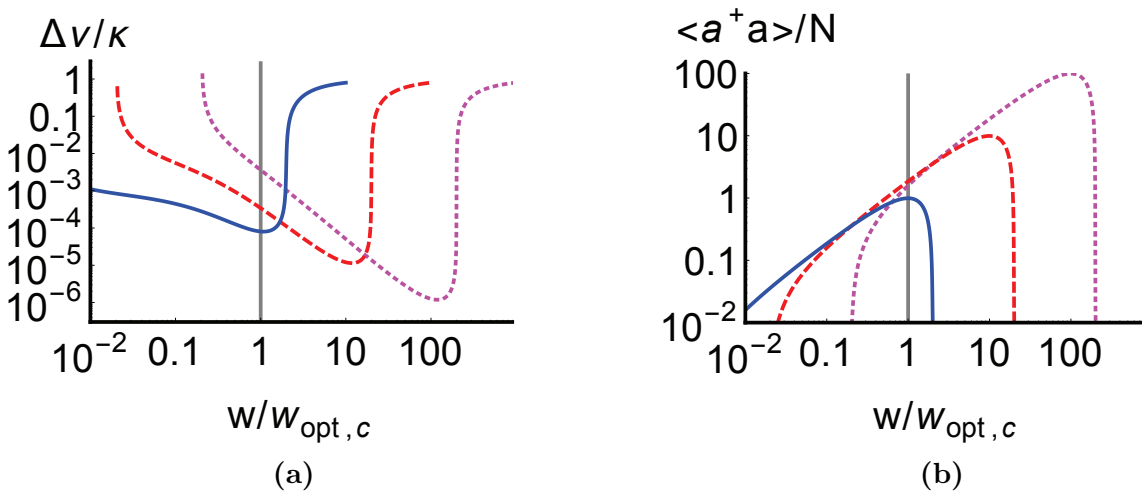
Figure 5.3: Comparison of (a) linewidth and (b) Intracavity intensity for a system operated in the crossover ($\xi = 1$) shown in blue solid, lasing ($\xi = 10$) shown in red dashed, and far lasing ($\xi = 100$) shown in magenta dotted, regions. $w_{opt,c}$ is the optimum w value in the crossover region. For all systems, $N = 10000$.

starts to linearly decrease as in the lasing regime. Therefore, a system in the crossover region displays characteristics of both superradiance and lasing.

When $1/T_2$ is increased to $1/T_2 = w_{\mathrm{opt}}/5$, Fig. 5.2 (b) shows that $\Delta\nu/\kappa$ increases for $w/w_{\mathrm{opt}} \ll 1$, but it is not significantly affected by $1/T_2$ as w/w_{opt} approaches unity. Note that the latter is the pumping region where the emitted light intensity is largest. Near $w \sim w_{\mathrm{opt}}$ we obtain both the largest intensity and the best frequency stability.

In the crossover region, seen in Fig. 5.2 (c), when $1/T_2 = w_{\mathrm{opt}}/5$, $\Delta\nu/\kappa$ increase for $w/w_{\mathrm{opt}} \ll 1$, where the system is displaying superradiant behavior. On the other hand, when $w \sim w_{\mathrm{opt}}$ where the system starts to display lasing behavior, $\Delta\nu/\kappa$ is insensitive to the inhomogeneous broadening of the atomic line.

Figure 5.2 (d) shows that $\Delta\nu/\kappa$ does not increase in the lasing region when $1/T_2 = w_{\mathrm{opt}}/5$. Rather the linewidth decrease in the region slightly below $w/w_{\mathrm{opt}} = 1$, when compared to the $1/T_2 = 0$ case. This reduction has also been observed for smaller atom numbers using the exact SU(4) code. It can be shown that the value of $1/T_2$ that maximally reduces the linewidth is $1/T_2 = \frac{w_{\mathrm{opt}}}{1+\sqrt{2}}$.

As mentioned previous, a laser normally operates just above threshold, where $w/w_{\mathrm{opt}} \ll 1$. As seen in Fig. 5.3 (a), for the same pump strength w, and a fixed N, a system in the crossover region can operate with $w/w_{\mathrm{opt}} = 1$, allowing the crossover system to have a linewidth orders of magnitude smaller than the linewidth of the lasing system. Fig. 5.3 (b) shows that this improvement in linewidth can be achieved without paying the penalty of a reduced output intensity. Another way of saying this is that, for the same output intensity, one can achieve greater brightness of the light source by using atoms with a smaller linewidth.

5.4.3   Effect of Cavity and Atomic Level Instabilities on the Spectrum

The effect of instabilities in the cavity frequency and atomic frequency on the linewidth is now investigated. Cavity frequency instability can be caused by fluctuations in cavity length due to the thermal fluctuations of the cavity mirrors, which are unavoidable in an experiment. The
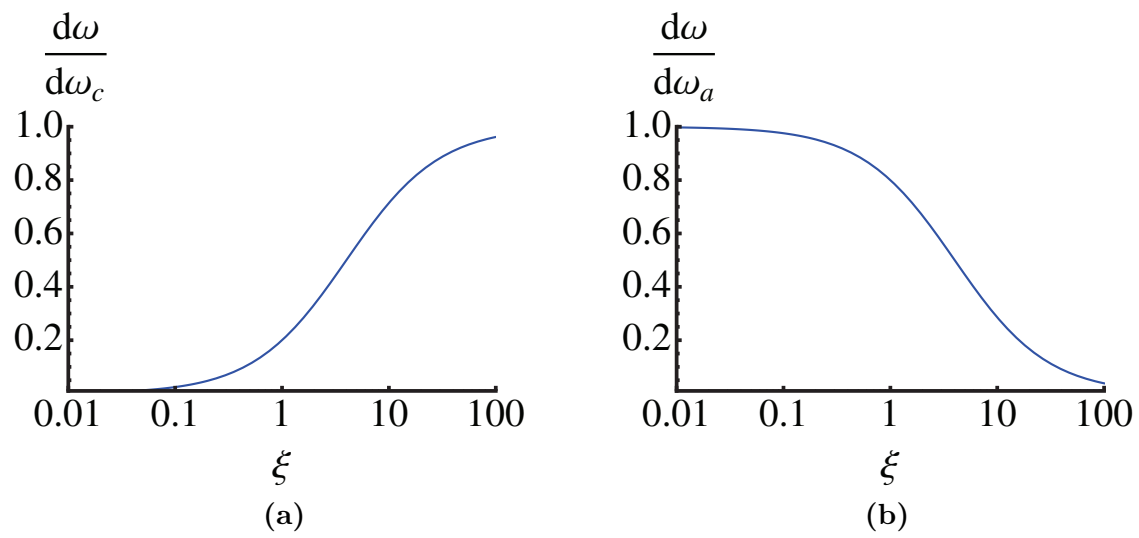
Figure 5.4: Instability in the atom-cavity system frequency ω with respect to (a) the cavity frequency ω_c and (b) atomic frequency ω_a as a function of crossover parameter ξ

energy levels in an atom can also be shifted by stray electromagnetic fields. The frequency of the combined atom-cavity system ω lies somewhere between the bare atom and cavity frequencies, and is given by Eq. 5.28.

If ω is varied, the resultant time averaged linewidth will be an average over these values, and will hence be much broader than the quantum limited linewidth. Therefore, the derivative of ω with respect to ω_c, and with respect to ω_a, gives us an idea as to how much of an effect an instability in these frequencies will have on broadening the linewidth. These derivatives are plotted in Fig. 5.4.

Fig. 5.4 (a) tells us that on the lasing side of the crossover, ω is shifted proportionally to the shift in ω_c, while on the superradiant side, ω is insensitive to shifts in ω_c. Conversely, in Fig. 5.4 (b) it can be seen ω is shifted proportionally to the shift in ω_a on the superradiance side of the crossover, while on the lasing side, ω is insensitive to shifts in ω_a. In the intermediate regime ($\xi = 1$), ω is not as sensitive to a shift in the ω_c as it is in the laser regime, and it is not as sensitive to a shift in the ω_a, as it is on the superradiance side.

5.5   Conclusion

A model that is capable of describing a system operating in any parameter region of the crossover between steady state superradiance and lasing has been introduced, and three solution methods to that model were demonstrated. The first method solves a set of c-number Langevin equations that approximate the quantum Langevin equations that are equivalent to our model. This method was seen to have outstanding agreement with the exact SU(4) method. Also, analytic expressions for the expectation values of the quantum Langevin equations were derived. Along with these solutions, an analytic solution for the linewidth of the power spectrum, which assumes Gaussian phase fluctuations, and neglects amplitude fluctuations was derived. It is demonstrated that these analytical results agree with SU(4) and c-number Langevin methods in the region in which the value of re-pumping is such that the system has the maximum number of intra-cavity photons, but disagree far from this region. Finally, a closed set of equations to second order in a

cumulant expansion were derived, and shown to agree qualitatively with the SU(4) and *c*-number Langevin methods.

Although a system in the lasing parameter region is capable of possessing the smallest linewidth, typically lasers operate with a re-pumping rate that puts them just above threshold, which does not allow the smallest linewidth for the system to be realized. For the same re-pumping rate, a system operating in the crossover region will be much farther above threshold, potentially allowing for a linewidth orders of magnitude smaller than in the laser region. Also, a crossover system will have a larger intracavity intensity than a superradiant system, making the former more experimentally accessible.

It was also demonstrated that a system in all regions of the crossover is insensitive to atomic dephasing as long as the re-pumping rate is smaller than the dephasing rate. Also, as the crossover is traversed into the lasing region, atomic dephasing can actually cause a reduction in the linewidth.

Finally, it was shown that the linewidth on the superradiance side is insensitive to fluctuations in cavity length, and that these fluctuations become more important as the crossover is traversed toward the laser side. Conversely, it was shown that the linewidth on the lasing side is insensitive to fluctuations in the atomic energy levels, and that these fluctuations become more important on the superradiance side. A system in the crossover region will be less sensitive to cavity frequency fluctuations than a lasing system, and it will be less sensitive to atomic frequency instabilities than a superradiant system. Both of these fluctuations cause a broadening of the linewidth. These conclusions are significant since fluctuations in the cavity frequency are a principal limitation preventing further reduction of the linewidth in today's most ultrastable lasers.

Chapter 6

Laser Stabilization using Saturated Absorption in a Cavity QED System

The bulk of this chapter was published in Physical Review A as Phys. Rev. A 92, 013817 (2015) [80].

Today's ultra-precise and accurate atomic clocks continue to make important contributions to fundamental physics as well as applied technology. Atomic clocks have imposed significant constraints on the drift of fundamental constants [58, 45, 35], may have the potential to enhance the sensitivity of gravitational wave detectors, and have provided ultimate tests of the general theory of relativity [74]. With the current stability of optical clocks at the 1×10^{-18} level, there are prospects for applying atomic clocks for the detailed mapping of the Earth's gravity field [38, 11].

A highly stabilized laser is an integral component of high precision measurements, such as optical atomic clocks and precision spectroscopy. Current technology for achieving highly phase stable laser sources relies on locking a laser to a high-Q reference ultra low expansion (ULE) glass cavity [23, 91, 48]. The phase stability of this method is currently limited by the thermal noise induced in the mirrors, spacers, and coatings of the reference cavity [68], but has been significantly reduced over the past few years with new engineered materials [49, 62].

As an alternative approach to overcoming the thermal noise problem, it was recently proposed [63] to lock the laser to the saturated resonance feature exhibited by a collection of atoms with an ultra-narrow electronic transition trapped in an optical cavity. Here, the atoms were assumed to be trapped in an optical lattice inside the cavity. Due to the narrow atomic line, such a system would

typically operate in the parameter region corresponding to the bad cavity limit of cavity QED. There, the atomic linewidth is significantly narrower than the cavity linewidth. In contrast to the reference cavity stabilization method described above, the cavity QED method offers a distinct advantage since no drift compensation is needed.

The cavity QED system exhibits optical bistability in the intracavity intensity [12, 24] where several solutions exist for the steady-state intracavity field. Working at an input intensity in the region where bistability is present would in principle allow the greatest degree of stabilization [63]. However, it is not practical to work in the bistable region since quantum and classical fluctuations between the semi-classical eigenmodes cause the system to be dynamically unstable. Therefore, one is restricted to working at input intensities above the bistability, where the achievable stabilization is orders of magnitude worse. Still, it was shown [63] that phase stability corresponding to the sub-mHz level should be achievable.

Recently [86], an experimental effort to demonstrate the cavity QED system was made by probing the $\left|{}^1S_0\right\rangle - \left|{}^3P_1\right\rangle$ intercombination line of ^{88}Sr atoms (i.e. $\gamma_a/2\pi = 7.6$ kHz) inside an optical cavity. There, however, the atoms were not trapped in an optical lattice, but loaded into the center of the cavity using a MOT, which was then turned off during probing. Typical MOT temperatures correspond to a few millikelvin which is equivalent to a Doppler width of several MHz. Considering the narrow 7.6 kHz line of the optical transition, this implies that motional effects will be important.

In this chapter, we extend the many-atom cavity QED theory of [63] to include atomic motion, and study its effect on the stabilization precision. In spite of the large Doppler effect, the standing-wave nature of the cavity field induces sharp saturated absorption and dispersion features to appear in the considered observables. These features are nestled in the center of the overall Doppler broadened features [77, 32, 76, 59]. The stabilization that is achievable by utilizing these sharp features is impeded by multi-photon scattering processes that occur when an atom's velocity matches one of its Doppleron resonances [1, 79]. The dependence of the stabilization on the number of atoms and the temperature due to the Dopplerons is discussed. We demonstrate that the motion
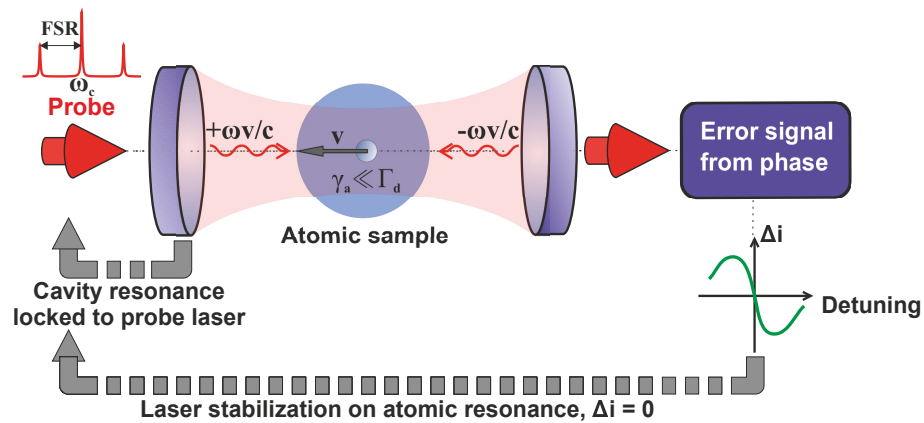
Figure 6.1: Schematic of the cavity QED experiment with a thermal sample of atoms with Doppler width Γ_d, each of which have a narrow optical transition of width $\gamma_a << \Gamma_d$. The atoms are probed with a carrier with frequency ω_c, and two sidebands located at $\omega_c \pm$FSR, where FSR is the free spectral range of the cavity. The carrier frequency ω_c, which is close to the atomic frequency ω_a, is locked on the cavity mode frequency ω, while the sidebands are assumed far off resonance, typically $\sim 10^4$ atomic linewidths. By demodulating the light transmitted through the cavity at the FSR, detection of the non-linear phase response of the transmitted light is achieved. This phase response results in a photocurrent that serves as a frequency discriminating error signal that stabilizes the laser frequency through the requirement $\Delta i = 0$.

of the atoms causes the bistability region to disappear, so that no restrictions on input power are necessary to avoid the dynamic instability that would otherwise result.

6.1   Model

We model our system as a collection of N two-level atoms inside a single mode optical cavity using the quantum Born-Markov master equation to describe the open quantum system,

$$\frac{d}{dt}\hat{\rho} = \frac{1}{i\hbar}\left[\hat{H},\hat{\rho}\right] + \hat{\mathcal{L}}\left[\hat{\rho}\right],\tag{6.1}$$

where,

$$\hat{H} = \frac{\hbar\Delta}{2}\sum_{j=1}^{N}\hat{\sigma}_j^z + \hbar\eta\left(\hat{a}^\dagger + \hat{a}\right) + \hbar\sum_{j=1}^{N}g_j(t)\left(\hat{a}^\dagger\hat{\sigma}_j^- + \hat{\sigma}_j^+\hat{a}\right),\tag{6.2}$$

and $\hat{\mathcal{L}}\left[\hat{\rho}\right]$ denotes the Liouvillian.

The Hamiltonian H describes the coherent evolution of the coupled atom cavity system in an interaction picture which rotates at the frequency of the cavity, and Δ is the atom-cavity detuning. The Pauli spin matrices for the atoms are $\hat{\sigma}_j^+$,$\hat{\sigma}_j^-$ and $\hat{\sigma}_j^z$, and $\hat{a}$ is the annihilation operator of the cavity mode. Furthermore, $\eta = \sqrt{(\kappa P_{in})/(\hbar\omega)}$ is the classical drive amplitude, where κ is the decay rate of the cavity, P_{in} is the input power, and ω is the frequency of the cavity mode. The atom-cavity coupling rate is $g_j(t) = g_0\cos(\delta_j t)$, where g_0 is the maximum coupling amplitude, and $\delta_j = kv_j$ is the Doppler shift in terms of the velocity v_j of the jth atom, and wave number k of the light.

The incoherent evolution describes the various forms of dissipation in this system and is described by the Liouvillian $\hat{\mathcal{L}}\left[\hat{\rho}\right]$,

$$\begin{aligned}\hat{\mathcal{L}}\left[\hat{\rho}\right] &= -\frac{\kappa}{2}\left\{\hat{a}^\dagger\hat{a}\hat{\rho} + \hat{\rho}\hat{a}^\dagger\hat{a} - 2\hat{a}\hat{\rho}\hat{a}^\dagger\right\}\\ &\quad -\frac{\gamma}{2}\sum_{j=1}^{N}\left\{\hat{\sigma}_j^+\hat{\sigma}_j^-\hat{\rho} + \hat{\rho}\hat{\sigma}_j^+\hat{\sigma}_j^- - 2\hat{\sigma}_j^-\hat{\rho}\hat{\sigma}_j^+\right\}\\ &\quad +\frac{1}{2T_2}\sum_{j=1}^{N}\left\{\hat{\sigma}_j^z\hat{\rho}\hat{\sigma}_j^z - \hat{\rho}\right\},\end{aligned}\tag{6.3}$$

where $\hat{\rho}$ is the system's density matrix, γ is the spontaneous emission rate for the atoms, and $\frac{1}{T_2}$ is the inhomogeneous dephasing rate.

We derive Langevin equations corresponding to Eq. 6.1. Assuming that the classical drive η is sufficiently strong, a mean-field description provides an accurate representation [37]. We define the mean values for the field $\alpha = -i\langle\hat{a}\rangle$, and for the atoms, $\sigma_j^- = \left\langle\hat{\sigma}_j^-\right\rangle, \sigma_j^+ = \left\langle\hat{\sigma}_j^+\right\rangle, \sigma_j^z = \left\langle\hat{\sigma}_j^+\right\rangle$, which evolve according to the semiclassical evolution,

$$\dot{\alpha} = -\kappa\alpha + \eta + \sum_{j=1}^{N} g_j(t)\sigma_j^-, \tag{6.4}$$

$$\dot{\sigma}_j^- = -\left(\gamma_p + i\Delta\right)\sigma_j^- + g_j(t)\alpha\sigma_j^z, \tag{6.5}$$

$$\dot{\sigma}_j^z = -\gamma\left(\sigma_j^z + 1\right) - 2g_j(t)\left(\alpha\sigma_j^+ + \alpha^*\sigma_j^-\right), \tag{6.6}$$

where $\gamma_p \equiv \frac{1}{T_2} + \frac{\gamma}{2}$ is the total decay rate of the atomic dipole. In the moving frame of reference of the jth atom, the cavity field appears as a traveling wave, containing two frequencies shifted above and below the cavity frequency by the Doppler shift δ_j (refer to Fig. 6.1).

It is convenient to approximate Eqns. 6.4 – 6.6 as a function of the continuous variable $\delta = kv$,

$$\dot{\alpha} = -\kappa\alpha + \eta + g_0\int d\delta P(\delta)\cos(\delta t)\sigma^-, \tag{6.7}$$

$$\dot{\sigma}^- = -\left(\gamma_p + i\Delta\right)\sigma^- + g_0\cos(\delta t)\alpha\sigma^z, \tag{6.8}$$

$$\dot{\sigma}^z = -\gamma\left(\sigma^z + 1\right) - 2g_0\cos(\delta t)\left(\alpha\sigma^+ + \alpha^*\sigma^-\right), \tag{6.9}$$

where $P(\delta)$ is the Maxwell velocity distribution of width δ_0, which is related to the temperature by the equipartition theorem.

To solve this problem that intrinsically contains a bi-chromatic drive, we proceed in two ways. Our first approach is to numerically integrate Eqns. 6.7 – 6.9, partitioning the integral into finite-size velocity bins. The velocity partition must be chosen with care, since the system exhibits Doppleron resonances, which have a strong dependence on the atomic velocity. Specifically, at lower velocity, more resolution in the partition is required.

Our second approach is semi-analytic, and involves a Floquet analysis [31, 2], in which we

expand σ^-, σ^+, and σ^z in terms of their Fourier components,

$$
\begin{aligned}
\sigma^- &= \sum_l e^{il\delta t} x_1^{(l)}, \\
\sigma^+ &= \sum_l e^{il\delta t} x_2^{(l)}, \\
\sigma^z &= \sum_l e^{il\delta t} x_3^{(l)},
\end{aligned}
\tag{6.10}
$$

where $x_1^{(l)}, x_2^{(l)}$, and $x_3^{(l)}$ are the amplitudes of the lth Fourier component. Upon substitution of Eqns. 6.10 into Eqns. 6.7 – 6.9, equations for the amplitudes are found:

$$
\dot{x}_1^{(l)} = -\left(i(\Delta + l\delta) + \gamma_p\right) x_1^{(l)} + \frac{g_0 \alpha}{2} \left(x_3^{(l+1)} + x_3^{(l-1)}\right),
\tag{6.11}
$$

$$
\dot{x}_2^{(l)} = \left(i(\Delta + l\delta) - \gamma_p\right) x_2^{(l)} + \frac{g_0 \alpha^*}{2} \left(x_3^{(l+1)} + x_3^{(l-1)}\right),
\tag{6.12}
$$

$$
\begin{aligned}
\dot{x}_3^{(l)} = {}& -\gamma \delta_{l,0} - (il\delta + \gamma) x_3^{(l)} \\
& - g_0 \left(\alpha x_2^{(l+1)} + \alpha^* x_1^{(l+1)} + \alpha x_2^{(l-1)} + \alpha^* x_1^{(l-1)}\right).
\end{aligned}
\tag{6.13}
$$

In order to find a steady state solution, we set the time derivatives in Eqns. 6.11 – 6.13 to zero, and substitute Eqns. 6.11 – 6.12 into Eq. 6.13, yielding,

$$
0 = \gamma \delta_{l,0} + a_l x_3^{(l)} + d_l x_3^{(l+2)} + b_l x_3^{(l-2)},
\tag{6.14}
$$

where $\delta_{l,0}$ is a Kronecker delta, and

$$
a_l \equiv il\delta + \gamma + \frac{g_0^2 |\alpha|^2}{2} \left(\frac{1}{Q_{l+1}} + \frac{1}{P_{l+1}} + \frac{1}{Q_{l-1}} + \frac{1}{P_{l-1}}\right),
\tag{6.15}
$$

$$
b_l = d_{l-2} \equiv \frac{g_0^2 |\alpha|^2}{2} \left(\frac{1}{Q_{l-1}} + \frac{1}{P_{l-1}}\right),
\tag{6.16}
$$

where,

$$
P_l = i(l\delta + \Delta) + \gamma_p,
\tag{6.17}
$$

$$Q_l = i(l\delta - \Delta) + \gamma_p. \tag{6.18}$$

For a given α, Eq. 6.14 defines a tridiagonal linear system that can be solved by truncating l at some finite value, and applying the Thomas algorithm for matrix inversion [70].

Since the atoms have motion, the condition for resonance between an atom and photon is achieved when the atomic frequency and photon frequency are offset by δ. However, higher order multi-photon processes, known as Doppleron resonances, involving $2n + 1$ photons where n is an integer, are also possible. The nth order Doppleron resonance corresponds to the terms of order $l/2$ in the Floquet theory [1, 79]. This correspondence is why only even values of l can couple into Eq. 6.14.

In steady state, Eq. 6.7 simplifies to,

$$\alpha = \frac{\eta}{\kappa} + \frac{g_0^2 N}{2\kappa} \int d\delta P(\delta) \left(x_1^{(-1)} + x_1^{(1)} \right). \tag{6.19}$$

Since x_1^{-1} and x_1^1 depend on α, the self-consistent field amplitude α that solves Eq. 6.19 is found numerically by applying Newton's method for root finding [70].

We have seen excellent agreement between the two previously described solution methods, and for the remainder of the chapter, focus our attention on the Floquet solution, which most transparently illuminates the underlying physics.

6.2   Discussion of Steady State Solutions

We first consider the lowest order solution to Eq. 6.19, by truncating at $l = 0$, which means we have not included higher order Doppleron processes. We have verified that this solution displays the correct physics qualitatively by comparing to higher order solutions that are truncated at increasing values of l. We define scaled intracavity and input field amplitudes $x \equiv \alpha/\sqrt{n_0}$, $y \equiv \eta/(\kappa\sqrt{n_0})$, where $n_0 = (\gamma\gamma_p)/(4g_0^2)$ is the saturation photon number. Eq. 6.19 then becomes,

$$y = x\left(1 + \frac{NC_0}{4} \int d\delta P(\delta)\left\{ \frac{1 - i(\Delta + \delta)/\gamma_p}{1 + \frac{(\Delta+\delta)^2}{\gamma_p^2} + \frac{|x|^2}{4}\left(1 + \xi^+\right)} \right.\right.$$
$$\left.\left. + \frac{1 - i(\Delta - \delta)/\gamma_p}{1 + \frac{(\Delta-\delta)^2}{\gamma_p^2} + \frac{|x|^2}{4}\left(1 + \xi^-\right)} \right\}\right), \tag{6.20}$$

where $C_0 \equiv \frac{g_0^2}{\kappa \gamma_p}$, and $\xi^\pm = \frac{\gamma_p^2 + (\Delta \pm \delta)^2}{\gamma_p^2 + (\Delta \mp \delta)^2}$.

It is interesting to consider the relation corresponding to Eq. 6.20 for a ring cavity system that has a field traveling in only one direction, assuming equal intracavity power. The corresponding expression is given by,

$$y = x\left(1 + \frac{NC_0}{2} \int d\delta P(\delta) \frac{1 - i(\Delta + \delta)/\gamma_p}{1 + \frac{(\Delta+\delta)^2}{\gamma_p^2} + \frac{|x|^2}{2}}\right). \tag{6.21}$$

In the experiment described in [86], the measured observables are the cavity transmitted power $T \equiv |x/y|^2$ and transmitted phase shift $\phi \equiv arg(x/y)$ of the intracavity light relative to the input light. Fig. 6.2 shows that the presence of $\xi^\pm$ in Eq. 6.20 results in extra absorption and dispersive features (blue solid) around resonance in the transmission and phase shift, as compared to a ring cavity field (red dashed) where $\xi^\pm = 0$.

These extra absorption and dispersive features are caused by the following: The distribution of atomic velocities results in a different Doppler frequency shift of the light for each atomic velocity class, so that each velocity class will be resonant at a different detuning Δ. When $|\Delta| \ll \gamma_p|x|$, the resonant velocity class of the atoms is interrogated by both components of the standing wave field, whereas when $|\Delta| \gg \gamma_p|x|$, the resonant velocity class of atoms is interrogated by only one component of the standing wave field. Thus, there is an increased saturation in atomic absorption, with a corresponding saturated dispersive feature, for $|\Delta| \ll \gamma_p|x|$. These sharp features are absent from the traveling wave cavity situation where there is only one propagating field.

As seen in Fig. 6.2 (a), for low input intensities, there is no atomic saturation at any detuning. In Fig. 6.2 (b), the atoms in the velocity class around resonance are saturated by both components of the field, and the velocity classes away from resonance are saturated by only a single component of the standing wave field. Therefore, the features caused by the two component saturation and the features caused by the single component saturation are clearly able to be distinguished. It can be seen in Fig. 6.2 (c) that as the amount of saturation becomes large, the central feature becomes power broadened, but is still identifiable. Fig. 6.2 (d) shows the intracavity intensity for a given
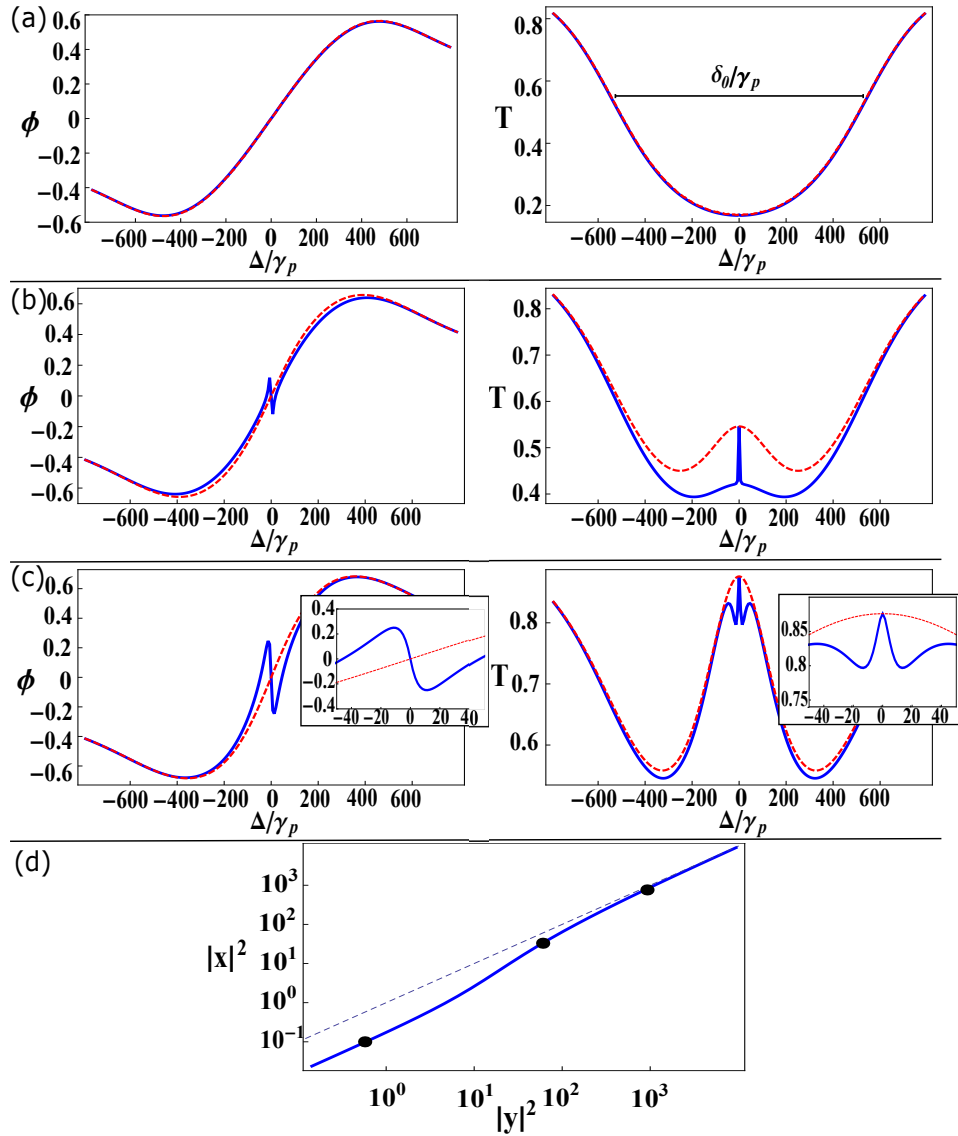
Figure 6.2: Development of the extra absorption and dispersion features in the transmission (T) and phase shift (ϕ), as the input intensity is increased. Blue (dark gray) solid curves are for a standing wave cavity, red (light gray) dashed are for a traveling wave cavity. For all plots, $NC_0 = 600$ and $\delta_0/\gamma_p = 260$, which in the case of ^{88}Sr, corresponds to a temperature of $\sim 15\ mK$. (a) $|y|^2 = 5 \times 10^{-1}$, (b) $|y|^2 = 6 \times 10^1$, (c) $|y|^2 = 9 \times 10^2$; The inset is zoomed in to emphasize the central features. (d) Input vs intracavity intensity at resonance. The black dots label the input and intracavity intensities of (a) (b) and (c), and the dashed line is $|y|^2 = |x|^2$ for reference. Note that there is no bistability.

input intensity with the values used in Figs. 6.2 (a-c) labeled by black dots.

In Fig. 6.3 and Fig. 6.4, a comparison between the solutions to Eq. 6.19, with l truncated at $l = 6$, and the experimental results of [86] can be seen. Fig. 6.3 shows the transmitted phase shift $\phi \equiv arg(x/y)$ of the intracavity light relative to the input light around resonance for several systems of varying input probe laser power. Here is demonstrated a linear increase in phase slope as the input laser power is reduced. Fig. 6.4 shows the transmitted phase shift for several systems with varying numbers of atoms. Here is demonstrated a linear increase in phase slope as the number of atoms is increased. In both figures, an excellent agreement between the theory and experimental results can be seen.

6.3   Shot Noise Limited Laser Stabilization

For laser stabilization, the central part of the phase response close to the atomic resonance serves as an error signal, see Fig. 6.2 (c), and allows for the generation of a feedback signal to the laser frequency. Through the photodetector, the error signal is converted to a measurable photocurrent. Any photocurrent measured by the photo detector should, in principle be zeroed by an ideal feedback loop of infinite bandwidth to the laser frequency.

To determine the potential phase stability that could be achievable using our system, we consider the shot noise limited stabilization linewidth assuming a strong local oscillator, as derived in [63],

$$\Delta\nu = \frac{\hbar\omega}{8\pi\varepsilon P_{sig}\left(\frac{\partial\phi}{\partial\Delta}\right)^2} = \frac{C_0}{4\pi\varepsilon\gamma|x|^2\left(\frac{\partial\phi}{\partial\Delta}\right)^2}, \tag{6.22}$$

where P_{sig} is the signal power, ε is the photo-detector efficiency and $\left(\frac{\partial\phi}{\partial\Delta}\right)$ is the dimensionless phase slope at resonance $\Delta = 0$. In the case that FM spectroscopy, such as NICEOHMS [86], is used for the detection of the absorption or cavity transmitted phase, Eq. 6.22 must be modified as follows. In general, in a configuration where sidebands are applied at the free spectral range of the cavity, Eq. 6.22 must be multiplied with $(1 + P_{sig}/2P_{sideband})$, where $P_{sideband}$ is the sideband power.
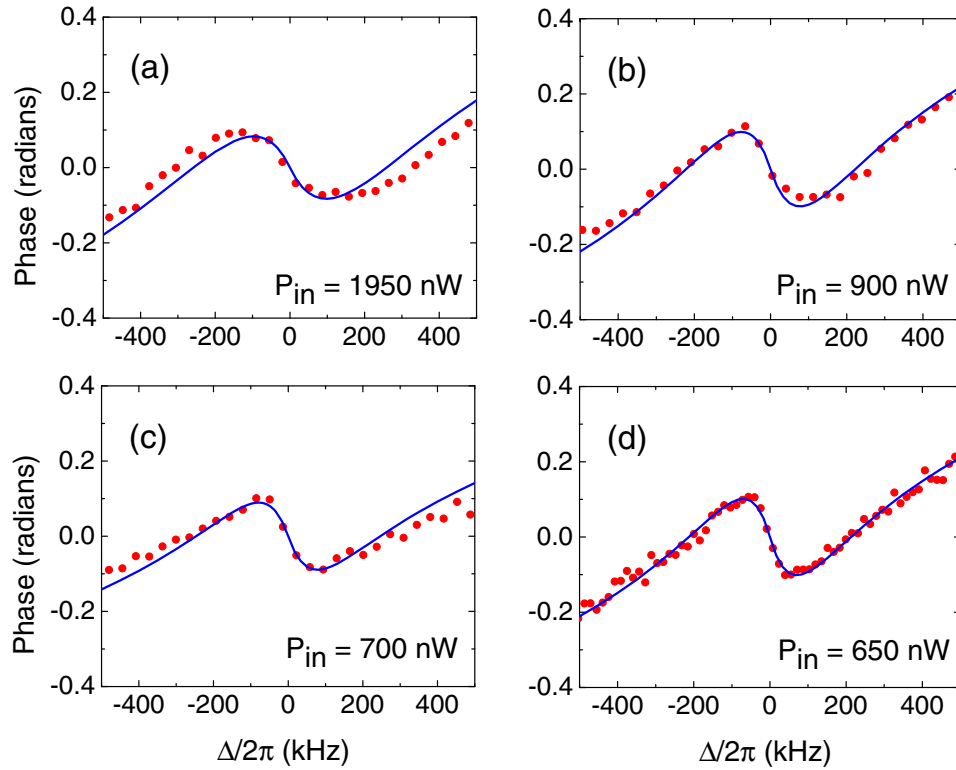
Figure 6.3: Measured phase shift of the cavity transmitted field when scanned across the atomic resonance. The input probe laser power, P_{in}, is progressively decreased from 1950 nW (a), 900 nW (b), 700 nW (c) to 650 nW (d). The number of atoms is about 2.5×10^7. Each point is an average of three data points. The solid lines are the predictions of the theoretical model.
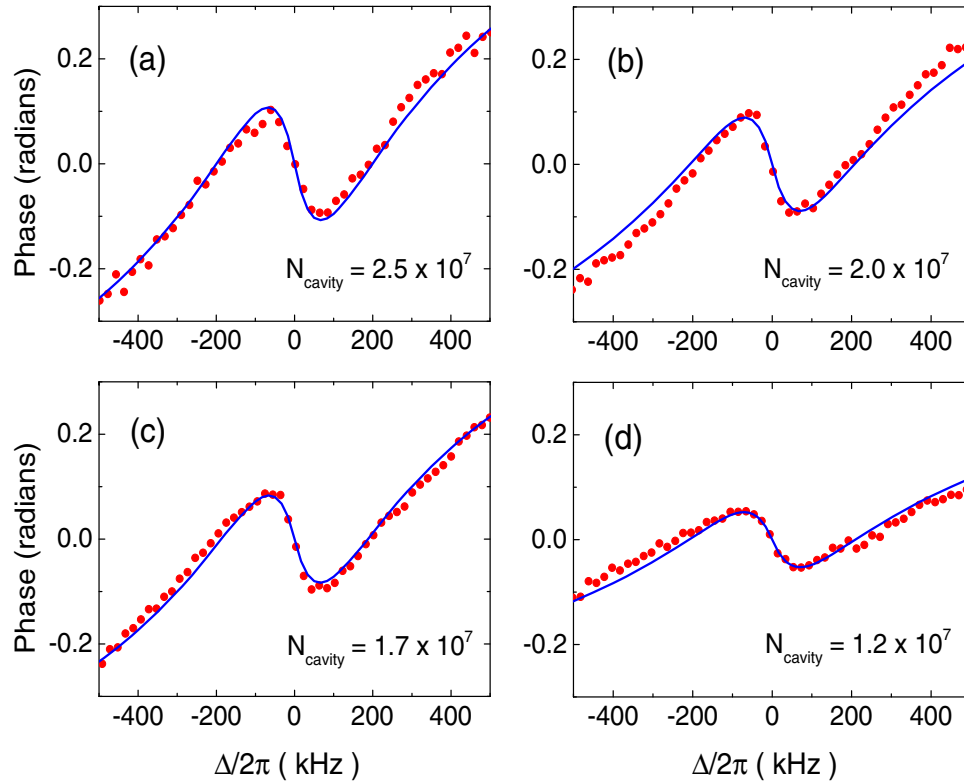
Figure 6.4: Measured phase shift of the cavity transmitted field when scanned across the atomic resonance. The number of atoms in the cavity, N_{cavity}, is progressively decreased from 2.5×10^7 (a), 2.0×10^7 (b), 1.7×10^7 (c) to 1.2×10^7 (d). The input power used for all plots was 650 nW. Each point is an average of three data points. The solid lines are the predictions of the theoretical model.

Eq. 6.22 is the smallest, and hence the phase is most stable, when the product of the slope around resonance and the intracavity intensity is as large as possible. The optimal input intensity, which allows this product to be as large as possible, is the value used in Fig. 6.2 (c), and is labeled by the black dot at $|y|^2 \approx 10^3$ in Fig. 6.2 (d).

To achieve a quantitative agreement between theory and experiment [86], higher orders in l in Eq. 6.19 must be included. These higher order terms correspond to Doppleron resonances, i.e. multi-photon scattering processes between the atoms and cavity mode.

To study the importance of these higher order Dopplerons, we calculate the linewidth from Eq. 6.22 at the optimum input power while varying the order of l at which the truncation occurs.

Fig. 6.5 shows the dependence of the linewidth at the optimum input intensity on the order of l at which the truncation occurs for 3 different sets of parameters. The first set, shown in blue circles, converges by $l = 12$. The linewidth calculated with up to $l = 12$ included before truncation is around 5 times larger than the linewidth with only $l = 0$ included. This shows that Doppleron effects are crucial to include for a correct quantitative analysis of this system.

Shown in red squares, we increase the number of atoms by a factor of 10, and again calculate the linewidth as a function of the order of l at which the truncation occurs. As a result of N being increased, the optimum value of $|y|^2$ is also increased. Convergence occurs around $l = 16$. Now, the difference between the converged linewidth and the linewidth with only $l = 0$ included has increased by a factor of around 2. This demonstrates that as N is increased, higher order Dopplerons play an increasing role.

We also decrease the temperature by a factor of 10, and again calculate the linewidth at the new optimum value of $|y|^2$, as shown by the black diamonds. Even though the optimum $|y|^2$ occurs at a lower value, there is still an increase in the difference between the converged linewidth and the $l = 0$ linewidth. Convergence occurs around $l = 12$. This shows that as the temperature is decreased, higher order Dopplerons also play an increasing role.

We next study the effect of optical bistability, and its effects on the optimum input intensity. As can be seen in Fig. 6.6 (a), when $\delta_0/\gamma_p = 0$ there is a bistability in input ($|y|^2$) vs intracavity
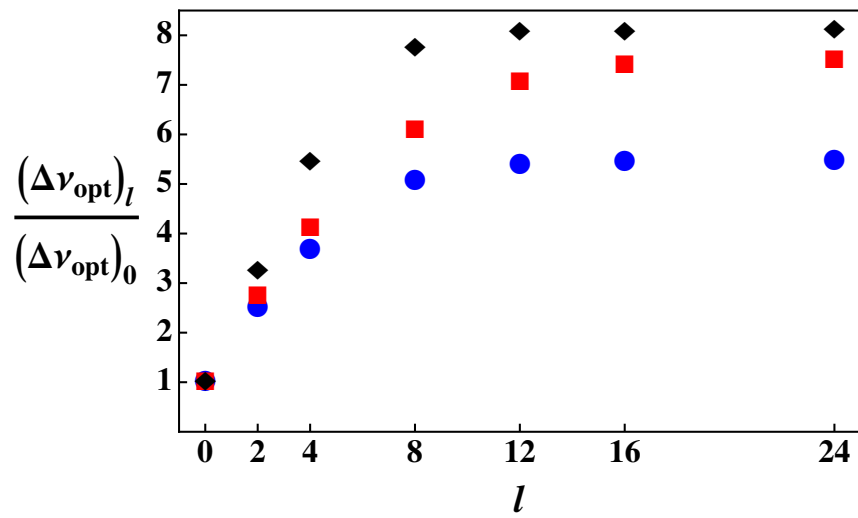
Figure 6.5: Linewidth at the optimum $|y|^2$, which gives the smallest linewidth, as a function of included orders of l, normalized by the $l = 0$ linewidth. Blue circles: $NC_0 = 600$, $\delta_0/\gamma_p = 260$, $|y|^2 = 1270$. Red squares: $NC_0 = 6000$, $\delta_0/\gamma_p = 260$, $|y|^2 = 7700$. Black diamonds: $NC_0 = 600$, $\delta_0/\gamma_p = 80$, $|y|^2 = 850$.

($|x|^2$) intensities. As the temperature is increased, the bistability becomes less pronounced, until eventually it disappears entirely, which can be seen in the $\delta_0/\gamma_p = 30$ curve.

The slope at resonance, which can be seen in Fig. 6.6 (b), has very a different behavior for the zero and non zero temperature cases. For $\delta_0/\gamma_p = 0$, the slope is largest on the lower branch, decreases slightly in the bistable region, and then drops exponentially to zero as the intensity is increased on the upper branch. When the temperature is increased, the bistability disappears, and a dispersion feature with negative slope appears. Then the slope goes to a maximally negative value before power broadening eventually causes it to increase to zero.

The disappearance of the bistability is important for achieving the highest possible degree of stabilization. In the zero temperature case, the optimal combination of $|x|^2$ and $\frac{\partial \phi}{\partial \Delta}$ to give the smallest $\Delta\nu$ occurs on the far left side of the upper branch, when the input intensity has the fixed value $|y|^2 = 4NC_0$, labeled with the black dot in Fig. 6.6 (a) and (b). However, this value of intensity is in the bistable region, so the system is dynamically unstable when the full quantum dynamics are accounted for. If the tunneling rate between the different branches is not small, we are constrained to work at input intensities that are above the bistable region where the achievable frequency precision is much less. The grey dot in Fig. 6.6 (a) and (b) is at the far right side of the bistable region, at the fixed input intensity value $|y|^2 = (NC_0)^2/4$. The stabilization linewidth is orders of magnitude worse here, because the slope is so small. Nonetheless, working above the bistability allows for shot noise limited stabilization line widths of ~ 1 mHz [63].

Fig. 6.6 (c) shows the stabilization linewidth as a function of NC_0 for several temperatures. In the $\delta_0/\gamma_p = 0$ limit of zero temperature, the black dashed curve corresponds to the input intensity corresponding to the black dot, and the black solid curve corresponds to the input intensity of the gray dot. When the temperature is increased sufficiently, the bistability disappears. Then, there are no longer any regions of dynamic instability and therefore no restrictions on input intensity. Each of the $\delta_0/\gamma_p \neq 0$ cases in this plot are calculated at their respective optimal input intensity, and stop at a critical value of NC_0, where the bistability reappears. It follows as reciprocal information that for a given value of NC_0, there exists a critical temperature at which the bistability disappears.
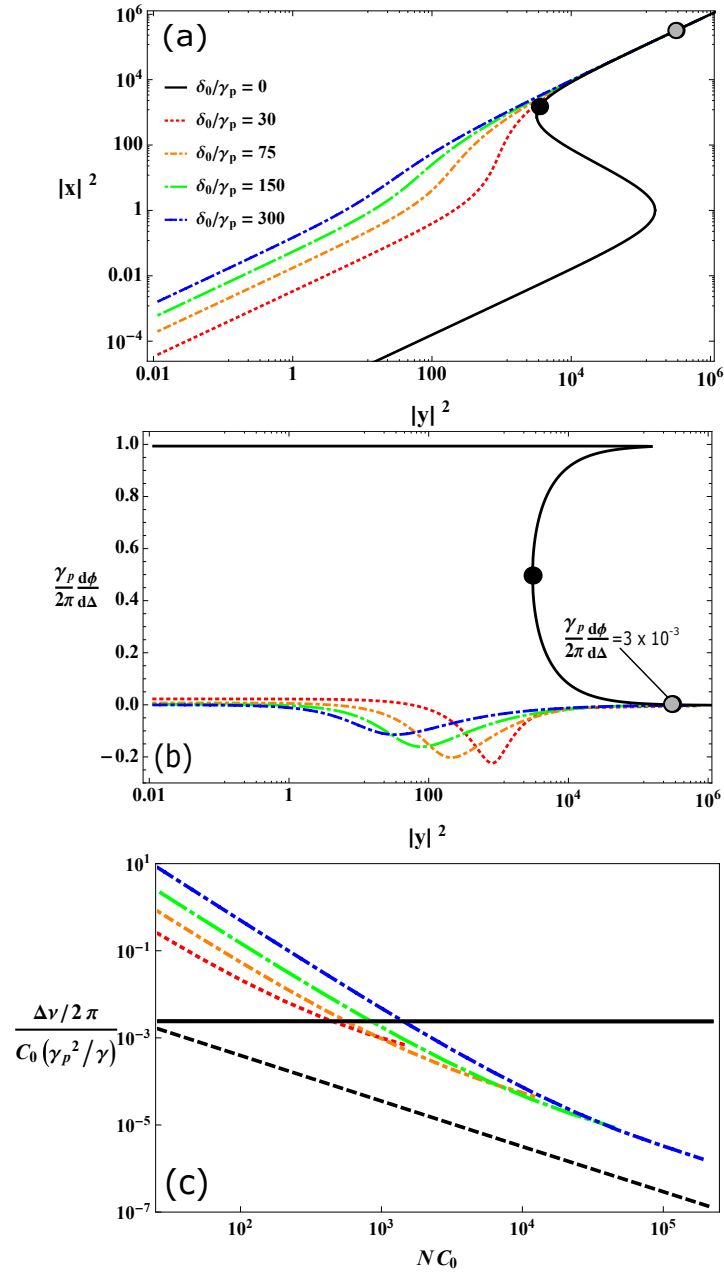
Figure 6.6: (a) Scaled input ($|x|^2$) vs intracavity ($|y|^2$) intensities for several temperatures with $NC_0 = 800$ (b) Slope at resonance for several temperatures with $NC_0 = 800$ (c) Stabilization linewidth as a function of NC_0 for several temperatures. For $\delta_0/\gamma_p = 0$, black dashed is calculated at the fixed input intensity $|y|^2 = 4NC_0$; black solid is calculated at the fixed input intensity $|y|^2 = (NC_0)^2/4$. For $\delta_0/\gamma_p \neq 0$, the linewidth is calculated with the input intensity fixed to the optimum value that gives the smallest linewidth. In the case of ^{88}Sr, $\delta_0/\gamma_p = 150$ corresponds to a temperature of $\sim 5\ mK$.

Therefore, by using Fig. 6.6 (c) to note the values of temperature and NC_0 at which the bistability disappears for the different curves, it is seen that the critical temperature increases as NC_0 increases.

In general, a lower temperature will yield a smaller linewidth. However, because one must avoid working in a region of optical bistability, the optimal shot noise limited linewidth for certain values of NC_0 and δ_0/γ_p in which there is no bistability can actually be smaller than the $\delta_0/\gamma_p = 0$ linewidth which is constrained above the bistability.

6.4   Conclusion

We have seen that thermal atoms in a standing wave cavity field exhibit additional phenomena that were not observed when considering a frozen arrangement of atoms. Specifically, when the detuning of the laser and atoms is less than the power broadened linewidth, the system interacts with both components of the standing wave field. This causes new absorptive and dispersive features in the observables, which are the features that can be used as an error signal for frequency stabilization. Multi-photon scattering processes due to Doppleron resonances cause the stabilization linewidth to increase. This effect becomes more dominant as the collective cooperativity NC_0 is increased, and as the temperature is decreased. A system with sufficient NC_0 and no atomic motion will exhibit optical bistability. Atomic motion may cause this bistability to disappear. When optical bistability occurs, one is generally restricted to using an input intensity that lies outside of the bistable region in order to prevent hopping between semiclassical solutions. When there is no optical bistability, there are no dynamically unstable regions, so that no such restrictions on input intensity are necessary, allowing the optimally smallest stabilization linewidth to be achieved.

Chapter 7

Conclusion

In this thesis, we have examined a variety of open quantum systems in an attempt to discover a scheme in which an extremely spectrally pure coherent light source might be realized. Before these systems were examined, the necessary preliminary material was provided. To begin, the electromagnetic field was quantized. This was necessary to correctly describe the Hamiltonian dynamics of our open quantum systems when only a few photons are present. Also, a quantized field is needed in order to describe spontaneous irreversible processes, such spontaneous emission. The power spectrum, and its relation to the two-time correlation functions through the Wiener-Khinchin theorem was also discussed. This allowed the spectral properties of a system, such as the linewidth of the power spectrum, to be calculated.

Next, we derived the master equation, which describes the Schrödinger evolution for a system that is weakly coupled to a much larger reservoir. The coupling was treated in time dependent perturbation theory, and the reservoir was approximated as having infinite bandwidth, and then averaged over. Exact solution methods to the master equation, such as the quantum jump and quantum state diffusion methods were presented, and computer simulations of these methods were demonstrated. The cumulant expansion method, which consists of an approximate set of coupled equations for expectation values of system observables, was also demonstrated.

The quantum Langevin equations, which describe open quantum systems in the Heisenberg picture of quantum mechanics, were then derived. The same infinite bandwidth approximation that was made in the master equation derivation was made here. Since these equations prove

difficult for computer simulations, a Fokker-Planck equation for a quasi-probability distribution describing the system was derived. It was shown that a set of c-number Langevin equations are equivalent to the Fokker-Planck equation. These c-number Langevin equations can be simulated on a computer with relative ease. Once this procedure for deriving the c-number Langevin equations from the Fokker-Planck equation was demonstrated, an easier, but less mathematically rigorous way to derive c-number Langevin equations was shown. This new procedure becomes increasingly advantageous as the system complexity increases. Finally, computer simulations of the c-number Langevin equations for several systems were demonstrated.

The theory of the crossover between lasing and steady state superradiance was presented. It was shown how lasing and steady state superradiance can actually be thought of as the extreme limits of a single and more general phenomenon. In a laser, the phase information that allows for coherence is stored in the light field. In steady state superradiance, this phase information is stored in the atomic ensemble. In the crossover region between these two limits, the phase information that allows for coherence can be stored in the light field and the atomic ensemble simultaneously. The parameter space between these two extreme limits was explored, and the benefits and drawbacks of operating a system at a given set of parameters, to achieve the most spectrally pure light source, were discussed.

Specifically, it was shown that for a given rate of re-supplying energy, a crossover system will be much farther above threshold than a laser, which is typically operated just above threshold. This can allow the linewidth of a crossover system to be orders of magnitude smaller than the laser, while maintaining a similar intracavity intensity. A crossover system also exhibits a much larger intracavity intensity than a superradiant system, so that the crossover system is more experimentally accessible. The linewidth and intracavity intensity were shown to be insensitive to atomic dephasing in all parameter regions, so long as the rate of atomic dephasing is smaller than the rate of energy being resupplied to the system.

The sensitivity to fluctuations in cavity length and cavity frequency were also discussed. The superradiance region was shown to be insensitive to fluctuations in cavity frequency, while a

lasing system is insensitive to fluctuations in the atomic frequency. A crossover system was shown to be less sensitive to fluctuations in cavity frequency than a laser system, and less sensitive to fluctuations in atomic frequency than a superradiant system. This is important, since fluctuations in cavity length are the bottleneck in further reducing the linewidth in today's narrowest linewidth lasers.

Finally, we considered the phase stability of a local oscillator locked to a cavity QED system comprised of atoms with an ultra-narrow optical transition. The atoms were modeled as being cooled to millikelvin temperatures and then released into the optical cavity. Even though the atomic motion introduced Doppler broadening, the standing wave nature of the cavity caused saturated absorption features to appear, which are much narrower than the Doppler width. These features can be used to achieve an extremely high degree of phase stabilization, competitive with the current state-of-the-art. A comparison between the developed theory, and the results of an experiment on the system that was considered was given. It was demonstrated that the inhomogeneity introduced by finite atomic velocities can cause optical bistability to disappear so that there exist no regions of dynamic instability that would otherwise restrict operational parameters in the experiment to be outside the optimum region where the minimum linewidth occurs.

Bibliography

[1] G. S. Agarwal and Yifu Zhu. Velocity-tuned resonances and resonance fluorescence in a standing-wave field. Phys. Rev. A, 46:479–484, Jul 1992.

[2] G. S. Agarwal, Yifu Zhu, Daniel J. Gauthier, and T. W. Mossberg. Spectrum of radiation from two-level atoms under intense bichromatic excitation. J. Opt. Soc. Am. B, 8(5):1163–1167, May 1991.

[3] A. Ashkin, J. M. Dziedzic, Bjorkholm J. E., and S. Chu. Observation of a single-beam gradient force optical trap for dielectric particles. Optics Letters, 11:288–290, 1986.

[4] Claude Audoin and Bernard Guinot. The measurement of time: time, frequency and the atomic clock. Cambridge University Press, 2001.

[5] Claus Bagger and Flemming O Olsen. Review of laser hybrid welding. Journal of laser applications, 17(1):2–14, 2005.

[6] Barry C Barish and Rainer Weiss. Ligo and the detection of gravitational waves. Physics Today, 52:44–50, 1999.

[7] S Blatt, AD Ludlow, GK Campbell, Jan Westenkær Thomsen, T Zelevinsky, MM Boyd, J Ye, X Baillard, M Fouché, R Le Targat, et al. New limits on coupling of fundamental constants to gravity using sr 87 optical lattice clocks. Physical Review Letters, 100(14):140801, 2008.

[8] BJ Bloom, TL Nicholson, JR Williams, SL Campbell, M Bishof, X Zhang, W Zhang, SL Bromley, and J Ye. An optical lattice clock with accuracy and stability at the 10-18 level. Nature, 506(7486):71–75, 2014.

[9] Justin G Bohnet, Zilong Chen, Joshua M Weiner, Kevin C Cox, and James K Thompson. Relaxation oscillations, stability, and cavity feedback in a superradiant raman laser. Physical review letters, 109(25):253602, 2012.

[10] Justin G. Bohnet, Zilong Chen, Joshua M. Weiner, Dominic Meiser, Murray J. Holland, and James K. Thompson. A steady-state superradiant laser with less than one intracavity photon. Nature, 484:78–81, April 2002.

[11] Ruxandra Bondarescu, Mihai Bondarescu, Gyrgy Hetnyi, Lapo Boschi, Philippe Jetzer, and Jayashree Balakrishna. Geophysical applicability of atomic clocks: direct continental geoid mapping. Geophysical Journal International, 191(1):78–82, 2012.

[12] R. Bonifacio and L. A. Lugiato. Optical bistability and cooperative effects in resonance fluorescence. Phys. Rev. A, 18:1129–1144, Sep 1978.

[13] Jingbiao Chen. Active optical clock. Chinese Science Bulletin, 54(3):348–352, 2009.

[14] JingBiao Chen. Active optical clock. Chinese Science Bulletin, 54:348–352, 2009.

[15] Bjarke TR Christensen, Martin R Henriksen, Stefan A Schäffer, Philip G Westergaard, Jun Ye, Murray Holland, and Jan W Thomsen. Non-linear spectroscopy of sr atoms in an optical cavity for laser stabilization. arXiv preprint arXiv:1507.05757, 2015.

[16] G. D. Cole, W. Zhang, M. J. Martin, Jun Ye, and M. Aspelmeyer. Tenfold reduction of brownian noise in high-reflectivity optical coatings. Nature Photonics, 7:644, 2013.

[17] Jean Dalibard, Yvan Castin, and Klaus Mølmer. Wave-function approach to dissipative processes in quantum optics. Phys. Rev. Lett., 68:580–583, Feb 1992.

[18] G John Dick. Local oscillator induced instabilities in trapped ion frequency standards. Technical report, DTIC Document, 1987.

[19] R. H. Dicke. Coherence in spontaneous radiation processes. Phys. Rev., 93:99–110, Jan 1954.

[20] SA Diddams, JC Bergquist, SR Jefferts, and CW Oates. Standards of time and frequency at the outset of the 21st century. Science, 306(5700):1318–1324, 2004.

[21] J.A. Dixon. Surgical application of lasers. 2nd edition. Year Book Medical Publishers,Chicago, IL, Jan 1987.

[22] Peter Domokos and Helmut Ritsch. Collective cooling and self-organization of atoms in a cavity. Phys. Rev. Lett., 89:253003, Dec 2002.

[23] RWP Drever, John L Hall, FV Kowalski, J Hough, GM Ford, AJ Munley, and H Ward. Laser phase and frequency stabilization using an optical resonator. Applied Physics B, 31(2):97–105, 1983.

[24] P D Drummond and D F Walls. Quantum theory of optical bistability. i. nonlinear polarisability model. Journal of Physics A: Mathematical and General, 13(2):725, 1980.

[25] FJ Duarte. Broadly tunable external-cavity semiconductor lasers. Tunable Laser Applications (CRC, 2009), pages 143–178, 2008.

[26] F.J.E.K.C. Duarte. Two-laser therapy and diagnosis device, September 28 1988. EP Patent App. EP19,880,302,468.

[27] R. Dum, P. Zoller, and H. Ritsch. Monte carlo simulation of the atomic master equation for spontaneous emission. Phys. Rev. A, 45:4879–4887, Apr 1992.

[28] L Essen. Atomic time and the definition of the second. Nature, 1956.

[29] L Essen and JVL Parry. An atomic standard of frequency and time interval: a caesium resonator. Nature, 1955.

[30] Louis Essen and JVL Parry. The caesium resonator as a standard of frequency and time. Philosophical Transactions of the Royal Society of London A: Mathematical, Physical and Engineering Sciences, 250(973):45–69, 1957.

[31] Z. Ficek and H. S. Freedhoff. Resonance-fluorescence and absorption spectra of a two-level atom driven by a strong bichromatic field. Phys. Rev. A, 48:3092–3104, Oct 1993.

[32] Charles Freed and Ali Javan. Standing-wave saturation resonance in the co_2 10.6-μ transitions observed in a low-pressure room-temperature absorber gas. Applied Physics Letters, 17(2):53–56, 1970.

[33] James G Fujimoto, Mark E Brezinski, Guillermo J Tearney, Stephen A Boppart, Brett Bouma, Michael R Hee, James F Southern, and Eric A Swanson. Optical biopsy and imaging using optical coherence tomography. Nature medicine, 1(9):970–972, 1995.

[34] Crispin W Gardiner et al. Handbook of stochastic methods, volume 4. Springer Berlin, 1985.

[35] R. M. Godun, P. B. R. Nisbet-Jones, J. M. Jones, S. A. King, L. A. M. Johnson, H. S. Margolis, K. Szymaniec, S. N. Lea, K. Bongs, and P. Gill. Frequency ratio of two optical clock transitions in ^{171}yb$^+$ and constraints on the time variation of fundamental constants. Phys. Rev. Lett., 113:210801, Nov 2014.

[36] Leon Goldman. Dye lasers in medicine. In F.J. DuarteLloyd W. Hillman, editor, Dye Laser Principles, Quantum ElectronicsPrinciples and Applications, pages 419 – 432. Academic Press, San Diego, 1990.

[37] J. Gripp, S. L. Mielke, and L. A. Orozco. Evolution of the vacuum rabi peaks in a detuned atom-cavity system. Phys. Rev. A, 56:3262–3273, Oct 1997.

[38] J. Guéna, M. Abgrall, D. Rovera, P. Rosenbusch, M. E. Tobar, Ph. Laurent, A. Clairon, and S. Bize. Improved tests of local position invariance using ^{87}Rb and ^{133}Cs fountains. Phys. Rev. Lett., 109:080801, Aug 2012.

[39] H. Haken. Theory of intensity and phase fluctuations of a homogeneously broadened laser. Z. Phys., 190:327, 1966.

[40] Hermann Haken. Laser Theory. Springer Berlin Heidelberg, 1983.

[41] John L Hall. Nobel lecture: Defining and measuring optical frequencies. Reviews of Modern Physics, 78(4):1279, 2006.

[42] TW Hansch and B Couillaud. Laser frequency stabilization by polarization spectroscopy of a reflecting reference cavity. Optics communications, 35(3):441–444, 1980.

[43] Stephan Hartmann. Generalized dicke states. arXiv, 1201.1732, 2012.

[44] N Hinkley, JA Sherman, NB Phillips, M Schioppo, ND Lemke, K Beloy, M Pizzocaro, CW Oates, and AD Ludlow. An atomic clock with 10–18 instability. Science, 341(6151):1215–1218, 2013.

[45] N. Huntemann, B. Lipphardt, Chr. Tamm, V. Gerginov, S. Weyers, and E. Peik. Improved limit on a temporal variation of m_p/m_e from comparisons of yb$^+$ and cs atomic clocks. Phys. Rev. Lett., 113:210802, Nov 2014.

[46] Steve Jefferts. Nist-f1 cesium fountain atomic clock, 2009. `http://www.nist.gov/pml/div688/grp50/primary-frequency-standards.cfm`.

[47] James Jespersen and Jane Fitz-Randolph. From sundials to atomic clocks: understanding time and frequency. Courier Corporation, 1999.

[48] YY Jiang, AD Ludlow, ND Lemke, RW Fox, JA Sherman, L-S Ma, and CW Oates. Making optical atomic clocks more stable with 10-16-level laser stabilization. Nature Photonics, 5(3):158–161, 2011.

[49] T. Kessler, C. Hagemann, C. Grebing, T. Legero, U. Sterr, F. Riehle, M. J. Martin, L. Chen, and J. Ye. A sub-40-mhz-linewidth laser based on a silicon single-crystal optical cavity. Nat. Photon, 6:687–692, Sep 2012.

[50] T Kessler, C Hagemann, C Grebing, T Legero, U Sterr, F Riehle, MJ Martin, L Chen, and J Ye. A sub-40-mhz-linewidth laser based on a silicon single-crystal optical cavity. Nature Photonics, 6(10):687–692, 2012.

[51] H. J. Kimble, Benjamin L. Lev, and Jun Ye. Optical interferometers with reduced sensitivity to thermal noise. Phys. Rev. Lett., 101:260602, Dec 2008.

[52] P.E. Kloeden and E. Platen. Numerical Solution of Stochastic Differential Equations. Stochastic Modelling and Applied Probability. Springer Berlin Heidelberg, 2011.

[53] R Kodama, PA Norreys, K Mima, AE Dangor, RG Evans, H Fujita, Y Kitagawa, K Krushelnick, T Miyakoshi, N Miyanaga, et al. Fast heating of ultrahigh-density plasma as a step towards laser fusion ignition. Nature, 412(6849):798–802, 2001.

[54] R Kodama, H Shiraga, K Shigemori, Y Toyama, S Fujioka, H Azechi, H Fujita, H Habara, T Hall, Y Izawa, et al. Nuclear fusion: Fast heating scalable to laser fusion ignition. Nature, 418(6901):933–934, 2002.

[55] M. I. Kolobov, L. Davidovich, E. Giacobino, and C. Fabre. Role of pumping statistics and dynamics of atomic polarization in quantum fluctuations of laser sources. Phys. Rev. A, 47:1431–1446, Feb 1993.

[56] Ryogo Kubo. Generalized cumulant expansion method. Journal of the Physical Society of Japan, 17(7):1100–1120, 1962.

[57] S. J. M. Kuppens, M. P. van Exter, and J. P. Woerdman. Quantum-limited linewidth of a bad-cavity laser. Phys. Rev. Lett., 72:3815–3818, Jun 1994.

[58] R. Le Targat, L. Lorini, Y. Le Coq, M. Zawada, J. Guna, M. Abgrall, M. Gurov, P. Rosenbusch, D. G. Rovera, B. Nagrny, R. Gartman, P. G. Westergaard, M. E. Tobar, M. Lours, G. Santarelli, A. Clairon, S. Bize, P. Laurent, P. Lemonde, and J. Lodewyck. Experimental realization of an optical second with strontium lattice clocks. Nat. Commun., 4(2109), Jul 2013.

[59] Marc Levenson. Introduction to Nonlinear Laser Spectroscopy. Elsevier, 2012.

[60] TH MAIMAN. Stimulated optical radiation in ruby. Nature, 1960.

[61] Eckhard Mandelkow and Eva-Maria Mandelkow. Kinesin motors and disease. Trends in cell biology, 12(12):585–591, 2002.

[62] M. J. Martin, M. Bishof, M. D. Swallows, X. Zhang, C. Benko, J. von Stecher, A. V. Gorshkov, A. M. Rey, and J. Ye. A quantum many-body spin system in an optical lattice clock. Science, 341(6146):632–636, 2013.

[63] M. J. Martin, D. Meiser, J. W. Thomsen, Jun Ye, and M. J. Holland. Extreme nonlinear response of ultranarrow optical transitions in cavity qed for laser stabilization. Phys. Rev. A, 84:063813, Dec 2011.

[64] D. Meiser and M. J. Holland. Intensity fluctuations in steady-state superradiance. Phys. Rev. A, 81:063827, Jun 2010.

[65] D. Meiser and M. J. Holland. Steady-state superradiance with alkaline-earth-metal atoms. Phys. Rev. A, 81:033847, Mar 2010.

[66] D. Meiser, Jun Ye, D. R. Carlson, and M. J. Holland. Prospects for a millihertz-linewidth laser. Phys. Rev. Lett., 102:163601, Apr 2009.

[67] Pierre Meystre and Murray Sargent. Elements of quantum optics. Springer Science & Business Media, 2007.

[68] Kenji Numata, Amy Kemery, and Jordan Camp. Thermal-noise limit in the frequency stabilization of lasers with rigid cavities. Physical review letters, 93(25):250602, 2004.

[69] M. B. Plenio and P. L. Knight. The quantum-jump approach to dissipative dynamics in quantum optics. Rev. Mod. Phys., 70:101–144, Jan 1998.

[70] William H. Press, Saul A. Teukolsky, William T. Vetterling, and Brian P. Flannery. Numerical Recipes 3rd Edition: The Art of Scientific Computing. Cambridge University Press, New York, NY, USA, 3 edition, 2007.

[71] Audrey Quessada, Richard P Kovacich, Irène Courtillot, André Clairon, Giorgio Santarelli, and Pierre Lemonde. The dick effect for an optical frequency standard. Journal of Optics B: Quantum and Semiclassical Optics, 5(2):S150, 2003.

[72] Norman F Ramsey. History of atomic clocks. J. Res. Nat. Bur. Stand, 88:301, 1983.

[73] A. L. Schawlow and C. H. Townes. Infrared and optical masers. Phys. Rev., 112:1940–1949, Dec 1958.

[74] S. Schiller, G.M. Tino, P. Gill, C. Salomon, U. Sterr, E. Peik, A. Nevsky, A. Grlitz, D. Svehla, G. Ferrari, N. Poli, L. Lusanna, H. Klein, H. Margolis, P. Lemonde, P. Laurent, G. Santarelli, A. Clairon, W. Ertmer, E. Rasel, J. Mller, L. Iorio, C. Lmmerzahl, H. Dittus, E. Gill, M. Rothacher, F. Flechner, U. Schreiber, V. Flambaum, Wei-Tou Ni, Liang Liu, Xuzong Chen, Jingbiao Chen, Kelin Gao, L. Cacciapuoti, R. Holzwarth, M.P. He, and W. Schfer. Einstein Gravity Explorera medium-class fundamental physics mission, volume 23. Springer Netherlands, 2009.

[75] Marlan O. Scully and M. Suhail Zubairy. Quantum Optics. Cambridge University Press, 1 edition, September 1997.

[76] Stig Stenholm. Foundations of Laser Spectroscopy. Dover Publications, 2005.

[77] Stig Stenholm and Willis E Lamb Jr. Semiclassical theory of a high-intensity laser. Applied Physics Letters, 181(2):618, 1969.

[78] Karel Svoboda, Christoph F. Schmidt, Bruce J. Schnapp, and Steven M. Block. Direct observation of kinesin stepping by optical trapping interferometry motility. Nature, 365(6448):721–727, 1993.

[79] Andrée Tallet. Raman emission versus dopplerons in a two-level atomic cell. J. Opt. Soc. Am. B, 11(8):1336–1349, Aug 1994.

[80] D. A. Tieri, J. Cooper, Bjarke T. R. Christensen, J. W. Thomsen, and M. J. Holland. Laser stabilization using saturated absorption in a cavity-qed system. Phys. Rev. A, 92:013817, Jul 2015.

[81] D. A. Tieri, Minghui Xu, D. Meiser, J. Cooper, and M. J. Holland. The crossover between lasing and steady state superradiance, 2015. In preperation.

[82] Charles H. Townes. How the laser happened : adventures of a scientist / Charles H. Townes. Oxford University Press New York, 1999.

[83] Th Udem, Ronald Holzwarth, and Theodor W Hänsch. Optical frequency metrology. Nature, 416(6877):233–237, 2002.

[84] M. P. van Exter, S. J. M. Kuppens, and J. P. Woerdman. Theory for the linewidth of a bad-cavity laser. Phys. Rev. A, 51:809–816, Jan 1995.

[85] Daniel F Walls and Gerard J Milburn. Quantum optics. Springer Science & Business Media, 2007.

[86] Philip G. Westergaard, Bjarke T. R. Christensen, David Tieri, Rastin Matin, John Cooper, Murray Holland, Jun Ye, and Jan W. Thomsen. Observation of motion-dependent nonlinear dispersion with narrow-linewidth atoms in an optical cavity. Phys. Rev. Lett., 114:093002, Mar 2015.

[87] H. M. Wiseman and G. J. Milburn. Quantum theory of field-quadrature measurements. Phys. Rev. A, 47:642–662, Jan 1993.

[88] Minghui Xu, D. A. Tieri, and M. J. Holland. Simulating open quantum systems by applying su(4) to quantum master equations. Phys. Rev. A, 87:062101, Jun 2013.

[89] Minghui Xu, DA Tieri, EC Fine, James K Thompson, and MJ Holland. Synchronization of two ensembles of atoms. Physical review letters, 113(15):154101, 2014.

[90] Minghui Xu, DA Tieri, and MJ Holland. Simulating open quantum systems by applying su (4) to quantum master equations. Physical Review A, 87(6):062101, 2013.

[91] B. C. Young, F. C. Cruz, W. M. Itano, and J. C. Bergquist. Visible lasers with subhertz linewidths. Phys. Rev. Lett., 82:3799–3802, May 1999.